SENSITIVITY OF A PHOTOMAGNETOMETER

by

John A. MacKinnon, BSc.

A thesis submitted to the Faculty of Graduate Studies and Research of McGill University, in partial fulfilment of the requirements for the degree of Master of Science.

Eaton Electronics Research Laboratory,
McGill University,
Montreal.

June 1963.

TABLE OF CONTENTS

ABSTRACT

A photomagnetometer is an instrument capable of measuring changes induced by external radiation in the macroscopic magnetic moment of a solid. The system described here is a source-modulated detector. The solid being studied is fixed in the presence of a uniform magnetic field and radiation in the optical region modulated at a low frequency (1000 c.p.s.) is allowed to strike the solid. Any changes in the magnetic moment are measured by the voltage induced in detection coils suitably arranged adjacent to the sample. These signals are detected by a phase sensitive electronics system.

The sensitivity, frequency response, and thermal noise level of the system were measured. Studies were made of the spurious signals which can arise from vibration of the detection coils in the magnetic field, irregularities in modulation due to imperfections in the chopping disc, and stray light falling on the detection coils. The bandwidth of the electronic detection system, and the photomagentism to be expected in a small parallelepiped of solid arising from the photogeneration of free carriers were calculated.

The characteristics of the important component instruments were measured.

ACKNOWLEDGEMENTS

The author wishes to thank Dr. Stevenson who designed and built the Photomagnetometer for his supervision and encouragement during the course of the experiment.

The research formed part of the work on the physics of photomagnetism, which is financed at the Eaton Laboratory by the Office of Naval Research (U.S.A.) and in part by the Defence Research Board.

The author is indebted to the National Research Council of Canada for financial assistance in the form of one Bursary and one Studentship.

CHAPTER I

INTRODUCTION

An experiment in which the macroscopic magnetic moment of a solid is altered due to incident optical radiation is called a photomagnetism experiment. The change in the macroscopic magnetic moment of materials (a magnetic field is applied to the sample) such as germanium and the alkali halides due to illumination has been the subject of experimental and theoretical investigation in recent years.[1]

For semiconductors it could be hoped to observe the Landau diamagnetism of photogenerated electrons, or the diamagnetism of photogenerated excitons. The first effect (per particle) is inherently small; the second, because of the possibly large orbits, might be appreciable. However, it could be difficult to create enough excitons to make the effect observable.

One photomagnetism experiment with a semiconductor has been reported, Kessler and Moore (1959,1960),[2] Moore and Kessler (1960),[3] in which a diamagnetic effect was observed at room temperature. This effect was considered to be related to the photogeneration of excitons. It seemed desirable to study the phenomenon with a completely different type of measuring system.

An apparatus-system called a photomagnetometer was designed and built to measure the change in the macroscopic magnetic moment of a sample of material as a result of illuminating the sample with light in the optical region.

Figure 1-1 is a block diagram of the apparatus-system. The important and central part of the apparatus was the cryostat (Figure 1-2) in which the sample was mounted. The sample was a small parallelepiped of material of dimensions 3/8" by 3/8" by 1/4". An opening of about one inch in diameter was provided in the cryostat stock for the illumination of the sample with light. The opening was provided with a fused silica window, and an "O" ring as a vacuum seal. A helium gas thermometer was installed on the cryostat for the approximate measurement of sample temperature.

Two small coils placed beneath the sample were used to detect the small changes in the magnetic moment due to illumination. Figure 1-3 is a schematic diagram of the sample, coils, and reference coil. This reference coil was a permanent part of the apparatus-system, but not the one used during the calibration and sensitivity measurements.

The brass spools on which the coils were wound had no lip on the end upon which the sample rested. Eddy

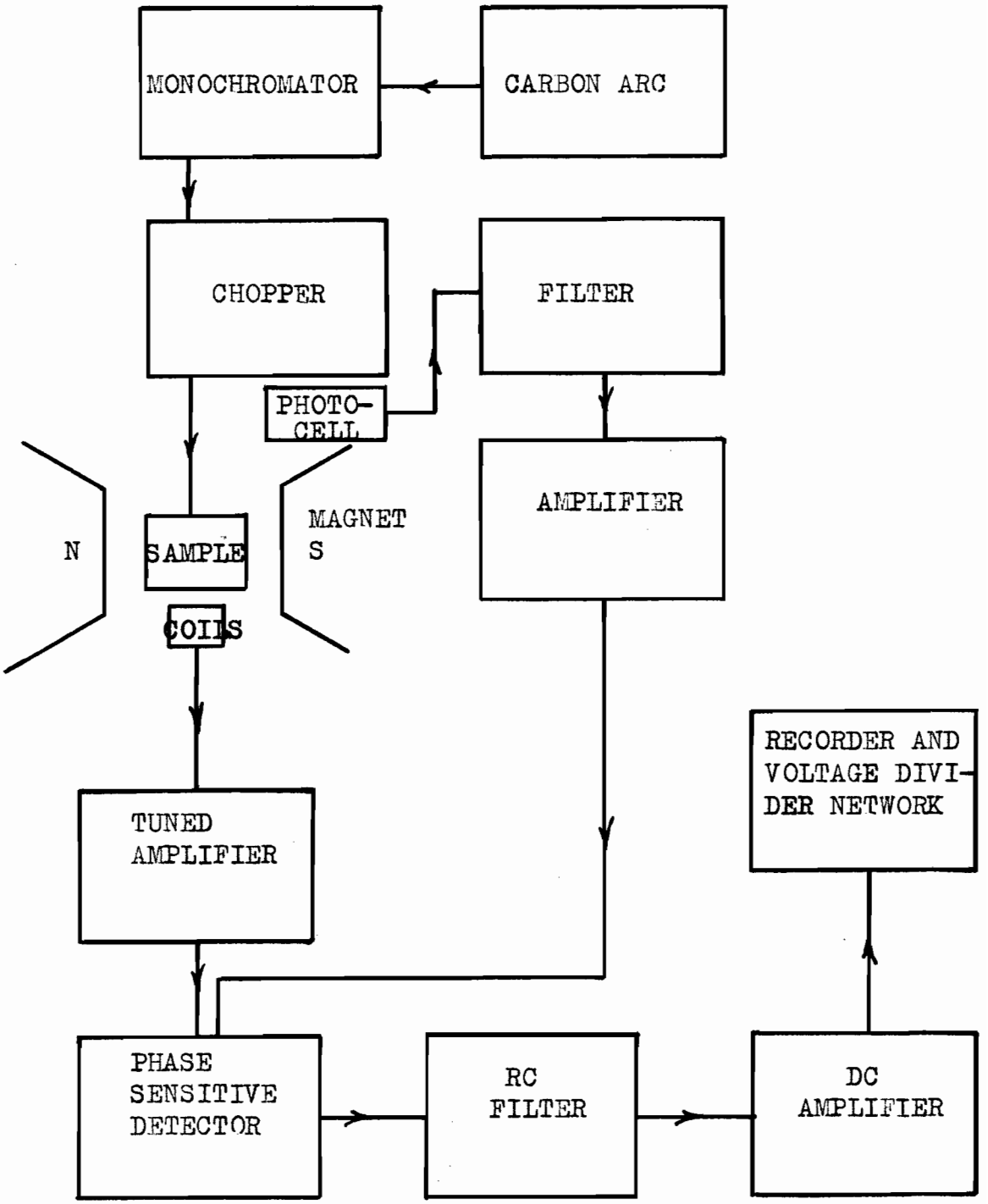

Fig. 1-1 Block Diagram of Apparatus-System

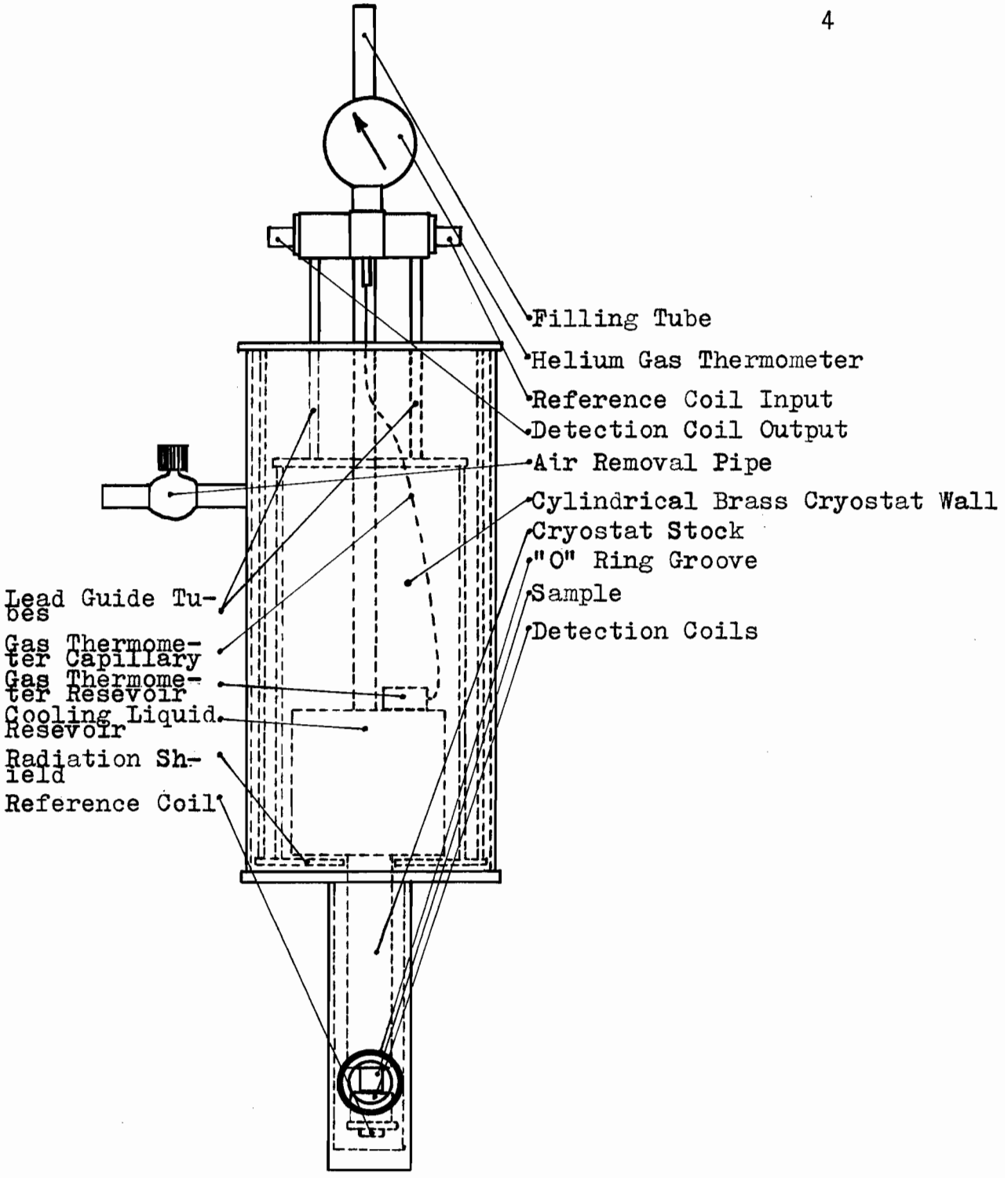

Fig. 1-2 Schematic of Cryostat

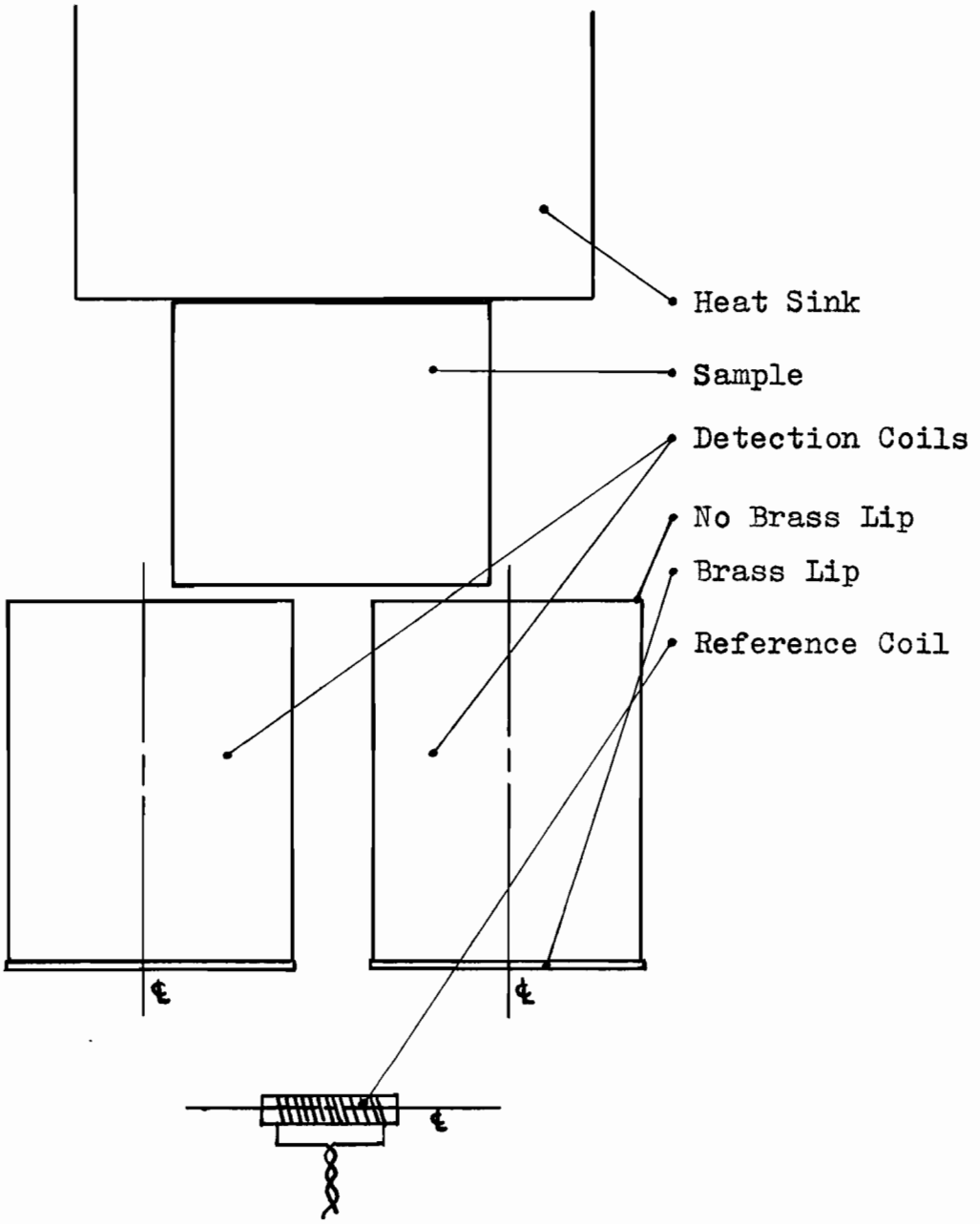

Fig. 1-3 Schematic of Sample, Coils, and Reference Coil

currents generated in the brass lip of the spool would magnetically shield the coil, with a subsequent loss in sensitivity. The coils were connected in parallel opposition. The advantage of this arrangement was that spurious signals due to stray magnetic fields and mechanical vibrations were minimized.

The cryostat was clamped firmly between the pole pieces of a Newport Instruments Magnet in order that there be no spurious signal generated as a result of the motion of the coils in the magnetic field. The entire magnet was mounted on a vibration isolating system tuned to 2 c.p.s..

Chopped light was guided onto the sample by means of a length of square copper tubing the inside of which had been polished (dimensions 3/8" by 3/8" by 12").

The light from the carbon arc source was chopped by means of a rotating disc in which radial slits had been etched. The source of light for the sample was a 1600 watt Leiss carbon arc lamp. For direct illumination of the sample by the carbon arc the glass lens of the lamp was in place. If the lamp was used in conjunction with the Leiss monochromator the lens of the carbon arc lamp was removed.

The monochromator was equipped with a sodium chloride prism.

The source of power for the carbon arc lamp was twelve, twelve volt automobile batteries connected in series.

The source of power for the Newport magnet was twelve, twelve volt automobile batteries connected in series, providing a maximum field of 6000 oersteds.

The power for the lamp and the magnet was supplied by batteries rather than AC rectified power supplies in order to avoid spurious signals which might have arisen due to AC ripple. A battery charger was provided so that the magnet power source and the lamp power source could be charged individually.

The electronics of the measuring system was relatively straightforward. The central part of the system was a phase sensitive detector. The timing signal for the phase sensitive detector was generated by a photocell having as its source of light a flashlight lamp arranged at another position along the sectored disc of the chopper. The power source for the photocell lamp was a six volt automobile battery. The signal from the photocell was filtered, amplified and then supplied to the reference terminals of the phase sensitive detector.

The signal from the detection coils was placed on the input terminals of a narrow band, high gain, tuned amplifier, the output of which supplied the input of the phase sensitive detector.

The DC output from the phase sensitive detector was put through a low pass filter, and then amplified. The

signal from the DC amplifier supplied a voltage divider network, the output of which drove a chart recorder. Table 1-1 gives the important instruments and their manufacturer.

Table 1-1 Important Component Instruments and their Manufacturer

Instrument	Manufacturer	Model
Recorder (Speedomax)	Leeds and Northrup	Type G
DC Amplifier	General Radio	
Low Pass Filter	Carbon Resistor in series with General Radio decade Capacitance	
Phase Sensitive Detector	Industrial Test Equip. Co.	100AH
Unit Amplifier & Power Supply	General Radio	1206-B
Band Pass Filter	Krohn-Hite Corporation	330 M
Photocell	RCA	5583
Magnet	Newport Instruments	
Magnet Supply	12, 12 volt storage batteries	
Tuned Amplifier & Null Detector	General Radio	1232-A
Carbon Arc Lamp	Carl Zeiss, Germany	
Oscilloscope	Allen B. Dument Laboratories	304-A
Battery Charger	Made in Shop	
Monochromator	Leiss, Germany	
Carbon Arc Lamp Supply	12, 12 volt storage batteries	

CHAPTER II

THEORY

2.1 Magnetism

If a magnetic field is applied to a sample of solid material, there is induced in the sample a macroscopic magnetic moment[4] given by the relation

$$\underline{M} = \chi \underline{H} \qquad (2\text{-}1)$$

where $\underline{M}$ is the magnetic moment induced in the sample of volume V, χ the magnetic susceptibility for the same volume, and $\underline{H}$ the applied magnetic field.

All materials possess a magnetic susceptibility[5] although in the majority of them it is of a very small magnitude compared to the ferromagnetic substances.

Most materials are diamagnetic, that is, the magnetic susceptibility is negative. A smaller number of materials such as the transition elements, rare earths, actinide elements, and others are paramagnetic, and for these materials the magnetic susceptibility is positive.

If a paramagnetic solid is illuminated with microwave radiation causing a change in the population distribution of the magnetic energy levels, then a change in the magnetic moment results. Analagous to this situation is the one in which a semiconductor material is illuminated with light in the optical region. It could be hoped to

observe the Landau diamagnetism of photogenerated electrons, or the diamagnetism of photogenerated excitons.

Any change in the magnetic susceptibility of a sample which can be attributed to the illumination of the sample with optical radiation is termed the photomagnetic susceptibility.

2.2 Semiconductor Absorption

Peierls[6] showed first that the optical absorption spectrum of an ideal insulating crystal in which the atoms are supposedly fixed in their mean positions would be similar to that of a vapour of free atoms. It consists of a series of sharp lines leading up to a series limit, beyond which there will be a continuous absorption band. In this respect the absorption spectrum of a non-metal is in sharp contrast to that of a metal, which consists of continuous bands only.

The reason for absorption bands is as follows. If the quantum of light has sufficient energy, a free hole and electron will be produced and they will move through the crystal independently. Sometimes, however, the quantum of energy is not sufficient to completely separate the hole electron pair. In the field of any positive charge there will exist a series of stationary, bound states for an electron, leading up to a series limit. The electron and hole may move through the crystal, or may be at rest. An electron and positive hole coupled in this way have been

called by Frenkel an 'exciton'.

For a crystal as a whole, each state of excitation of the exciton gives rise to a band of energy levels.

Suppose the limits of the energy bands plotted in $\underline{k}$ space are as shown in Figure 2-1a.[7] As can be seen, if the conduction band minimum and the valence band maximum occur at $\underline{k} = 0$ then the absorption edge occurs at $h\nu = E_g$; where E_g is the minimum width of the forbidden zone or activation energy of the semiconductor. Theoretically only 'vertical' transitions are allowed, that is electrons with a given wave number in a particular band can only make transitions to a state in a higher band having the same wave number. In practice 'nonvertical' transitions are observed but with diminished intensity. In the case of Figure 2-1a the absorption would cease more or less abruptly for $h\nu = E_g$.

It is possible for the maximum of the valence band and the minimum of the conduction band to occur at different points in $\underline{k}$ space as illustrated in Figure 2-1b. The intense absorption will cease for this case for a value of $E' = h\nu$ but less intense absorption will continue down to $E_g = h\nu$.

The absorption spectrum of a non-metal consists then of lines, broadened by the effect of lattice

vibrations, leading up to a series limit beyond which there is true continuous absorption.

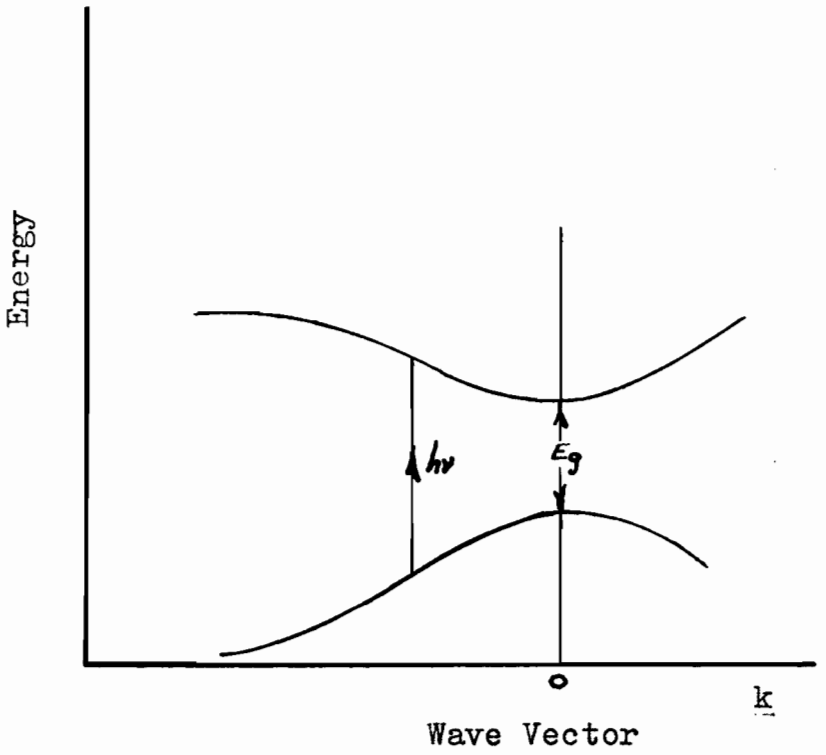

Figure 2-1a

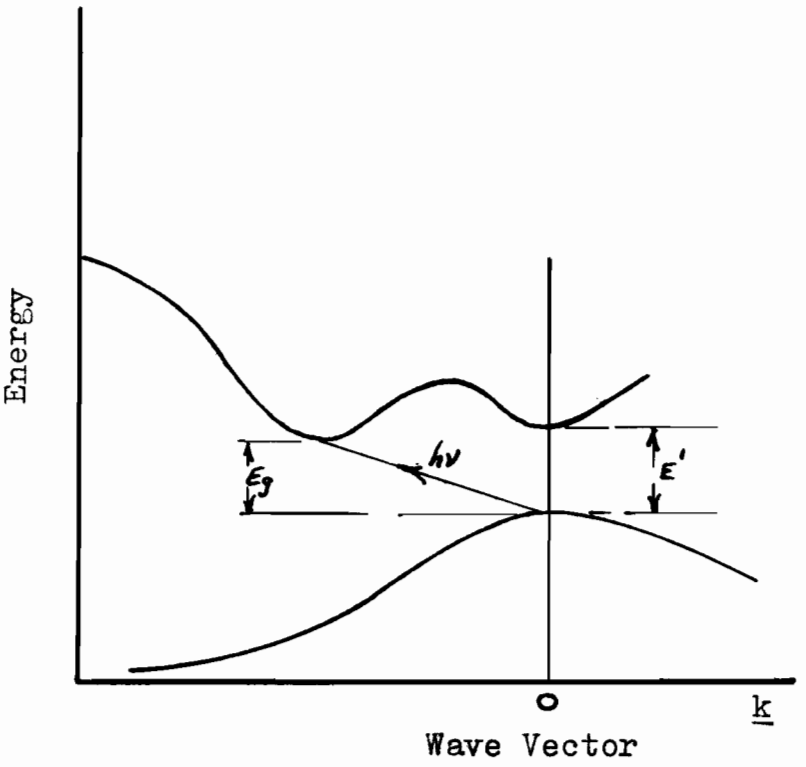

Figure 2-1b

2.3 Photomagnetism

The magnetic susceptibility χ of a semiconductor is due to several components: lattice impurities, bound carriers, and free carriers. By illuminating an 'intrinsic' semiconductor with light it would be hoped to change the numbers of carriers both bound and free. Hence, the following sources might contribute to a light generated magnetic susceptibility (photomagnetic susceptibility); excitons,[8] and free carriers.

Signals may be produced which fall into the category of photo-electric-magnetic effects,[9] which arise as a result of the interaction of the primary diffusion currents with the magnetic field. These signals can be eliminated by uniformly illuminating the specimen along the direction of the magnetic field. However, in this apparatus-system provision has not been made for the elimination of such signals.

2.4 Magnetic Susceptibility of Charge Carriers

Busch and Mooser[10] have shown that for an intrinsic semiconductor the magnetic susceptibility can be divided into two contributions, namely the susceptibility χ_c of charge carriers and the susceptibility χ_l of the lattice. Therefore the magnetic susceptibility may be written $\chi = \chi_l + \chi_c$. Busch and Mooser calculated the intrinsic

charge carrier contribution χ_c using Pauli's results for the spin paramagnetism and the Landau-Peierels expression for the diamagnetism of nearly free electrons. Therefore, the intrinsic charge carrier susceptibility can be written as

$$\chi_c = \frac{u^2 n_i}{3kT'}\left[6 - \left(\frac{\overline{m}}{m_n}\right)^2 - \left(\frac{\overline{m}}{m_p}\right)^2\right] \qquad (2\text{-}2)$$

where n_i is the intrinsic concentration, u the Bohr Magneton, T' the absolute temperature, k Boltzmann constant. The factors $\left(\frac{\overline{m}}{m_{n,p}}\right)^2$ are suitable averages over the effective masses which are independent of temperature. The carrier density n_i is given by

$$n_i = 2\left(\frac{2\pi kT'}{h^2}\right)^{3/2}(m_n \cdot m_p)^{3/4} N^{1/2} e^{-\frac{E_g}{2kT'}} \qquad (2\text{-}3)$$

where E_g is the energy gap of the semiconductor, and N the number of ellipsoids by which the conduction band edge can be represented.

When light is shone on a semiconductor the number of free electrons and holes increases. In the calculation which follows the quantity n_i will be replaced by the number of electrons injected into the conduction band by the incident radiation.

2-5 Light Sensitivity Calculation

The object of this calculation is to obtain an estimate of the magnitude of the photomagnetism which would result in a sample of germanium from the generation of free carriers by optical radiation.

The magnetic field and light direction are mutually perpendicular and are oriented with respect to the sample and coils as shown in the schematic diagram (Figure 2-2).

Assume the lamp, chopper, guide tube, and sample to be arranged as indicated in the schematic diagram (Figure 2-3).

The solid angle subtended at the arc by the sample is effectively that subtended by the lamp lens at the arc. If A is the area of the lamp lens, and R' the radius of the sphere which passes through the periphery of the lens, then the approximate solid angle subtended by the lens at the arc is A/R'^2.

If Q is the power supplied to the lamp by the batteries, A' the cross sectional area of the light guide tube, v' the efficiency with which thebattery energy is converted into radiation by the arc, and the efficiency with which the arc lens transmits the energy incident on its surface, v" the efficiency with which the lens, chopper, and guide tube place the energy on the sample, then the

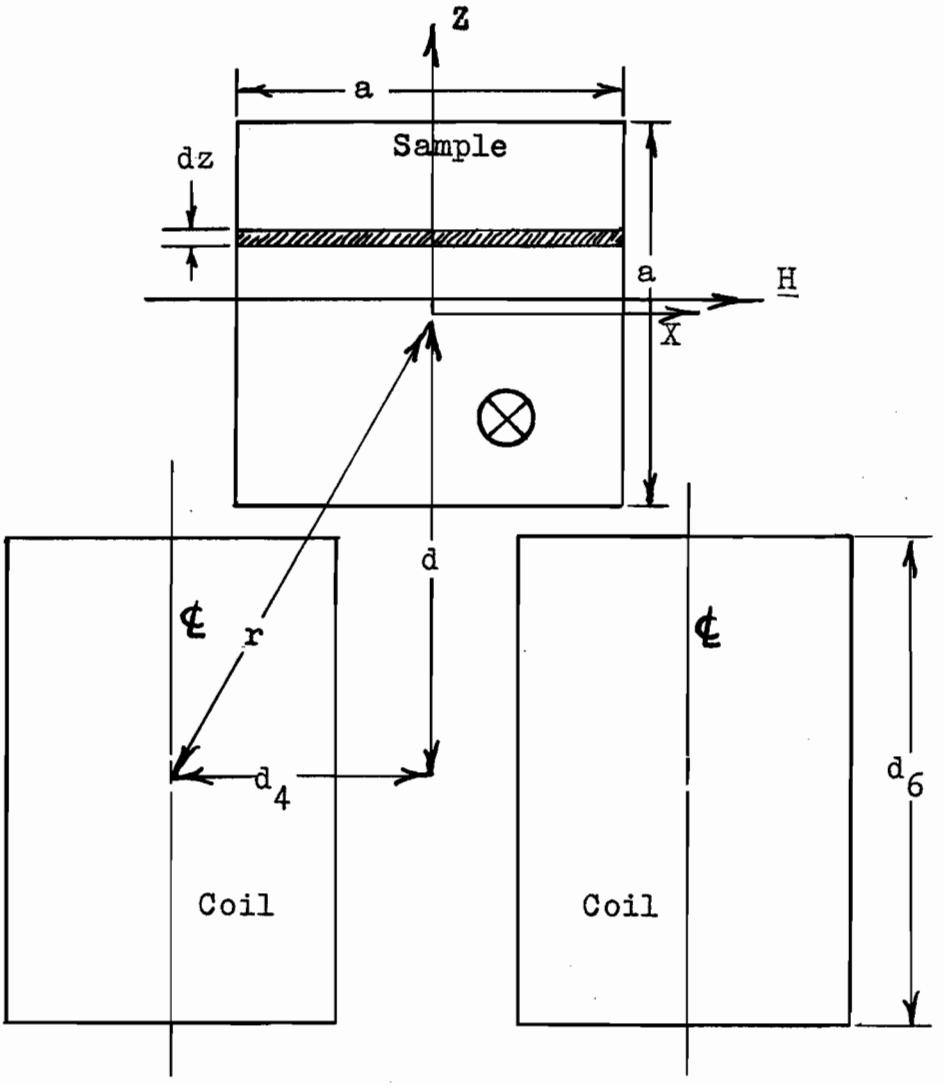

⊗ Direction of Illumination into Page

Figure 2-2 Orientation of Magnetic Field and Incident Light with respect to Sample and Coils

Figure 2-3 Schematic of Optical Arrangement for Light Sensitivity Calculation

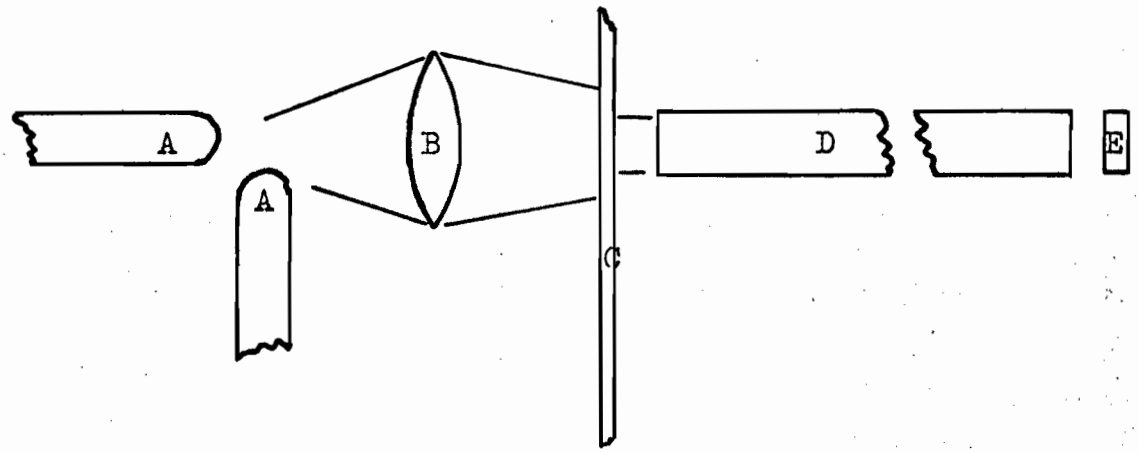

A Carbon Arc
B Lens of Carbon Arc
C Chopper
D Light Guide Tube
E Sample

incident power on the sample per unit area is $QAv'v''/4\pi R'^2 A'$.

If the relative amount of energy radiated by the lamp between the wave lengths λ and $\lambda + d\lambda$ is $g(\lambda)d\lambda$ (Figure 5-15), then the number of photons $n(\lambda)$ at any λ incident on the sample per unit area, per unit time is

$$n(\lambda) = \frac{QAv'v'' g(\lambda) d\lambda}{4\pi R'^2 A' h\nu} \qquad (2\text{-}4)$$

where ν is the frequency of the photon.

The energy from the lamp arrives at the sample perpendicular to the surface.

Let the refractive index of air be $N_0 = 1$, and the complex refractive index of the germanium sample be $N^1 = n^1 - ik^1$, then the number of photons for a given λ transmitted through the air germanium interface is

$$n(\lambda) \frac{4n'}{(n'+1)^2 + K'^2}$$

For semiconductors in the majority of cases of interest, n^1 is several times unity while k^1 is unity or less. Hence $n'^2 >> K'^2$. The number of photons of wavelength λ entering the germanium example is then approximately

$$n(\lambda) \frac{4n'}{(n'+1)^2}$$

The quantity n^1 depends on wavelength but in this calculation this variation is ignored, and the value of n^1 used is the zero frequency value.

Since a semiconductor is partially conducting the energy transmitted through the surface falls off exponentially. The number of photons of frequency ν absorbed at a distance y from the surface of the sample is

$$\frac{4n'}{(n'+1)^2}\frac{4\pi\nu k'}{c} e^{-\frac{4\pi\nu k' y}{c}} dy\, n(\lambda)$$

where $k' = \sqrt{\frac{\epsilon}{2}}\left[1-\left(1+\frac{\sigma^2}{\omega^2\epsilon^2\epsilon_0^2}\right)^{1/2}\right]^{1/2}$

ϵ_0 is the dielectric constant of free space, ϵ the dielectric constant of the semiconductor material, $\omega = 2\pi\nu$, σ the semiconductor conductivity at the optical frequency concerned.

The quantum efficiency (the number of hole electron pairs created per photon) in the optical and infrared regions is $\simeq 1$. Hence, the number of hole electron pairs produced at a distance y for a volume element a^2 dy is

$$\frac{a^2}{(n'+1)^2}\frac{4n'}{c}\frac{4\pi\nu k'}{c} e^{-\frac{4\pi\nu k' y}{c}} dy\, n(\lambda) \qquad (2\text{-}5)$$

The number of hole electron pairs I_{max} generated throughout a sample of thickness b then is

$$I_{max} = \frac{Q A \nu' \nu''}{4\pi R'^2 A'}\frac{4n'}{(n'+1)^2}\frac{4\pi a^2}{hc}\int_{\lambda_{gap}}^{\lambda_{max}}\int_{y=0}^{y=b} k' e^{-\frac{4\pi\nu k' y}{c}} g(\lambda)\, d\lambda\, dy \qquad (2\text{-}6a)$$

The symbol λ_{gap} is the wavelength corresponding to the energy gap E_g of the semiconductor, and λ_{min} to the highest energy photon incident on the sample.

This expression assumes that there is no carrier re-combination; this is taken into account now. Let n_i be the number of hole electron pairs present in the sample at any instant, τ the free carrier life time, and I the number of hole electron pairs formed per second, then dn_i/dt is given by

$$\frac{dn_i}{dt} = I - \frac{n_i}{\tau}$$

If I is caused to vary periodically with time such that $I = I_{max}\cos\omega' t$, then $n_i = \frac{\tau I_{max}}{\sqrt{1+\omega'^2\tau^2}} \cos(\omega' t - \theta')$

where $\theta' = \sin^{-1} \frac{\omega'\tau}{\sqrt{1+\omega'^2\tau^2}}$

The photomagnetic susceptibility of the sample due to photogencrated free carriers then is given by (using equation 2-2)

$$\chi_{sample} = \frac{\tau}{\sqrt{1+\omega'^2\tau^2}} \cos(\omega t - \theta') \frac{Q A \nu' \nu'' 4n' 4\pi a^2 (\text{times})}{4\pi R'^2 A' (n'+1)^2 hc}$$

$$\frac{\mu^2}{3kT'}\left[6 - \left(\frac{\bar{m}}{m_n}\right)^2 - \left(\frac{\bar{m}}{m_p}\right)^2\right] \int_{\lambda_{gap}}^{\lambda_{min}} \int_{y=0}^{y=b} \kappa' e^{-\frac{4\pi\nu k' y}{c}} g(\lambda)\, d\lambda\, dy$$

The photomagnetic moment of a sample of dimensions a by a by b due to photogenerated free hole electron pairs is then

$$M_{sample} = \chi_{sample} H \qquad (2\text{-}7)$$

The carbon arc energy spectrum curve can be described reasonably well by a curve characteristic of the energy spectrum of a black body. Such a curve[12] is given by

$$W_{B\lambda}\, d\lambda = \frac{c_1}{\lambda^5}\left(e^{c_2/\lambda T}-1\right)^{-1} d\lambda$$

where $W_{B\lambda}\, d\lambda$ denotes the emission of unpolarized radiation per square cm., per second in all directions in a range $d\lambda$, $c_1 = 3.7413 \times 10^{-5}$ ergcm^{2}sec^{-1}, $c_2 = 1.4388$ cmdeg., λ the wavelength, T absolute temperature in degrees Kelvin. If $W_{B\lambda}$ is the total energy in ergs emitted from the surface of a black body per square cm., per second, the Stefan-Boltzmann law states that $W_{B\lambda} = \sigma T^4$ where $\sigma = 5.669 \times 10^{-5}$ ergcm^{-2}sec^{-1} K^{-4}. The wavelength of the maximum of each curve λ_{max} depends on temperature according to Wien's displacement law, which states that $\lambda_{max} T = 0.2898$cmdeg.. The carbon arc energy spectrum peaks at 1.5 microns. Therefore the effective temperature of the carbon arc is 1,920 °K.

The quantity $g(\lambda)$ in formula 2-6b can be replaced by

$$g(\lambda) = \frac{c_1}{\sigma T^4 \lambda^5}\left(e^{c_2/\lambda T}-1\right)^{-1} \qquad (2\text{-}8)$$

Substituting the expression for g (λ) (2-8) into equation 2-6b and integrating with respect to y gives the following expression for the photomagnetic susceptibility

$$\chi_{\text{sample}} = \frac{\tau}{\sqrt{1+\omega'^2\tau^2}} \cos(\omega' t - \theta') \frac{Q A v' v'' 4n'}{4\pi R'^2 A' (n'+1)^2} \frac{a^2}{hc} \text{(times)}$$

$$\frac{u^2}{3kT'}\left[6-\left(\frac{m_n}{m_n}\right)^2-\left(\frac{m_n}{m_p}\right)^2\right]\frac{C_1}{6T^4}\int_{\lambda_{gap}}^{\lambda_{min}} \frac{\left(1-e^{-\frac{6\pi\nu k'}{c}}\right)}{\left(e^{c_2/\lambda T}-1\right)\lambda^4}\, d\lambda \qquad (2\text{-}9)$$

At room temperature $k' \simeq 10^4/4\pi\nu$ for germanium, hence the term $\exp\left(-\frac{6\pi\nu k'}{c}\right)$ is negligible and can be ignored.

For wavelengths < 1.5 micron $\exp\left(c_2/\lambda T\right) \gg 1$, therefore $\left(\exp\left(c_2/\lambda T\right) - 1\right)$ can be replaced by $\exp\left(c_2/\lambda T\right)$ alone. The integral in equation 2-9 simplifies to

$$\int_{\lambda_{gap}}^{\lambda_{min}} \left(\frac{1}{\lambda^4}\right) \exp\left(-c_2/\lambda T\right) d\lambda \,.$$

The energy gap of germanium at room temperature corresponds to a wavelength of 1.5 micron (0.81 eV).

The factors v' and v" are rather arbitrary and their numerical value is at best an informed guess. It is assumed that the efficiency with which the carbon arc converts the power available to it to radiation, and the efficiency with which the lens transmits the energy incident on its surface is 50%; hence v' = 0.5. The factor v" was arrived at in the following way. The carbon arc can focus the energy landing on its lens into an area of 0.44 in.^{2}. The area of the chopper baffle opening is 0.12 in.^{2}. The factor v" was assumed to have a value of 0.12/0.44 or approximately 0.3.

The photomagnetic susceptibility for a sample of intrinsic germanium of dimensions 3/8" by 3/8" by 1/4" at

room temperature is from formula 2-9, $-5.6X10^{-10}$ amp^{2}m^4/ joule. The magnetic moment for a magnetic field of 6000 oersteds is from formula 2-7, $-4.2X10^{-16}$ wm.

The relevent quantities and their values used in this calculation are tabulated in section 5.4 of the appendix.

2.6 Theory of Detection

Q (Figure 2-4) is a sample of magnetized material and as such each of its elemental parts possesses a small magnetic moment $d\underline{m}$. The magnetic potential[13][14] at a point of observation P(x',y',z') is

$$\phi(x',y',z') = -\frac{1}{4\pi}\int_V d\underline{m}\cdot\underline{\nabla}'(1/r) \qquad (2\text{-}10)$$

where the integration is performed over the volume of the sample Q. The magnetic induction $\underline{B}$ at the point of observation P(x',y',z') is

$$\underline{B}(x',y',z') = \frac{1}{4\pi}\underline{\nabla}'\int_V d\underline{m}\cdot\underline{\nabla}'(1/r) \qquad (2\text{-}11)$$

The ' implies that the differentiation is with respect to the point of observation P(x',y',z').

If the point of observation is sufficiently remote from the sample Q such that r is essentially constant during integration, then equations 2-10 and 2-11 become

$$\phi(x',y',z') \quad -\frac{1}{4\pi}\underline{M}\cdot\underline{\nabla}'(1/r) \qquad (2\text{-}12)$$

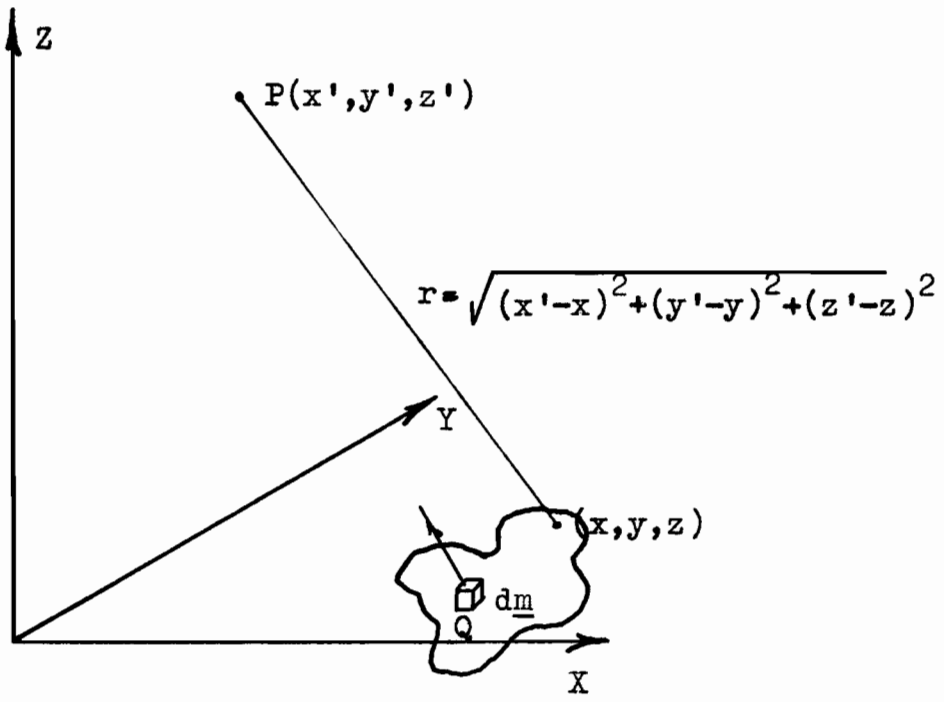

Figure 2-4

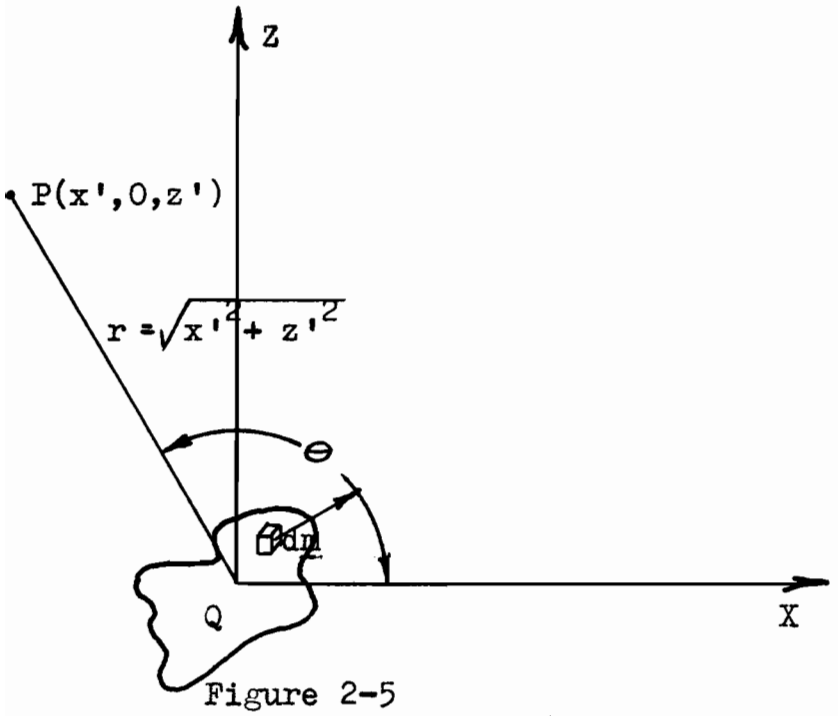

Figure 2-5

Fig. 2-6 Schematic of Magnetic Induction Pattern for Constant B''_z

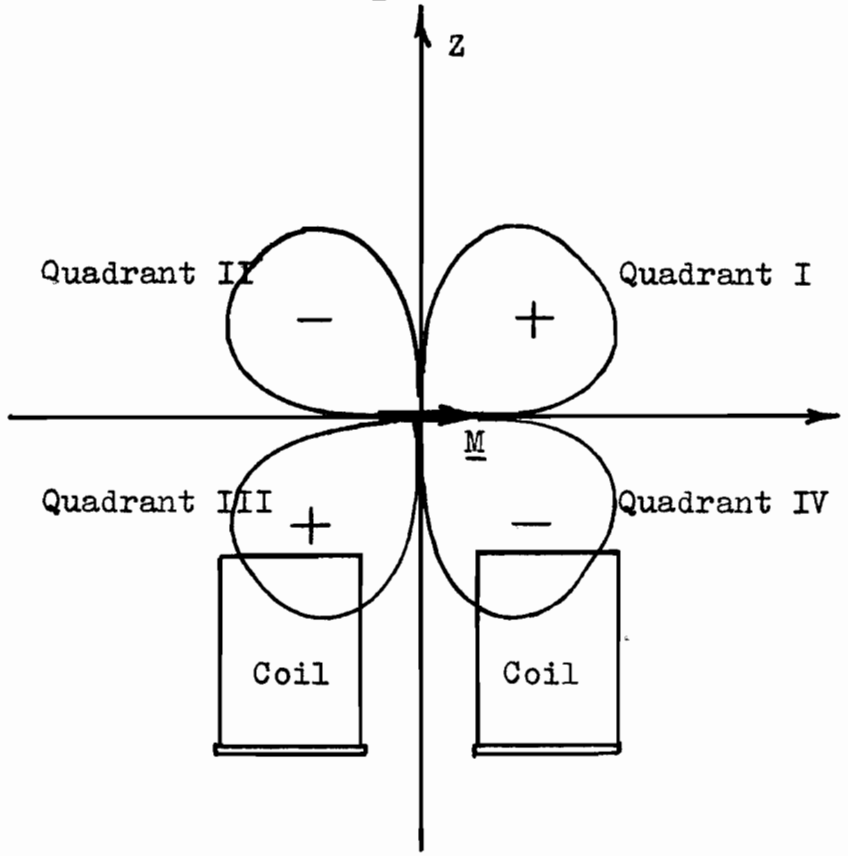

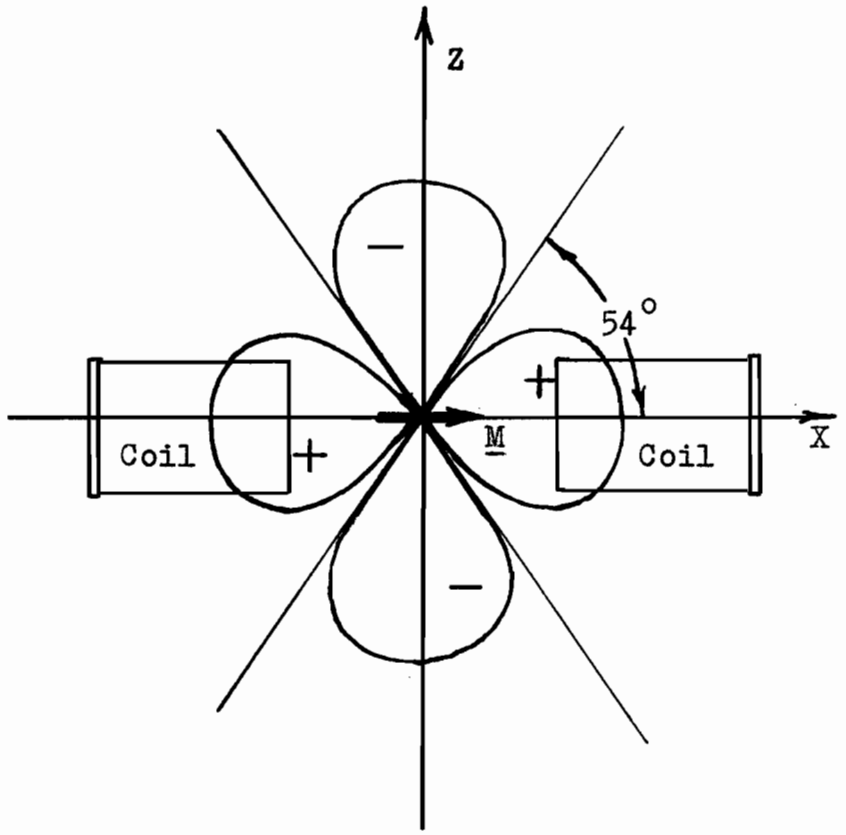

Fig. 2-7 Schematic of Magnetic Induction Pattern for Constant B''_x

and

$$\underline{B}(x',y',z') = \frac{1}{4\pi} \underline{\nabla}' \left[\underline{M} \cdot \underline{\nabla}' (1/r) \right] \tag{2-13}$$

where $\underline{M}$ is the total magnetic moment of the sample.

If the magnetic moment $\underline{M}$ is caused to vary periodically with time by some means such that

$$\underline{M} = \underline{M}_o + \underline{m}_o \exp(i\omega' t) \tag{2-14}$$

then 2-13 can be rewritten

$$\underline{B}(x',y',z't) = \frac{1}{4\pi} \underline{\nabla}' \left\{ \left[\underline{M}_o + \underline{m}_o \exp(i\omega' t) \right] \cdot \underline{\nabla}' (1/r) \right\} \tag{2-15}$$

Since it is only the time dependent part which can be detected, the useful part of 2-15 is

$$\underline{B}'(x',y',z',t) = \frac{1}{4\pi} \underline{\nabla}' \left[\underline{m}_o \cdot \underline{\nabla}' (1/r) \right] \exp(i\omega' t) \tag{2-16}$$

If the sample of magnetized material is placed at the origin of coordinates (Figure 2-5) and the part of $\underline{B}'$, which has as its source the x component of $\underline{m}_o$, is examined in the xz plane then 2-16 becomes simply

$$\underline{B}'(x',y',z',t) = \left[-\frac{i}{4\pi} |\underline{m}_{ox}| \left(\frac{1}{r^3} - \frac{3x'^2}{r^5} \right) + \frac{\underline{k}}{4\pi} |\underline{m}_{ox}| \left(\frac{3z'x'}{r^5} \right) \right] e^{i\omega' t} \tag{2-17}$$

The detection coils in the apparatus-system of this experiment were arranged so as to respond principally to the $\underline{k}$ component of 2-17 (see Figure 2-6); hence the applicable part of 2-17 is

$$\underline{B}''_z(x',z',t) = \frac{\underline{k}}{4\pi} |\underline{m}_{ox}| \left(\frac{3z'x'}{r^5} \right) \exp(i\omega' t) \tag{2-18}$$

In polar coordinates this becomes

$$\underline{B}''_z(r,\theta,t) = \underline{k}|\underline{m}_{ox}| \frac{3\sin 2\theta}{8\pi r^3} \exp(i\omega' t) \qquad (2\text{-}19)$$

or if

$$B''_z = |\underline{m}_{ox}| \frac{3\sin 2\theta}{8\pi r^3} \qquad (2\text{-}20)$$

becomes

$$\underline{B}''_z(r,\theta,t) = \underline{k}B''_z \exp(i\omega' t) \qquad (2\text{-}21)$$

A plot of B''_z in the xz plane for constant B''_z is as in Figure 2-6.

If we consider the source of the magnetic moment to be small in spatial extent compared to the distance to the detection coils, and consider the turns of the coils to be concentrated at their geometrical centres then the flux linkages for one coil are given by

$$\phi(\text{ one coil }) = 3|\underline{m}_{ox}| \frac{\sin 2\theta A_c N_c}{8\pi r^3} \exp(i\omega' t) \qquad (2\text{-}22)$$

A_c is the cross sectional area for a coil, and the radius used in the calculation is the average radius $(r_1 + r_2)/2$ (see Figure 3-15 for r_1 and r_2). N_c is the number of turns on a single coil.

The voltage induced in one coil is given by

$$\mathcal{E} = -d\phi/dt \qquad (2\text{-}23)$$

As can be seen from Figure 2-6 the direction of B''_z in the I and III quadrants is opposite to that in the II

and IV quadrants. If two coils wound in the same manner are to respond to the magnetic induction pattern as given in Figure 2-6 they must be connected in opposition. Assuming a coil configuration as shown in Figure 2-6 the formula for the induced voltage appearing between the terminals of the two coils connected in parallel opposition is then

$$\mathcal{E} = -\frac{3i\omega' |\underline{m}_o| \sin 2\theta A_c N_c}{8\pi r^3} \exp(i\omega' t) \qquad (2\text{-}24)$$

where $\mathcal{E}$ is the signal in r.m.s. volts, ω' the frequency of oscillating magnetic dipole, θ and r polar coordinates of the geometrical centre of one of the detection coils.

If the variational part of the magnetic moment, namely $\underline{m}_o \exp(i\omega' t)$, makes angles ϕ and β with the xy plane and x axis respectively, then equation 2-24 can be rewritten as

$$\mathcal{E} = -\frac{3i\omega' \sin 2\theta A_c N_c |\underline{m}_o|}{8\pi r^3} \cos\phi \cos\beta \exp(i\omega' t) \qquad (2\text{-}25)$$

In Chapter III dealing with measurements and their interpretation formula 2-25 is refined to take into account the fact that the coils have a finite size.

Other coil arrangements are possible. The $\underline{i}$ component of $\underline{B}'(x',y',z')$ in equation 2-17 is

$$B''_x = -\frac{|\underline{m}_o|}{4\pi} (1/r^3 - 3x'^2/r^5) \qquad (2\text{-}26)$$

This can be transformed into polar coordinates which gives

$$B''_x = -\frac{|\underline{m}|\alpha_x}{4\pi r^3}(1 - 3\cos^2\theta) \qquad (2\text{-}27)$$

A plot of constant B''_x gives a picture as shown in Figure 2-7. The B''_x component can be detected by two coils similarily wound and connected in parallel aiding if they are arranged with respect to the dipole as shown in Figure 2-7.

It is to be further noted that the coil arrangement previously discussed will not respond to the magnetic induction pattern as shown in Figure 2-7.

The coil configuration as shown in Figure 2-6 was used rather than the one shown in Figure 2-7, since, if the coils are connected in parallel opposition spurious signals resulting from stray magnetic fields are very small if not eliminated completely.

Other interesting situations arise when the magnetic dipole is physically vibrated with respect to the detection coils. These situations are explored further in section 5.2 of the appendix.

2.7 Bandwidth of Detection System

The bandwidth of a detection system is usually taken as the frequency band between the half power points (Figure 2-8). A signal at a frequency outside this band is

tramsmitted with less than one half the output power of a signal of similar strength at the resonant frequency.

The bandwidth and shape of the low pass filter circuit is important in determining the performance of the system. The narrower the pass band, the smaller the fluctuations in the pen recorder. However, the narrowing can only be accomplished at the expense of a sluggish recorder with the result that a long observation time is needed.

After detection by the small coils the bandwidth is narrowed to about 45 c.p.s. by the tuned amplifier ($Q_{effective} = f/\Delta f = 1000/45 = 22$). The bandwidth is further narrowed in the next stage which is the phase sensitive detector in conjunction with the low pass filter.

The multiplier output of the phase sensitive detector is proportional to the instantaneous product of the input signal and the reference signal. The meter of the phase sensitive detector accepts the output of the multiplier and produces a deflection D_m proportional to the time average product of the input signal and the reference signal or

$$D_m = \frac{k}{T}\int_o^T V_s \cdot V_r \, dt \qquad (2\text{-}28)$$

where k is a constant, T the period of a cycle.

Suppose that the detected signal V_s differs from the reference signal frequency by Δf, hence if

$$V_r = B\sin\omega' t \qquad (2\text{-}29a)$$

$$V_s = A\sin\left[(\omega' + \Delta\omega')t + \theta\right] \tag{2-29b}$$

$$\Delta\omega' = 2\pi\Delta f \tag{2-29c}$$

then

$$D_m = \frac{k}{T}\int_0^T AB\sin\omega' t \sin\left[(\omega' + \Delta\omega')t + \theta\right] dt \tag{2-30}$$

Now if it is assumed $\Delta\omega'$ is very small, i.e., $\Delta\omega' \ll \omega'$ then

$$D_m = \frac{kAB}{2}\cos(\Delta\omega' t + \theta) \tag{2-31}$$

As can be seen the meter needle of the phase sensitive detector will oscillate slowly with a frequency $\frac{\Delta\omega'}{2\pi}$. If the detected and reference signal are of the same frequency, as is the desired case 2-31 becomes

$$D_m = \frac{kAB}{2}\cos\theta \tag{2-32}$$

Therefore the meter deflection is proportional to the in-phase component of the detected signal.

A phase shifter is incorporated into the phase sensitive detector to change the phase of the detected signal by 90 degrees. When the phase shifter is introduced into the circuit equation 2-29b becomes

$$V_s = A\sin\left[(\omega' + \Delta\omega')t + \theta - 90^\circ\right] \tag{2-33}$$

By a similar argument the meter deflection is

$$D'_m = \frac{kAB}{2}\sin(\Delta\omega' t + \theta) \tag{2-34}$$

If the frequency of the detected signal and the reference signal are the same, then

$$D'_m = \frac{kAB}{2}\sin\theta \tag{2-35}$$

Hence, the meter output is proportional to the quadrature

component of the detected signal.

Suppose a small signal V_{in} as described in equation 2-31 is placed on the low pass filter input terminals. Then

$$V_{in} = \frac{kAB}{2} \cos(\Delta\omega' t + \theta) \tag{2-36}$$

The network and component values of the low pass filter are indicated in Figure 2-9. The input impedance of the RC filter and DC amplifier is then

$$Z_{in} = R_1 + (R_2 / 1 + j\Delta\omega' CR)$$

If V_{IN} is the signal into the low pass filter (RC filter) then the voltage V_c across the capacitor is

$$V_C = V_{in} / (1 + \frac{R_1}{R_2} + j\Delta\omega' C R_1) \tag{2-37}$$

Since $R_2 >> R_1$, then

$$V_c \simeq V_{in} / (1 + j\Delta\omega' C R_1) \tag{2-38a}$$

or

$$V_c \simeq \frac{kAB \cos(\Delta\omega' t + \theta)}{2\sqrt{1+\Delta\omega'^2 C^2 R_1^2}} \exp(-j\theta_1) \tag{2-38b}$$

where

$$\theta_1 = \tan^{-1} \Delta\omega' C R_1 \tag{2-38c}$$

Equation 2-38b can be rewritten as

$$V_c \simeq \frac{kAB \cos(\Delta\omega' t + \theta - \theta_1)}{2\sqrt{1+\Delta\omega'^2 C^2 R_1^2}} \tag{2-38d}$$

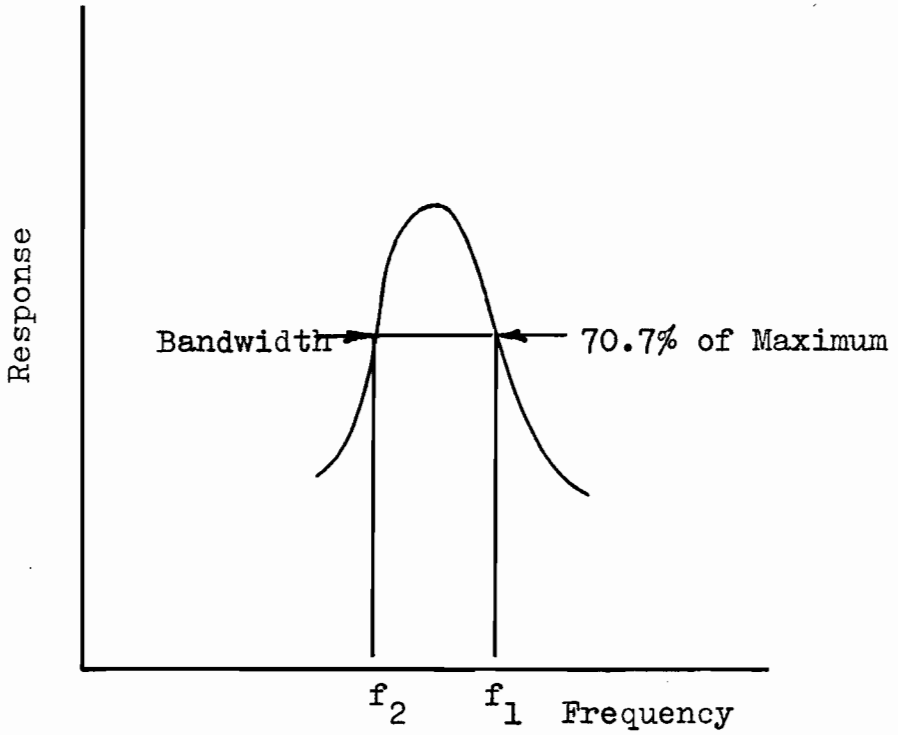

Figure 2-8 "Half Power" Frequencies

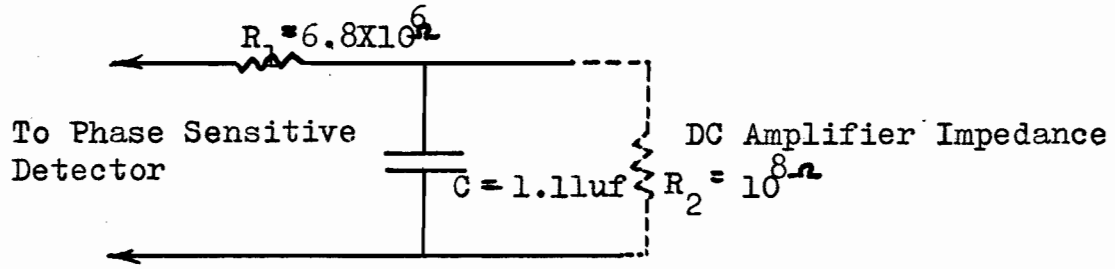

Figure 2-9 Low Pass (RC) Filter Circuit

The half power point occurs when

$$\Delta\omega' C R_1 = 1 \qquad (2\text{-}39)$$

For $R_1 = 6.8 \times 10^6 \Omega$ and C = 1.11uf then $\Delta\omega' = |\omega'_{sig} - \omega_{ref}| \simeq 0.13$ rad/sec, or $\Delta f \simeq 0.021$ c.p.s. ($Q_{effective} = 1000/0.021 = 4.7 \times 10^4$).

Equation 2-39 is but another example of the applicability of the uncertainty principle. The uncertainty principle states that the order of magnitude of the product of the uncertainties in the knowledge of two variables must be at least Planck's constant divided by 2π so that

$$\Delta t \cdot \Delta E \gtrsim h$$

Now $\Delta E = h\Delta f$, hence $\Delta f . \Delta t \simeq 1$. The same idea is embodied in the expression 2-39; if the bandwidth is decreased, the length of the observation time necessarily increases.

2.8 Phase Shift of Detection System

The difference in phase between the reference signal and detected signal can be due to: the phenomenon of photomagnetism, impedance of the detection coils, the tuned amplifier, the fact that the timing signal is taken from a different position of the sectored disc than that which is provided for the light beam, the phase sensitive detector, 90 degree lag due to electromagnetic induction.

2.8.1 The Phenomenon of Photomagnetism

The phase shift arising from the phenomenon of photomagnetism was not investigated. However, as was shown

in section 2.5 (formula 2-9) in which a light sensitivity calculation was done there exists the possibility of a phase shift θ' given by $\theta' = \sin^{-1} \frac{\omega'\tau}{\sqrt{1+\omega'^2\tau^2}}$

2.8.2 The Impedance of the Detection Coils

The phase shift from this source is temperature dependent seeing that the resistive component of the coil impedance is temperature dependent. This source of phase shift can be eliminated if wire is used, the resistivity of which varies little with temperature.

To obtain an idea of the phase shift to be expected from this source consider the following example. Two finely wound copper coils were used the resistance of which was 250Ω at room temperature and 2Ω at liquid helium temperature. The inductance of the two coils connected in parallel opposition was measured and found to be 37.5mh. If the impedance of the detection coils is $Z = R + j\omega L$, then the change in phase due to this source alone at a frequency of 1000 c.p.s. is $\Delta(\text{phase}) = 43^{\circ}$.

If the load into which the detection coils work (1MΩ as is the case with the tuned amplifier) is very high, the phase of the detected signal is not materially altered by a change in the resistance of the coils.

2.8.3. The Tuned Amplifier

The phase shift due to the tuned amplifier is that

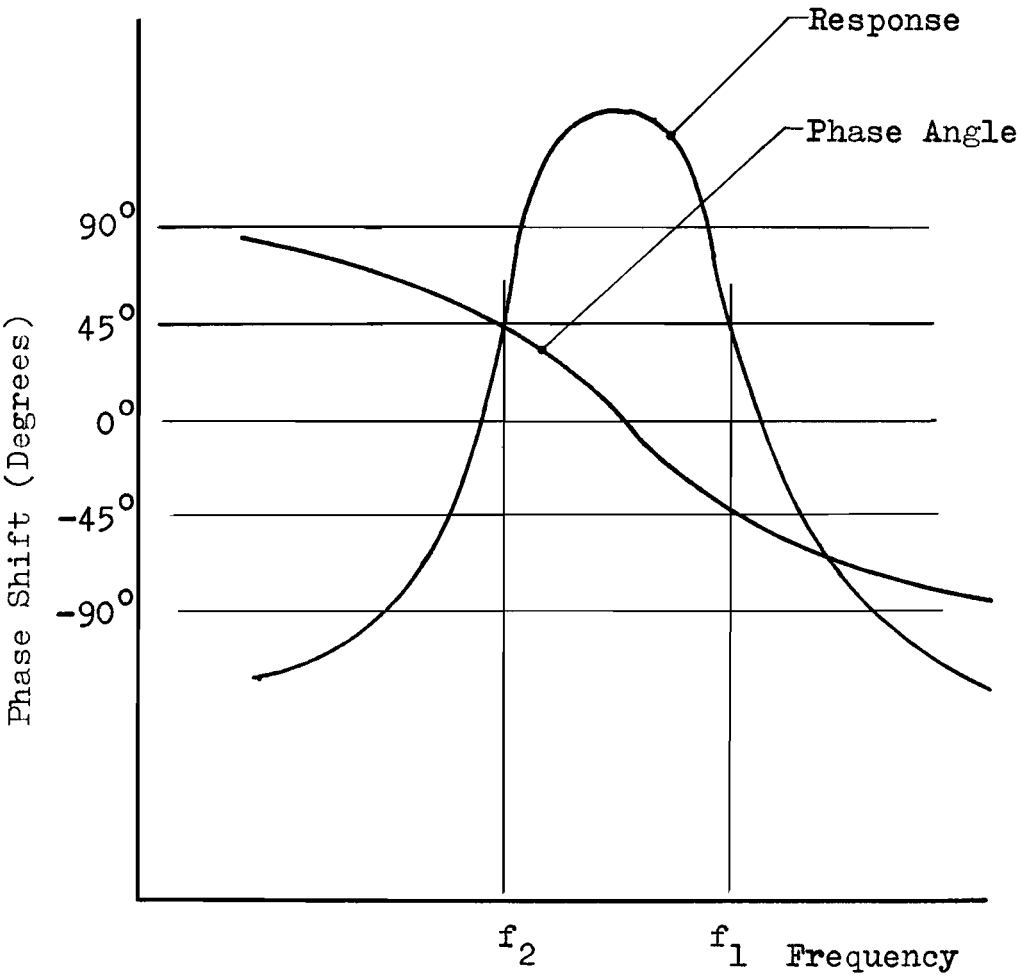

Figure 2-10 Phase Shift of Tuned Amplifier

characteristic of a bandwidth narrowing device. It can be seen from Figure 2-10 that any error in tuning, or a change in frequency can result in a possible phase shift of up to 45° (midband to half power point).

2.8.4. Timing Signal and Light Beam taken from different Positions of Sectored Disc

The phase shift due to the fact that the openings in the chopper light baffle for the timing signal and sample light beams are at different positions was measured and found to be a 1.5° lag.

The phase shift from this source depends on the angular separation of the two light beam openings in the baffle plate and the number of slits in the chopping disc. The above phase shift of 1.5 was for a disc of 18 slits (working frequency of 1000 c.p.s.).

This phase shift, although negligible for this disc, may be much larger for other discs giving different frequencies of interruption of the light beams.

2.8.5 The Phase Sensitive Detector

The phase shift due to the phase sensitive detector will be discussed more thoroughly in section 5.1.3 in the appendix.

2.8.6 The 90° Lag due to Electromagnetic Induction

The 90° lag due to electromagnetic induction is

a phase shift peculiar to this method of detection. This phase lag is predicted by formula 2-25.

2.9 Thermal Noise and Spurious Voltage Signals

The thermal noise and spurious voltage signals encountered during the course of the experiment will be considered under the following headings: thermal noise in the detection coils and electronic measuring instruments, irregularities in the timing signal and interrupted light beam as a result of the imperfections in the chopping disc, spurious signals due to the mechanical vibration of the coils in the magnetic field and stray magnetic fields, ground loop voltage signals, and spurious signals generated by light falling on the detection coils.

2.9.1 Thermal Noise in Detection Coils and Electronic Measuring Instruments

The thermal noise level of the detection system is determined primarily by the noise level of the tuned amplifier. Furthermore, the noise level of the tuned amplifier is independent of the source impedance.

To obtain an idea of the magnitude of the thermal noise generated by the detection coils the following calculation is given. The r.m.s. noise voltage generated in an impedance having a resistive component R is given by $e_n = \sqrt{4kTR\Delta f}$. For $k = 1.38 \times 10^{-23}$ joule/ degKelvin, $T = 290$ K°, $R = 6{,}150\ \Omega$, $\Delta f = 45$ c.p.s., $e_n = 6.6 \times 10^{-8}$ volts.

The internal noise of the tuned amplifier with input terminals shorted manifests itself as 10% of a full scale deflection of the tuned amplifier output meter. This is equivalent to an r.m.s. voltage of 0.13 volts at the output terminals of the tuned amplifier.

The noise into the input of the phase sensitive detector is of random phase, amplitude, and frequency. The noise signal from the tuned amplifier combines with the reference signal to give a small fluctuating signal on the output terminals of the phase sensitive detector. The phase sensitive detector reduces all noise and harmonics by 40 db. Hence for an r.m.s. noise voltage of 0.13 on the input terminals of the detector, a noise voltage of 1.3mv r.m.s. is to be expected on the output terminals. If the magnitude of the noise signal on the output terminals of the low pass filter is given by $e_{n\ (\text{low pass})} = e_n\ (\text{phase sensitive detector}) \sqrt{\frac{\Delta f_{(\text{low pass})}}{\Delta f(\text{tuned amplifier})}}$

then for $\Delta f_{(\text{low pass})} = 0.021\text{c.p.s.}$, $\Delta f_{(\text{tuned amplifier})} = 45\text{c.p.s.}$ $e_{n(\text{phase sensitive detector})} = 1.35\text{mv}$, $e_{n(\text{low pass})} = 29.1\text{uv}$. These are low frequency fluctuations and can be amplified by the DC amplifier.

If the DC amplifier is in its most sensitive position (30mv range), and the decade resistance box of the recorder voltage divider network set at 20.6Ω, the

measured peak to peak fluctuations of the chart recorder pen are about 0.9 recorder divisions. The calculated peak to peak value of thermal noise as should be observed on the recorder chart is 0.5 divisions. The calculated and measured values are in reasonable agreement.

In the analysis of the thermal noise present in the measuring system, the noise present in the timing signal was ignored. The reason is that the timing signal must be of a substantial size before there is any noticeable deflection on the meter of the phase sensitive detector, and the noise of the reference signal is just not large enough.

To gain an idea of the noise generated in the reference signal by the phototube, the following calculation is given. Assume the phototube is operating under temperature limited conditions, i.e., all the electrons generated by the cathode are collected by the anode. Then the Schottky[15] noise current is $\bar{i}_a^2 = 2eI_A \Delta f$, where e is the electronic charge, I_A the phototube current, Δf the bandwidth. The anode characteristic resistance of the phototube is infinite for temperature limited conditions hence, for all practical purposes, the tube is working into the input impedance Z of the band pass filter. The noise voltage at the input of the band pass filter is then $\bar{V}_a = |Z| \sqrt{2eI_A \Delta f}$. If the voltage gain of the band pass filter and unit amplifier in tandem is G', then the r.m.s.

noise voltage on the reference terminals of the phase sensitive detector due to the phototube is $V_a' = G' |Z|\sqrt{2eI_A\Delta f}$. For $G' = 150$, $Z = 22M\Omega$, $e = 1.59X10^{-19}$ coul., $I_A = 2X10^{-6}$ amp, $\Delta f = 302$ c.p.s., then $V_a' = 45.5$ mv.

The noise generated in the band pass filter (low position) is less than 100uv. The noise on the reference terminals of the phase sensitive detector due to this source is 5.0 mv.

The thermal noise from these two sources at the reference terminals of the phase sensitive detector is 45.8 mv.

The signal to noise ratio at a particular point in a circuit is $S/N = 20\log_{10} = \overline{V}_s/\overline{V}_t$ db, where $\overline{V}_s$ is the r.m.s. voltage signal, and $\overline{V}_t$ is the total rm.s. noise voltage. Since the minimum r.m.s. voltage required to operate the phase sensitive detector is 8 volts, the signal to noise ratio at the reference terminals of the phase sensitive detector is 45 db.

As was stated previously the noise level of the tuned amplifier determines the noise figure[16] of the detection system. The noise figure F of a receiver is a measure of the amount by which the noise output exceeds that which be obtained if the receiver were free of noise sources, and the only source of noise were the thermal agitation noise received from the resistance across the input terminals. The noise figure F of a receiver is given by

$F = \frac{S_i/N_i}{S_o/N_o}$ where S_i is the signal in, N_i the noise in, S_o the signal out, and N_o the noise out. The formula for F can be rewritten as $F = N_o/kTBG$ where k is Boltzmann's constant, T the ambient temperature, B the bandwidth, G the receiver gain.

Consider two networks arranged in tandem as shown in Figure 2-11. The overall noise figure is given by $F_{12} = F_1 + \left(\frac{F_2 - 1}{G_1}\right)$ As can be seen from the expression for F_{12}, if the G_1 gain of the initial stage of amplification is very high, the noise figure of the two networks in tandem is essentially that of the first high gain stage. The gain of the tuned amplifier is approximately 120 db. Hence the noise figure of the detection system is that of the tuned amplifier.

The noise figure of the tuned amplifier was measured by the small signal method[17] and found to be 2.4.

2.9.2. Irregularities in the Timing Signal and Interrupted Light Beam as a Result of Imperfections in the Chopping Disc.

This source of spurious signal is only mentioned and was not investigated in great detail.

For the optimum performance of the phase sensitive detector the reference terminals should be supplied with a distortionless sine wave. To provide as perfect a reference signal as possible, the radial slits in the chopping disc were etched out.

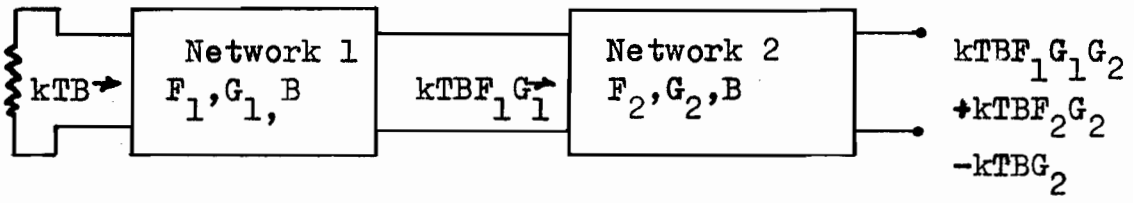

Figure 2-11 Noise Figure of Two Networks in Tandem

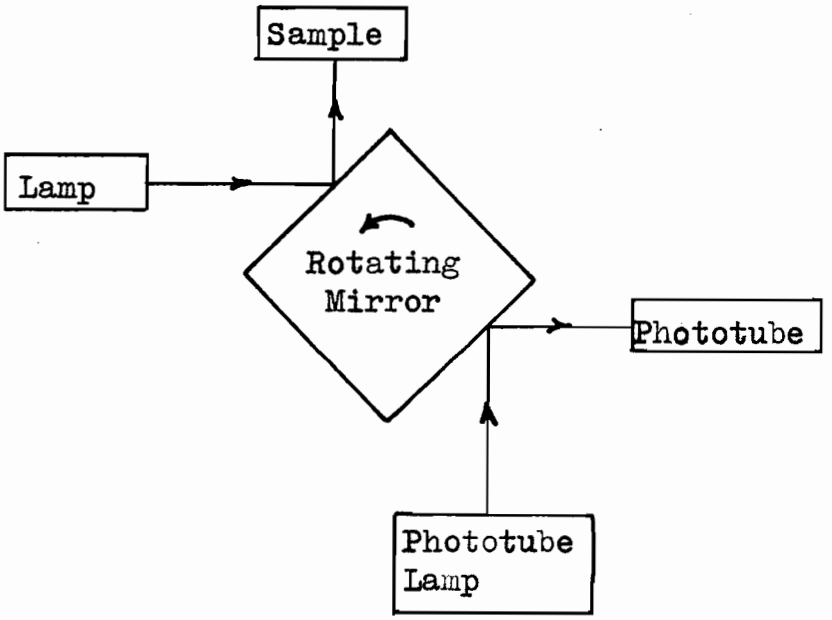

Figure 2-12 Alternate Method for Chopping Light Beam

This source of spurious signal could be eliminated by using for example (Figure 2-12) a four sided rotating mirror. Both timing signal and light beam for the sample could be obtained by reflection from the mirror's surfaces.

2.9.3 Spurious Signals due to Mechanical Vibration of the Coils in the Magnetic Field and to Stray Magnetic Fields.

The spurious signal due to mechanical vibrations was minimized by the precautions outlined in Chapter I. These included clamping the cryostat between the pole pieces of the magnet, and spring suspending the magnet and cryostat. The mechanical isolation afforded was good to the extent that there was no perceptible difference between the noise level with the magnetic field on and with it off.

The spurious signal due to stray magnetic fields was minimized by connecting the coils in parallel opposition.

In summary, the spurious signal from both these sources was less than the thermal noise of the tuned amplifier.

2.9.4. Ground Loop Voltage Signals

The detection system was extremely susceptible to ground loop signals if not exasperatingly so. The following system of grounding the instruments was adhered

to throughout the sensitivity measurements.

The ground wires provided with the instrument cables were grounded. The input and output negative terminals of the phase sensitive detector were joined and a ground lead applied to the input negative terminal of the same instrument. The output negative terminal of the tuned amplifier was joined to the negative terminal of the phase sensitive detector. The aluminum foil magnetic shield was grounded to the input negative terminal of the tuned amplifier (Figure 2-13).

During the calibration of the apparatus-system with the small magnetic current dipole, it was found that the dipole ground and the ground of the detection coils could not be connected; a large ground loop signal occurred if they were.

2.9.5 Spurious Voltage Signals Generated by Light Falling on the Detection Coils

This source of spurious signal, although unwanted, had all the appearances of a physical phenomenon. The phenomenon appeared under certain well defined conditions.

The apparatus used in the study of this spurious signal was as indicated in Figure 2-14. The coils were insulated electrically from the brass block and then rigidly fastened to the block with epoxy cement so as to prevent any spurious signal which might have arisen from

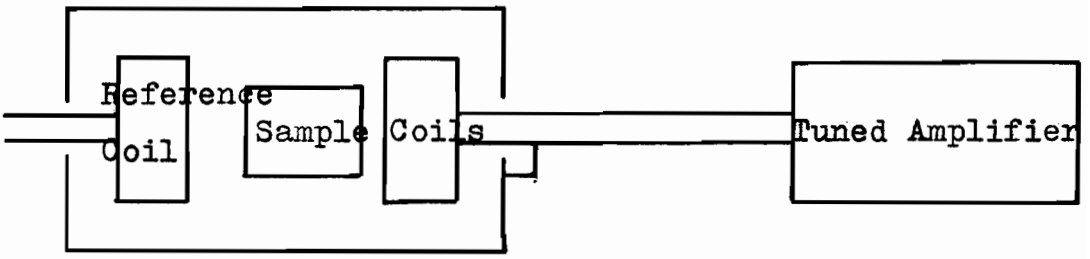

Figure 2-13 Grounding of Magnetic Shield

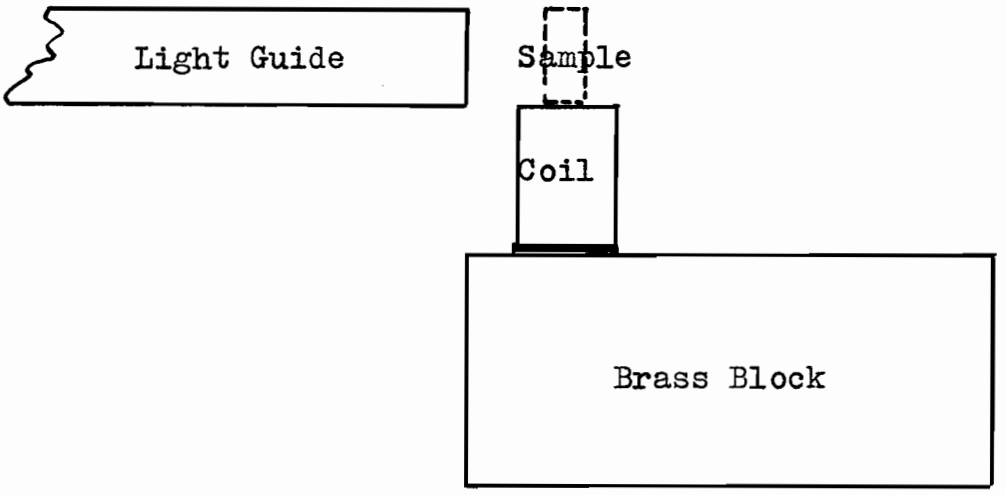

Figure 2-14 Side View Schematic of Coil, Sample,Brass Block and Light Guide

the vibration of the coils in the magnetic field. The coils were connected in parallel opposition and the leads braided. The braided leads were led out through a small opening in the top of the brass block to an amphenol output connector at the back of the block. The leads were fastened down with epoxy cement.

Copper and evanohm wire wound coils were used and both exhibited the same phenomenon.

The following section describes the experiments and the observations. The brass block holding the coils was arranged between the magnet pole pieces. The light guide was set up in such a way as to be symmetrically located with respect to the coils in the horizontal plane and shine no light or very little on the coils. Light was sent down the guide tube and the magnetic field applied; there was no signal.

An etched germanium sample was put in place as shown in Figure 2-14 so as to intercept the light from the light guide. Conditions of light and magnetic field were applied. A large signal was observed. The view that the signal was genuine was further strengthened by the fact that the signal showed a 180° phase shift upon reversal of the magnetic field.

A copper block with its faces dulled was used in place of the germanium sample. The same sequence of

trials was performed. There was no signal. The active face (face on which light was incident) was covered with a thin sheet of 0.001" aluminum foil (highly reflecting surface) and the copper block placed above the coils. When conditions of light and field were applied, the same observations characteristic of those observed for the germanium sample were obtained.

It appeared then that the source of the signal was from light reflected onto the coils by the high reflectivity surfaces.

The chopped light was then shone directly on one of the coils and the magnetic field applied. A large signal about 50 db above the noise level of the detection system was observed which reversed in phase by 180° when the field direction was reversed. When the light was shone on the other of the two coils a large signal was observed as in the previous situation, but it differed in phase by 180° from that noted for the other coil.

The coils were then shielded with 0.001" aluminum foil. The sensitivity of the detection system was measured and found to have been reduced by a factor of 450 by the aluminum foil shield.

Chopped light was shone on one of the coils (shielded) and the magnetic field applied. A small signal was observed thus demonstrating the inadequacy of the 0.001" aluminum foil as a thermal radiation shield.

An additional experiment was performed with a single evanohm wire wound coil mounted on a brass block. All the precautions previously taken to prevent a spurious vibrational signal were adhered to. The monochromator was inserted in front of the carbon arc, and the carbon arc lens removed. The carbon arc energy spectrum was measured with a thermocouple and the results are shown in Figure 5-15.

The light from the monochromator was shone on the single evanohm coil and the magnetic field applied (5000 oersted). The visible light and near infrared spectrum was scanned.

It was found that the absorption spectrum of the coil, and the energy spectrum of the carbon arc lamp both peaked at a wavelength of 1.5 microns.

This was a serious source of spurious voltage signal in view of the fact that the absorption edge of germanium at room temperature starts at a wavelength of 1.5 microns.

CHAPTER 3

MEASUREMENTS AND THEIR INTERPRETATION

Figure 3-1 is a schematic diagram of the special apparatus used in the calibration of the photomagnetometer, and in the investigation of photomagnetism in germanium at room temperature. Such a device avoids all the previously discussed sources of spurious voltage signal.

The coils were recessed into a thick hardwood block. A thin wafer of wood was fitted snugly over the coils into a recessed area which was larger than the coil area. The coils were glued firmly in place with glyptal cement. The coils were connected in parallel opposition and the braided leads taken out through the body of the block to an amphenol output connector. A wooden light guide was bolted onto the block holding the coils. The arrangement was painted black and then covered with 0.001" aluminum foil. The shielding was connected to the shield terminal of the amphenol output connector.

Sensitivity measurements were made by inserting a current dipole through the holes made in the body of the light guide.

3.1 Measurement of the Over All Electronic Sensitivity and Calibration of the Photomagnetometer

The purpose of these measurements was to calibrate the photomagnetometer and measure the sensitivity in the space above the detection coils. A small current dipole was used to calibrate the photomagnetometer.

Consider Figure 3-2. The electronic sensitivity was measured in the X direction, the Y direction, and the Z direction, the magnetic moment axis of the dipole being parallel to the X axis at all times.

The sensitivity of the photomagnetometer as a function of the angular orientation of the dipole was measured by rotating the current dipole about the y axis and in the xz plane, rotating the current dipole about the Z axis and in the xy plane.

The minimum detectable signal was measured for a frequency of 1000 c.p.s..

The calibration and sensitivity measurements were done with the coils and dipole at room temperature. However, the measurements are valid for lower temperatures, since the input impedance of the tuned amplifier is so high (1 MΩ) that the impedance of the coils is not important in determining the magnitude of the voltage signal applied to the tuned amplifier.

For all the measurements except those concerned with the frequency response of the photomagnetometer the frequency used was 1000 c.p.s..

The source of current for the dipole was a small portion of the signal taken from the output of the amplifier.

These measurements were made only after a great deal of trouble had been experienced with ground loops in the input of the tuned amplifier. It was found that the ground of the current dipole and that of the detection coils could not be joined.

Several dipoles were used in the calibration but the parameters for a typical one (Figure 3-3) are given in Table 3-1.

Table 3-1 Parameters of a Sample Current Dipole

Symbol	Meaning	Units	Value
l	length	in.	0.162
R	resistance	Ω	66.2
d'	dipole diameter	in.	0.125
d_w	wire diameter	in.	0.004
N	turns		25

Material - Evanohm

The circuit diagram for these measurements is the same as that indicated in Figure 1-1 except for a small additional circuit shown in Figure 3-4.

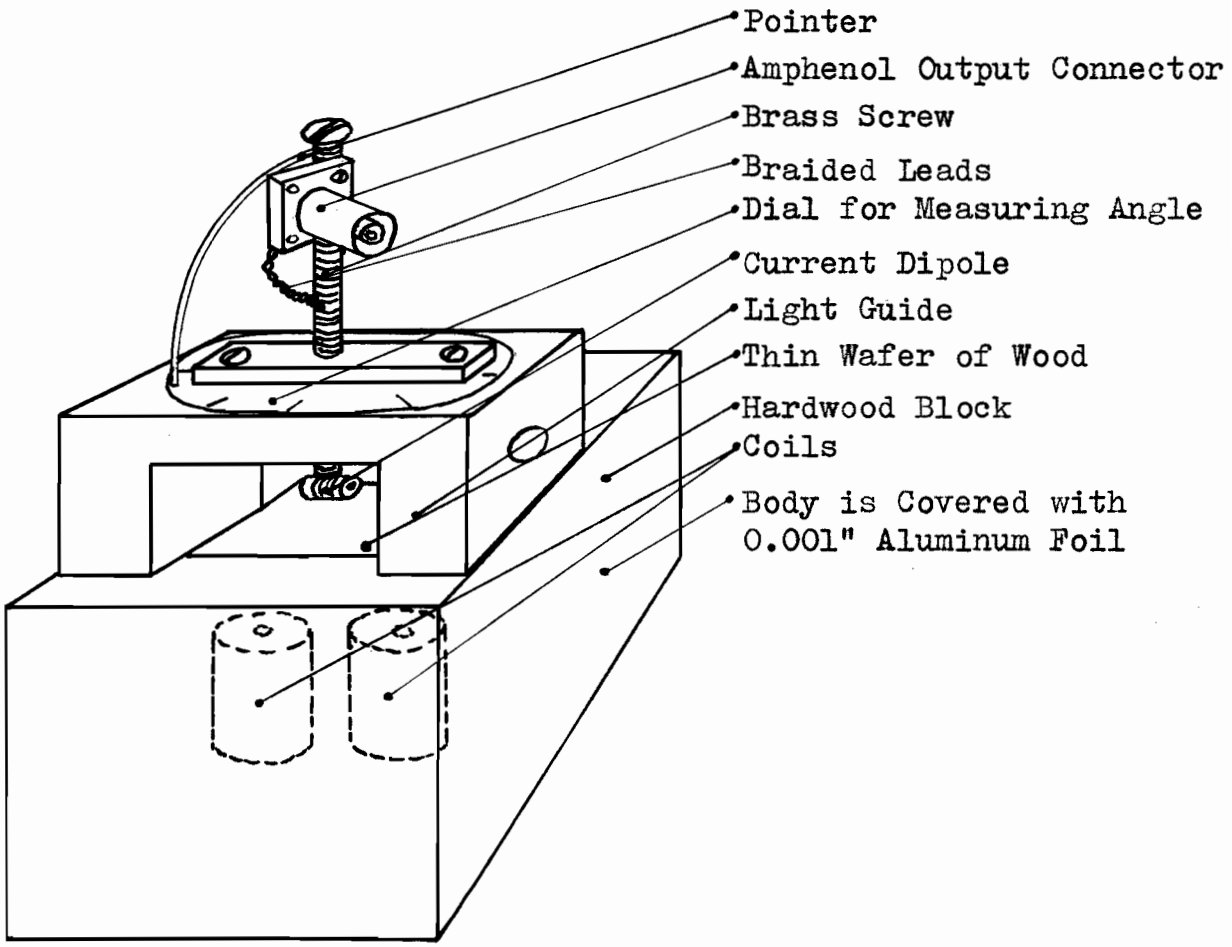

Figure 3-1 Schematic of Special Apparatus

The calibration measurements were not made with the phase sensitive detector or recorder decade resistance in their most sensitive positions. The gain setting of the phase sensitive detector was set at "low" and the decade resistance to 1.6Ω. If the phase sensitive detector is used in the "high" gain position the output meter of the same instrument fluctuates violently with a large amplitude. The optimum value of the recorder decade resistance is about 20Ω. By optimum is meant that the wandering of the recorder pen is large enough to be seen but not so large as to fill the whole chart.

3.1.1 Sensitivity in the X direction.

For these measurements the block holding the coils (without the light guide) was clamped in the vise of a lathe carriage and the dipole held stationary. By turning the micrometer handle of the lathe carriage the position of the dipole with respect to the coils could be changed. In practice the fineness of control permitted by the micrometer handle proved to be greater than that needed for the measurement.

The results for the sensitivity in the X direction are shown in Figure 3-6. Measurements were made for dipole distances (d) of 0.755, 0.535, and 0.355 inches. The magnetic moments of the current dipole were 6.22×10^{-14}, 3.00×10^{-14}

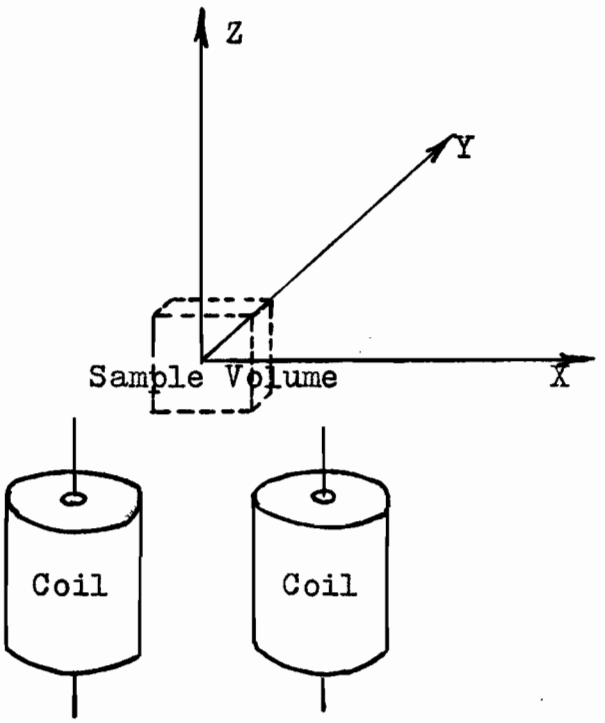

Figure 3-2 Sensitivity Measurements in Space Occupied by Sample

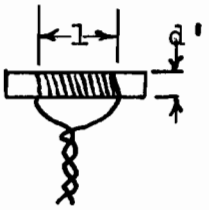

Figure 3-3 Magnetic Dipole (Small Coil)

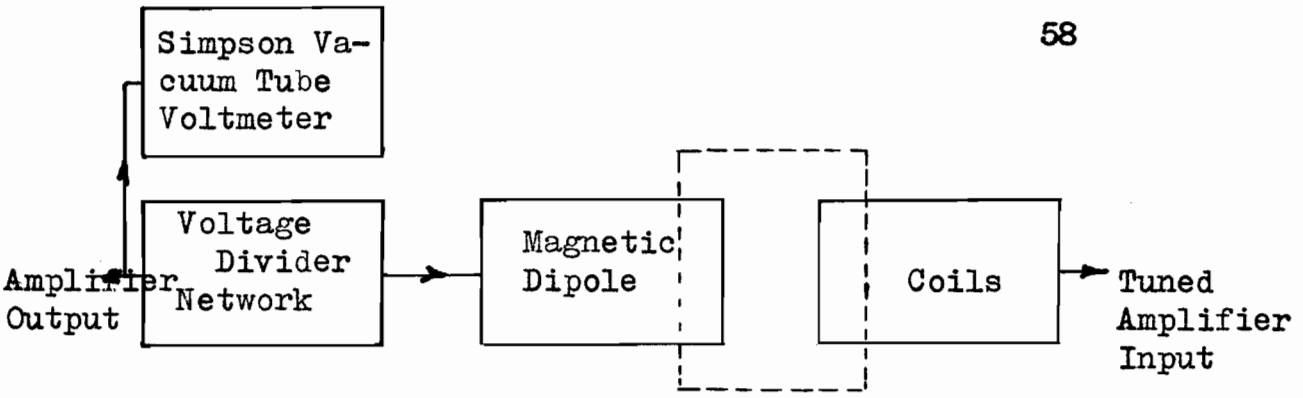

Figure 3-4 Additional Circuitry Used During Sensitivity and Calibration Measurements(All Sections Excluding Section 3.2)

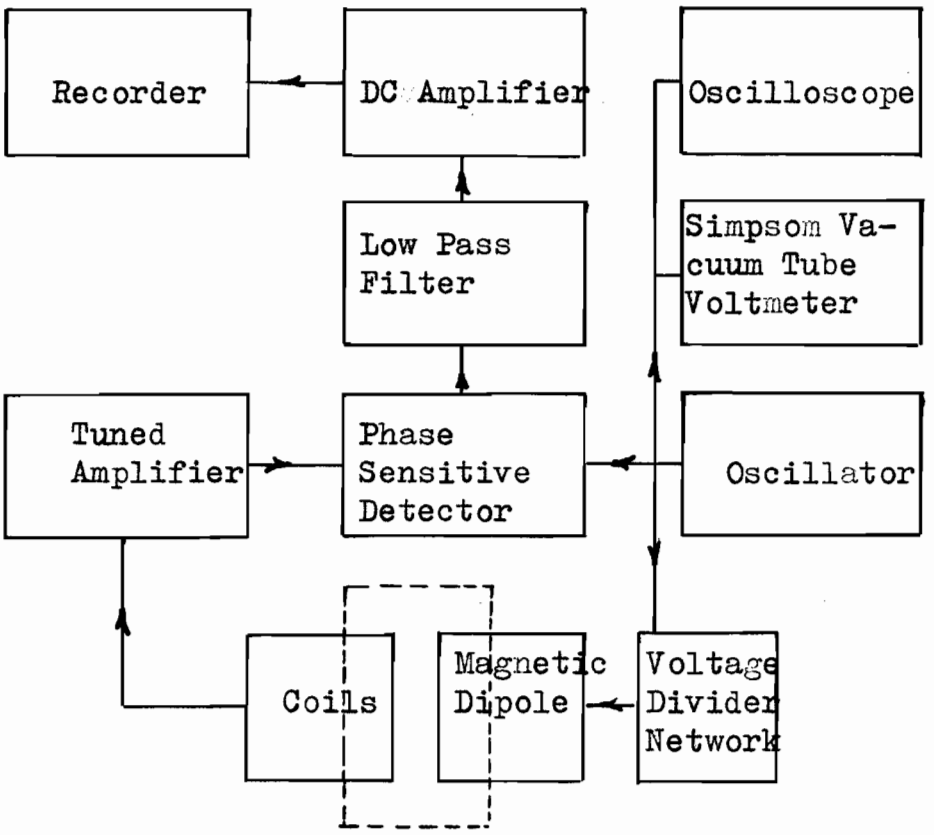

Figure 3-5 Block Diagram of Instruments Used in the Measurement of the Photomagnetometer Sensitivity as a Function of Frequency

Figure 3-6 Sensitivity in X Direction

Table of Parameters		
Point	Moment	Dipole Distance
×	3.03×10^{-14} wm	0.535 in.
⊗	6.8×10^{-15} wm	0.355 in.
⊠	6.22×10^{-14} wm	0.755 in.

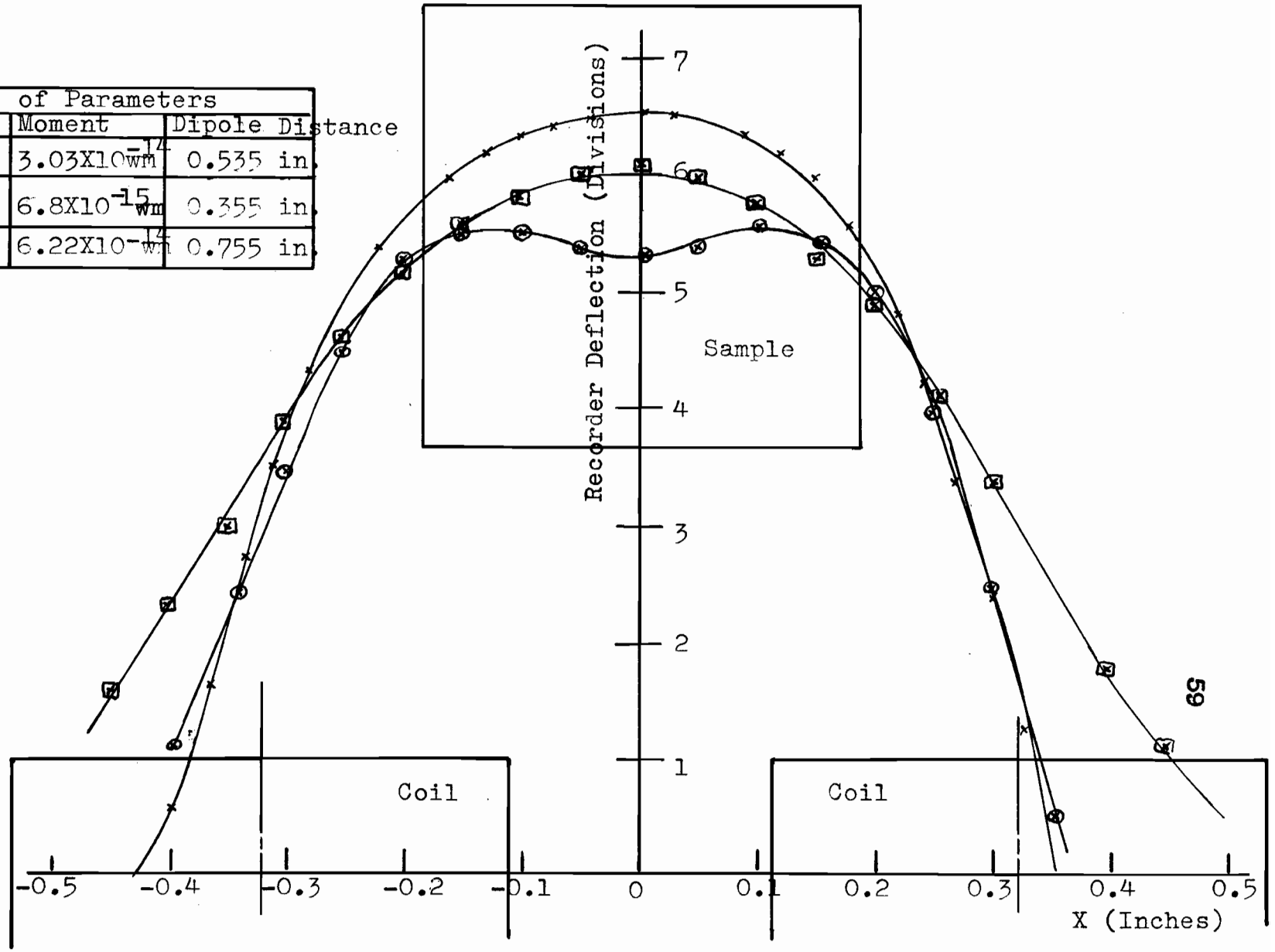

Figure 3-7 Sensitivity of Photomagnetometer in Y Direction

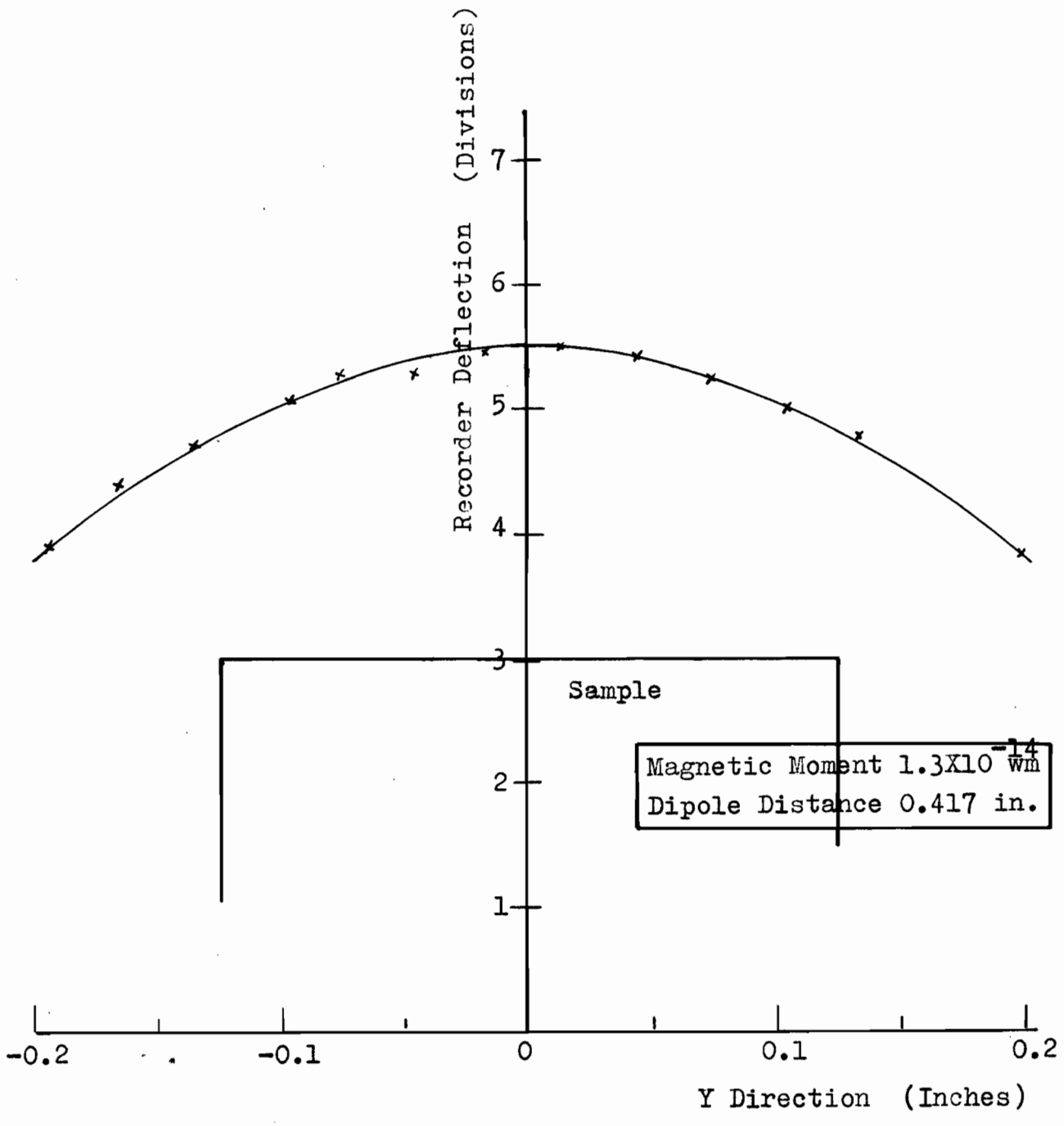

and $0.680X10^{-14}$ wm respectively. The spatial extent of the sample and coils is included in the Figure to show that the sensitivity was relatively constant across the breadth of the sample. The sensitivity decreases by 15% in going from the centre to the edge of the sample.

3.1.2 Sensitivity in the Y direction.

The same technique employed in the previous section for holding the coils and current dipole was used for these measurements.

The results for the sensitivity in the Y direction are shown in Figure 3-7. The sensitivity was measured for a dipole distance of 0.417 inches and a magnetic dipole strength of $1.30X10^{-14}$ wm. If the sample is placed such that the plane of its active surface contains the axes of the coils, then the decrease in sensitivity in going from the front face to the back is 51%. However, if the sample is placed symmetrically with respect to the coils, the decrease in sensitivity in going from the centre to a face is 12%.

3.1.3 Sensitivity in the Z direction.

For these measurements the coils were held stationary and the dipole moved along the Z axis.

The current dipole was glued to the bottom of a brass screw (32 threads per inch). A hole had been drilled down the axis of the screw to accommodate the leads from the current dipole. The leads were terminated in an amphenol output connector bolted in place at the head of the screw. The brass screw travelled up and down in a brass plate, which was screw-nailed onto the top of the wooden light guide (Figure 3-1).

The results for the sensitivity in the Z direction are shown in Figure 3-8. Measurements were made for dipole distances of 0.418, 0.437, 0.500, 0.625, 0.687 inches.

3.1.4 Rotation of the Dipole about the Y Axis.

For these measurements the dipole geometrical centre was held at some fixed distance from the coils, and rotated through 360^{o} taking measurements at 18^{o} intervals.

The magnetic moment was $1.97X10^{-14}$ wm and the dipole geometrical centre situated at a distance of 0.495 inches from the coils (Figure 3-9).

3.1.5 Rotation of the Dipole about the Z Axis.

As in section 3.4. the dipole geometrical centre was held at some fixed distance from the coils, and rotated through 360^{o}, taking measurements at 18^{o} intervals.

Figure 3-8 Sensitivity of Photomagnetometer in Z Direction

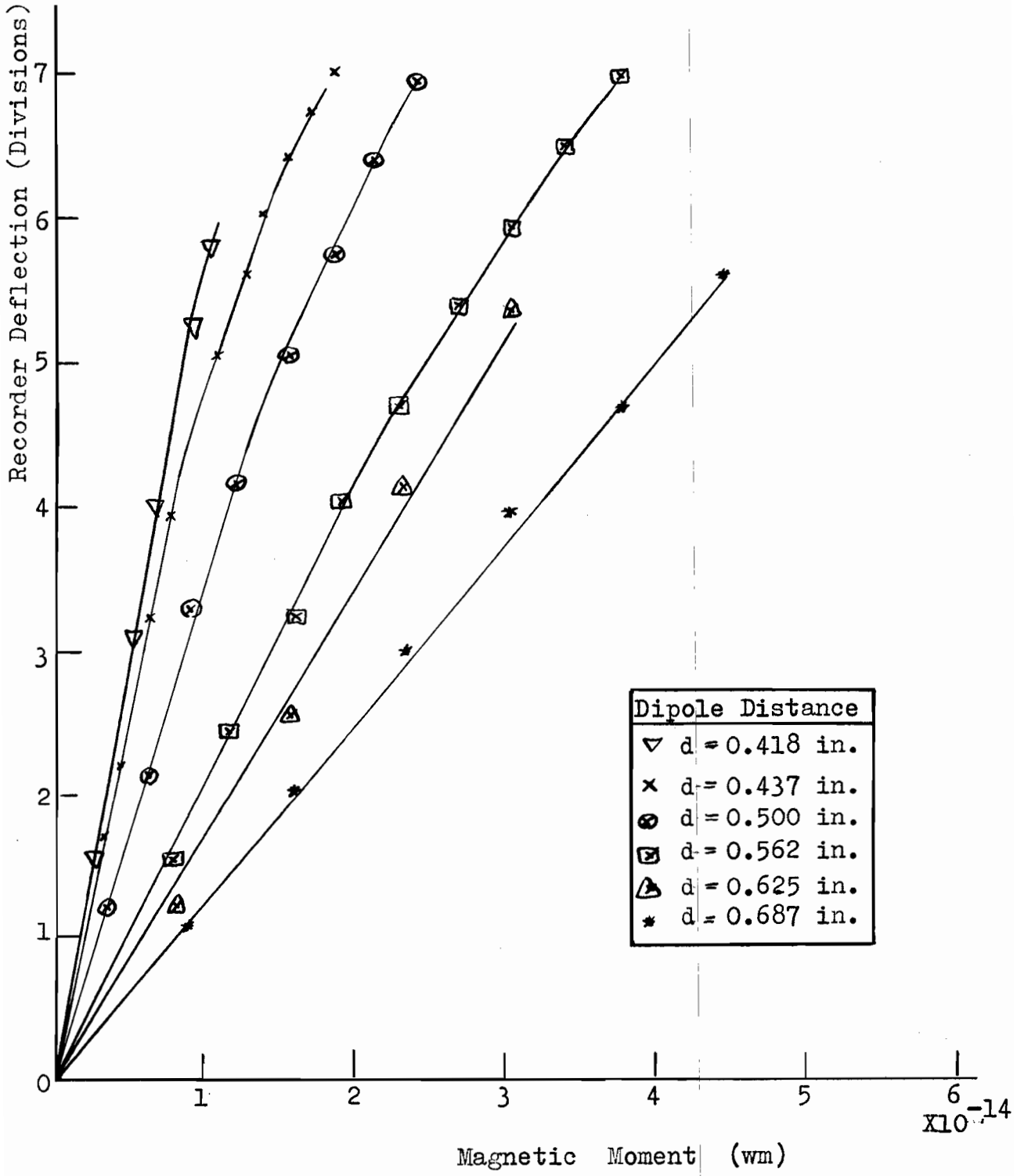

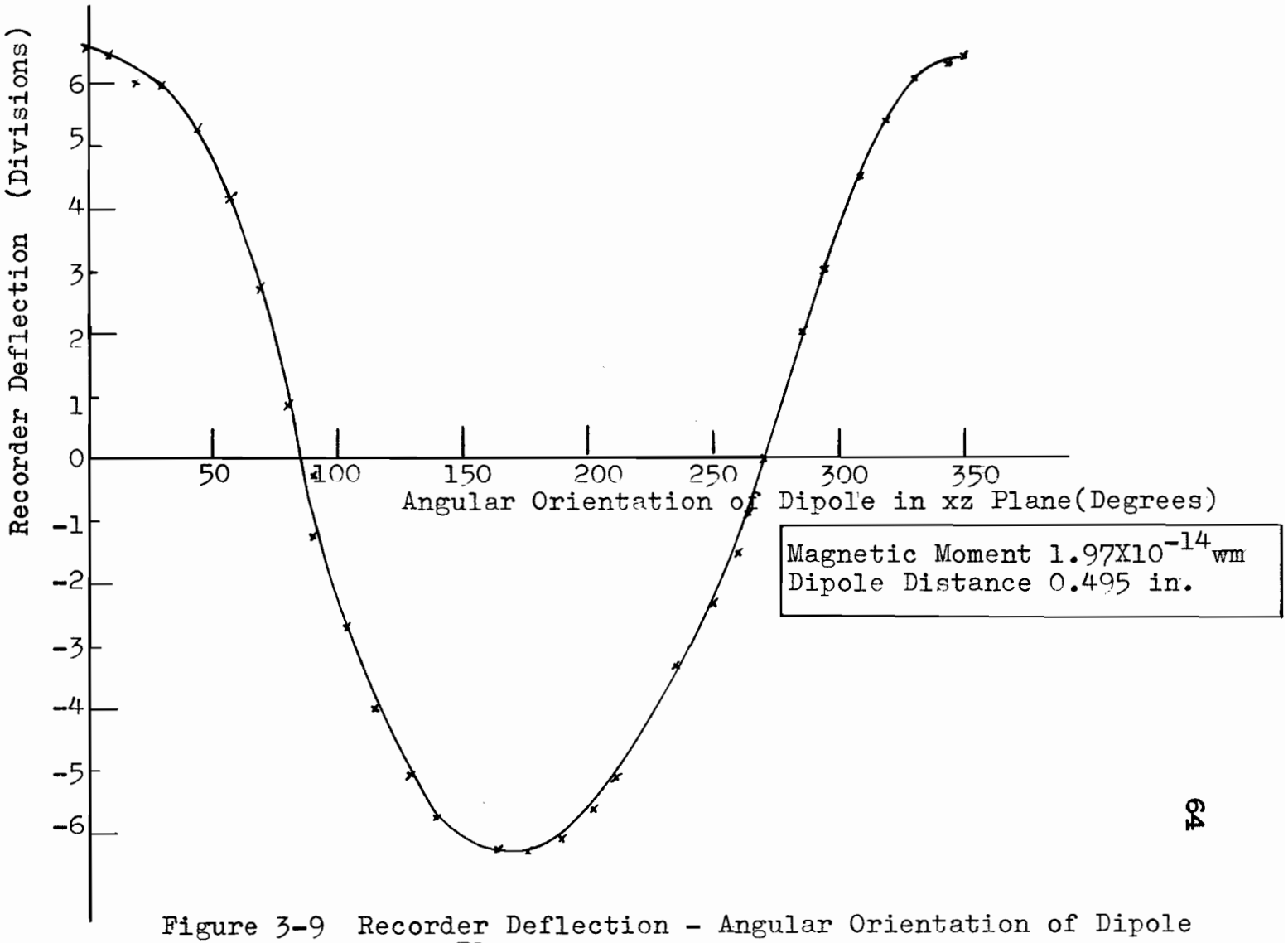

Figure 3-9 Recorder Deflection - Angular Orientation of Dipole in xz Plane

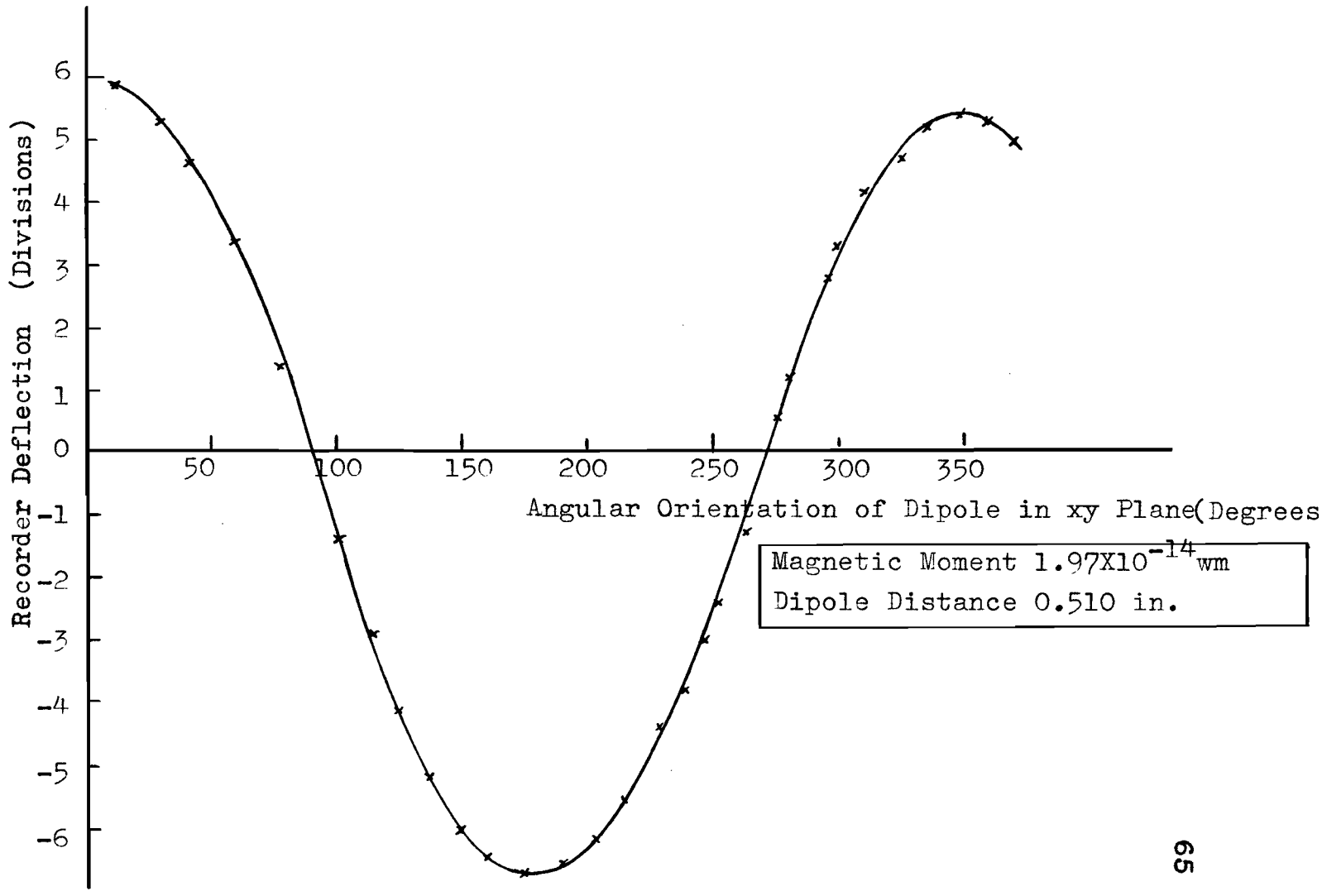

Figure 3-10 Recorder Deflection - Angular Orientation in xy Plane

Figure 3-11 Phase Angle of Signal - Angular Orientation of Dipole

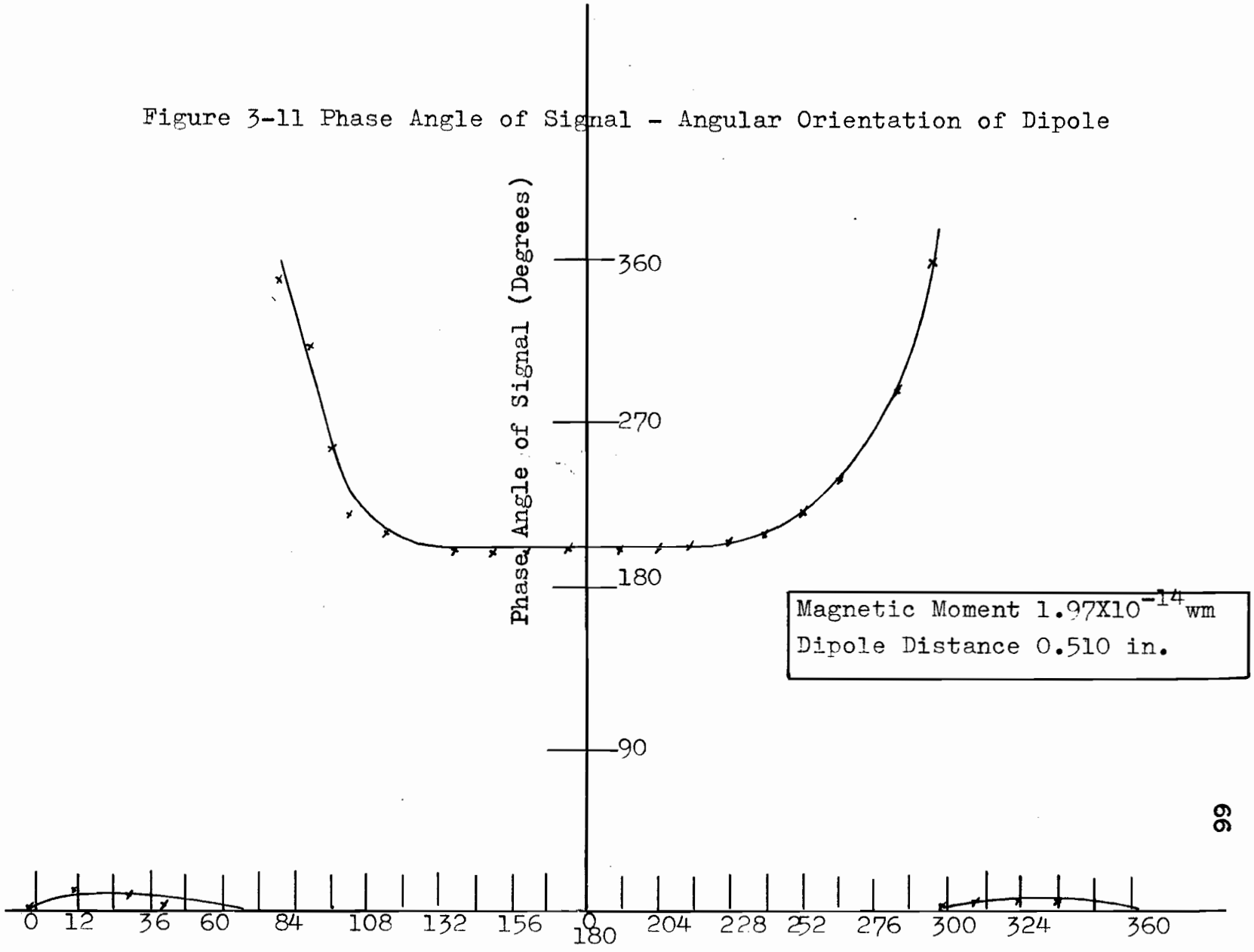

The magnetic moment was 1.97×10^{-14} wm and the dipole geometrical centre situated at 0.510 inches (Figure 3-10).

Figure 3-11 is included to demonstrate how the phase of the signal changes with dipole orientation. The results from this section were used in the calculation. The phase angle is relatively constant for 180° of travel of the dipole but quite abruptly changes to a new phase angle differing from the old by 180°. The phase of the signal remains relatively constant for the next 180°.

3.2 Calibration of the Photomagnetometer over the Frequency Range 200 c.p.s. to 6000 c.p.s.

For this set of measurements the timing signal from the photocell was not used. Instead the signal was obtained from an oscillator. Part of the signal was placed on the reference terminals of the phase sensitive detector and part was used to supply the current dipole. The ground arrangements were the same as in the previous measurements. Figure 3-5 is the block diagram of the instruments used in the measurement. Great care had to be exercised in shielding at frequencies greater than 2000 c.p.s. as the oscillator radiated badly for these frequencies. The results are indicated in Figure 3-12. The small kink in the curve was due to the tuned amplifier gain characteristic. The gain

Figure 3-12 Photomagnetometer Sensitivity - Frequency

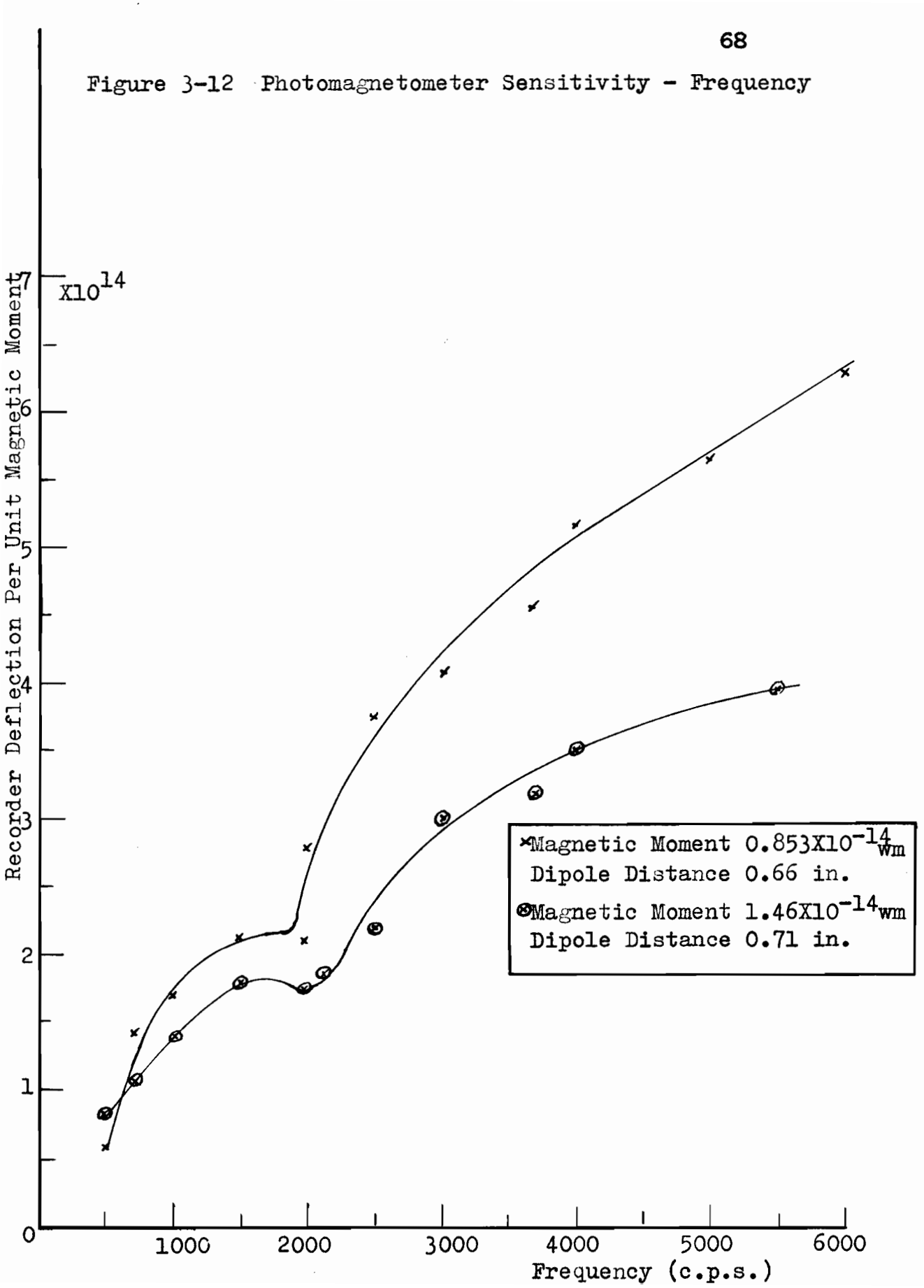

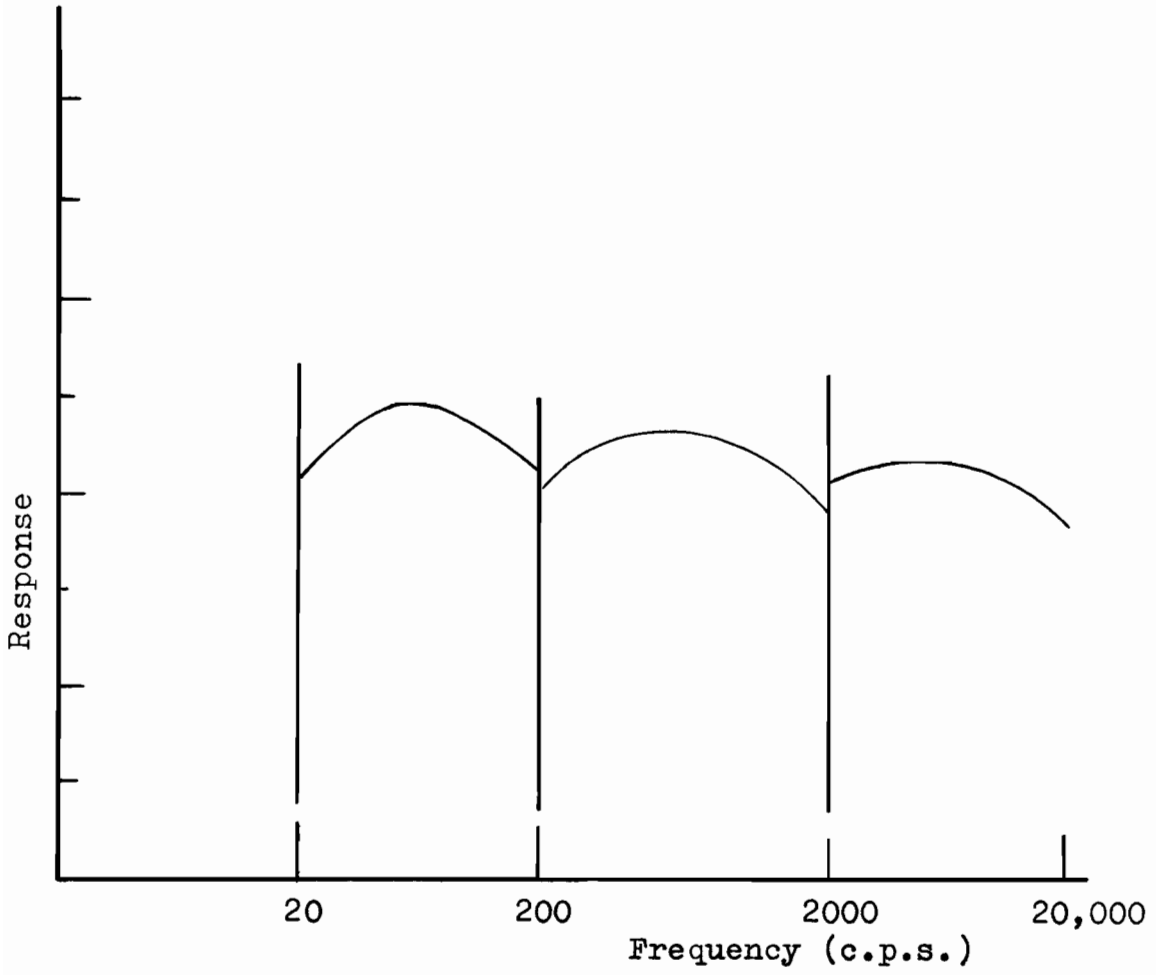

Figure 3-13 Schematic of Frequency Response of Tuned Amplifier

characteristic of the tuned amplifier (schematic) is as shown in Figure 3-13.

3.3 Measurement of the Minimum Detectable Signal.

The apparatus arrangement for this measurement was the same as that used in section 3.1.3. The dipole distance was 0.437 inches.

The recorder decade resistance was adjusted until the noise of the apparatus-system was visible on the recorder chart. The magnetic moment of the current dipole was increased until a small signal appeared on the recorder above the noise level. The minimum detectable signal corresponded to a magnetic moment of $3.89X10^{-16}$ wm. The voltage induced in the detection coils due to this moment was $1.58X10^{-8}$ volts. The thermal noise in the detection coils at room temperature was calculated to be $6.66X10^{-8}$ volts. The signal to noise ratio at the coil terminals then was -26 db. It is to be noted that this signal to noise ratio quoted does not include the thermal noise generated in the input impedance of the tuned amplifier.

3.4 Refinement of Formula 2-25 to take into Account the Finite Size of the Detection Coils

The recorder deflection in terms of the magnetic moment and orientation of the dipole with respect to the

coils is given quite generally by

$$D = G\left(\frac{|m_0|}{1.41}\right)\left(3\omega' \frac{\sin 2\theta A_c N_c}{8\pi r^3} \cos\phi \cos\beta\right)$$

where G is the electonic gain factor expressed in divisions/volt (r.m.s.).

As was mentioned previously, the fact that the coils are of a finite size, and the distance of the dipole to the coils is not large must be taken into account.

Figure 3-14 illustrates how the magnetic induction per unit magnetic moment varies across different sections of a detection coil.

The flux linkages per unit magnetic moment for a detection coil can be written as a definite integral. Considering Figure 3-15 the flux linkages per unit magnetic moment are given by

$$(\phi/M)_{coil} = \int_{r_1}^{r_2} \frac{dr'}{d_w} \int_{d_2}^{d_1} \frac{d(d)}{d_w} \int_{d_4 - r'}^{d_4 + r'} \frac{3M \sin 2\theta}{4\pi r^3} \sqrt{r'^2 - p^2} \left[d(d_4 + p)\right]$$

where d_w is the diameter of the wire and the other symbols are as indicated in the diagram.

This integral proved impossible to evaluate and so a simpler method was resorted to. The coil was divided up into thin sections of thickness d(d). The area-turns factor for a thin section was obtained from the formula

$$(\text{Area-turns})_{\text{section}} = \frac{d(d)\pi}{d_w 4}\left[d_1^2\left(\frac{d_2 - d_1}{2d_w}\right) \quad \frac{d_1}{2}(d_2 - d_1)\left(1 + \frac{d_2 - d_1}{2d_w}\right)\right.$$

$$\left. + \frac{d_w}{12}(d_2 - d_1)\left(\frac{d_2 - d_1}{2d_w} + 1\right)\left(\frac{d_2 - d_1}{d_w} + 1\right)\right] \qquad (3\text{-}1)$$

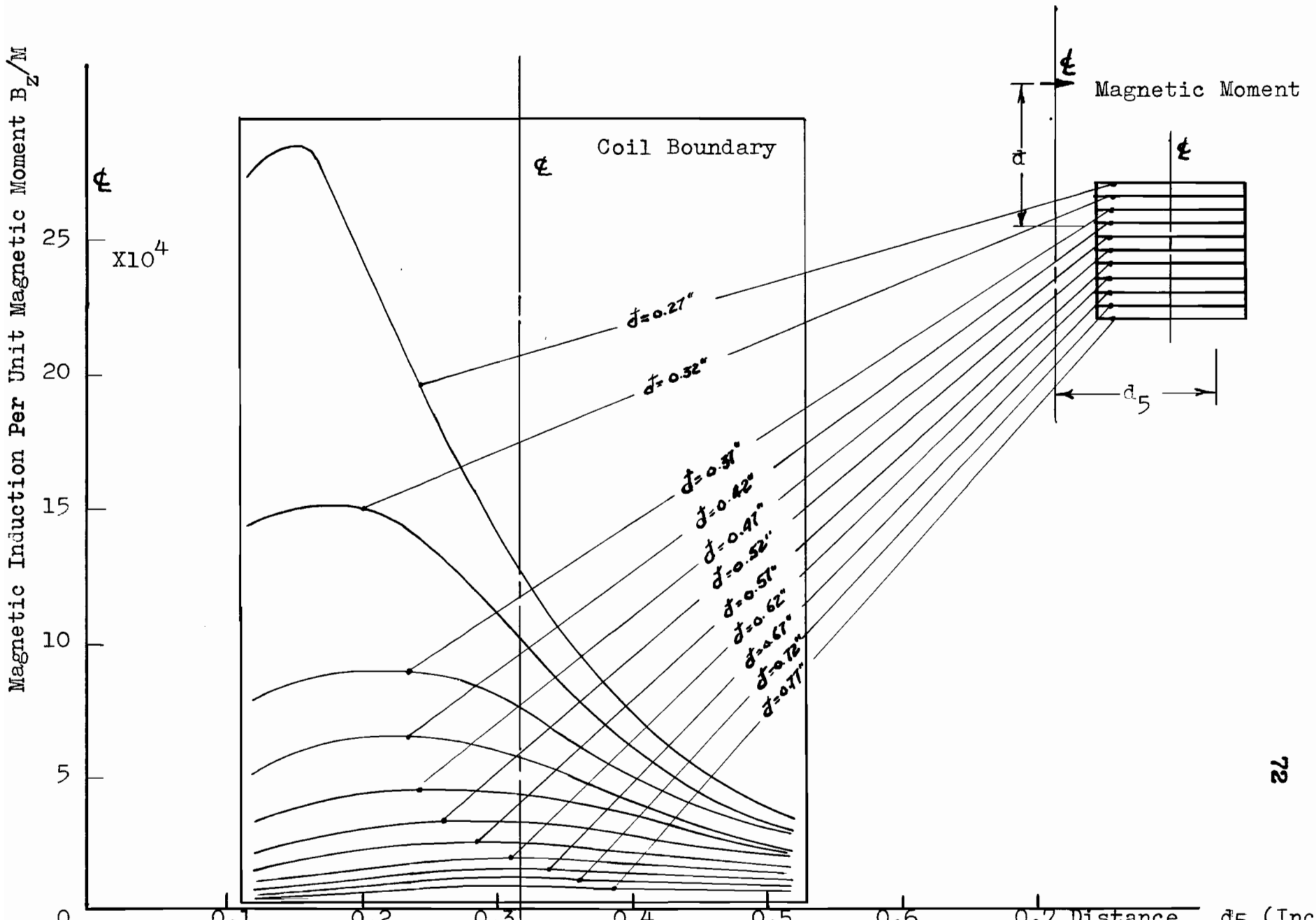

Figure 3-14 Magnetic Induction Per Unit Magnetic Moment Across Different Sections of a Coil

where d_1 and d_2 are the outside and inside diameters respectively of the coil. The flux linkages for a given section were obtained by taking the product of the magnetic induction at the centre of the coil section and the area-turns factor. The flux linkages for a single coil is then the sum of all such products.

Figure 3-16 gives the variation of B_z/M along the centre line of a coil as a function of the distance of the dipole to a cross sectional plane of the coil.

The flux linkages per unit magnetic moment for a single coil can be found by integrating the magnetic induction along the centre line of the coil. The integral is

$$(\phi/M)_{coil} = \int_{d+0.25"}^{d-0.25"} \frac{3M\sin 2\theta}{8\pi r^3} \left(\text{Area-turns per unit length}\right) d(d+z)$$

where $d+z = d$; d is the distance of the magnetic moment from the horizontal plane which passes through the geometrical centres of the coils. The result of the integration is

$$(\phi/M)_{coil} = \frac{A" d_4}{2.06 \times 10^{-4}} \left\{ \frac{1}{\left[d_4^2 + (d - 0.25)^2\right]^{3/2}} - \frac{1}{\left[d_4^2 + (d+0.25)^2\right]^{3/2}} \right\} \quad (3-2)$$

where A" is the area-turns (m^2 turns) factor per inch. The other terms are as indicated previously. The symbols d_4 and d are expressed in inches.

Expression 3-2 is plotted in Figure 3-17.

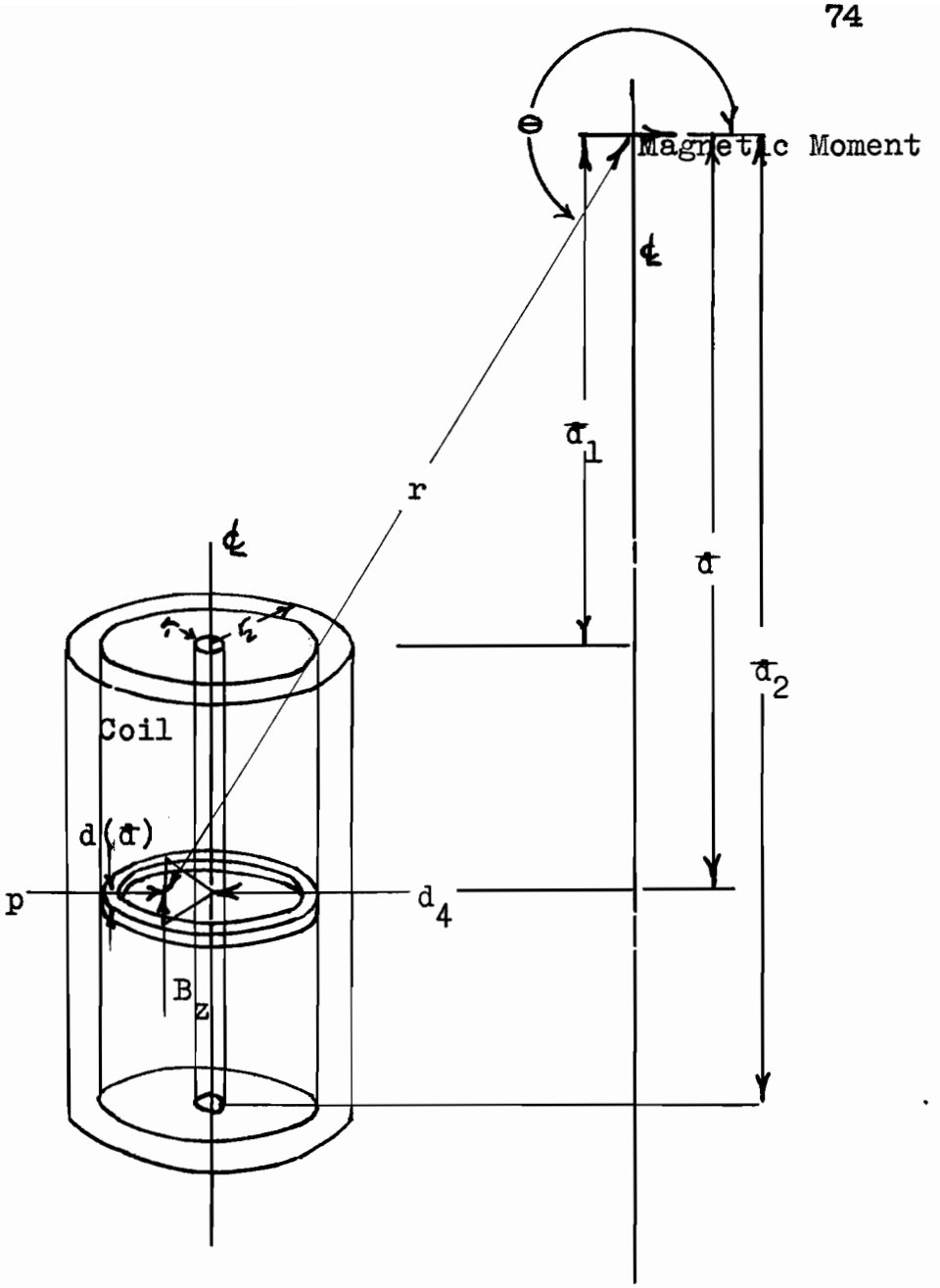

Figure 3-15 Flux Linkages for a Single Coil

Figure 3-16 Variation of B_z/M along ℄ of a Detection Coil

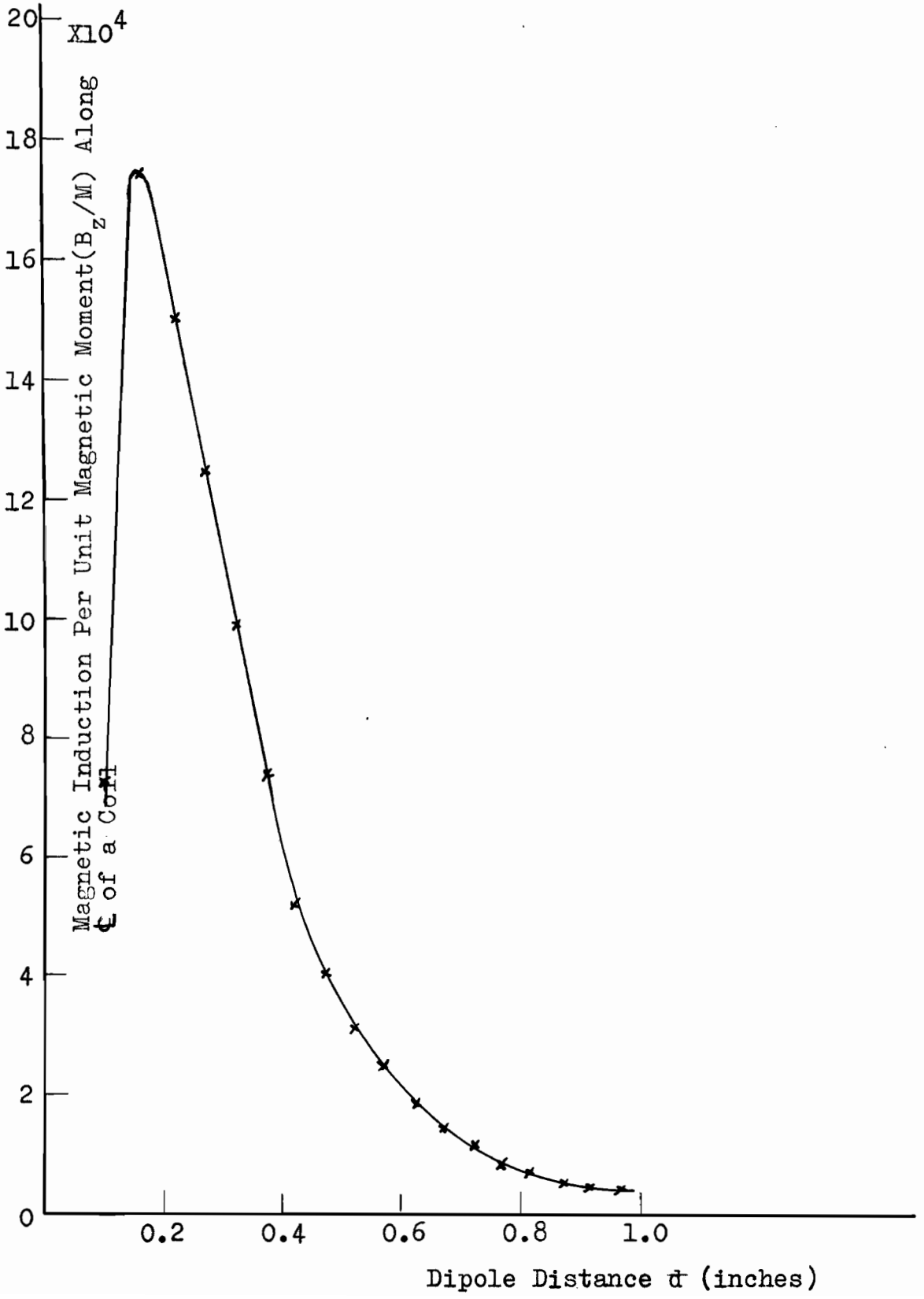

Figure 3-17 Flux Linkages $(\phi/M)_{Coil}$ - Dipole Distance d

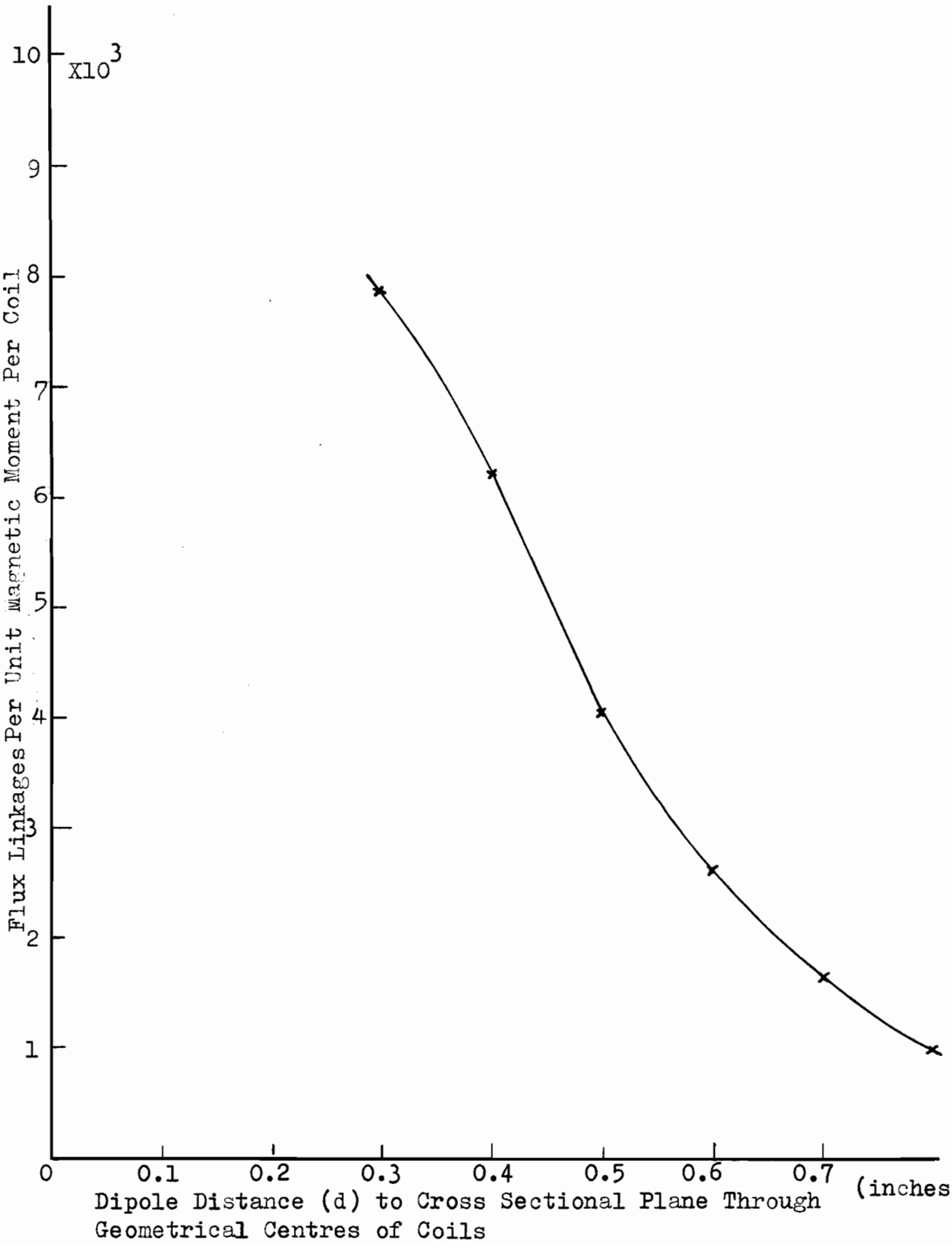

The refined expression for the recorder deflection as a function of the magnetic moment and dipole orientation is then

$$D = \omega'(\phi/M)_{coil} MG \cos\phi \cos\beta \qquad (3\text{-}3)$$

where D is the recorder deflection in divisions, ω' angular frequency of chopper, $(\phi/M)_{coil}$ the flux linkages per unit magnetic moment per coil, G the electronic gain factor in divisions/volt (r.m.s.), ϕ and β angles which describe the angular orientation of the dipole.

3.5 Sample Calculation illustrating how Formula 3-3 can be used.

The values used in the calculation are listed in Table 3-2, and were obtained from section 3.1.3 of the measurements.

Table 3-2 Table of Values for Sample Calculation

Symbol	Meaning	Unit	Value
i	dipole current	amp.	4.62×10^{-5}
d	dipole distance	in.	0.418
ω'	angular frequency	rad/sec	6.27×10^{3}
M	Magnetic monent	wm	1.16×10^{-14}
$(\phi/M)_{coil}$	flux linkages	m^{-1}	5.75×10^{3}
ε	signal into tuned amplifier	uv	0.42
G	gain factor	div/volt	1.2×10^{7}
$\cos\phi, \cos\beta$	dipole orientation angles		1
D	recorder signal	divisions (calculated)	5.0

D	recorder signal	divisions (measured)	5.3
% discrepancy			6%

The current i flowing in the dipole was obtained from a knowledge of the voltage across the voltage divider network which supplied the dipole, and the resistances of the voltage divider.

The magnetic moment M of the dipole was obtained from the formula $M = u_o AiN$, where $u_o = 12.57X10^{-7}$ w/ampm, A the cross sectional area of the dipole, N the number of turns on the dipole. When the dipole parameters as listed in Table 3-1 are used, the formula for M becomes $M = 2.51X10^{-10} i$ wm.

Knowing the value for d in inches $(\phi/M)_{coil}$ can be obtained from Figure 3-17.

The electronic gain factor, although relatively constant, varies slightly with the signal level into the tuned amplifier. Figure 3-18 gives the variation of G with signal level into the tuned amplifier.

The frequency $f = \frac{\omega'}{2\pi}$ was obtained with an oscilloscope. For the apparatus-system f = 1000 c.p.s.

Figure 3-18 Gain Factor - Signal Level Into Tuned Amplifier

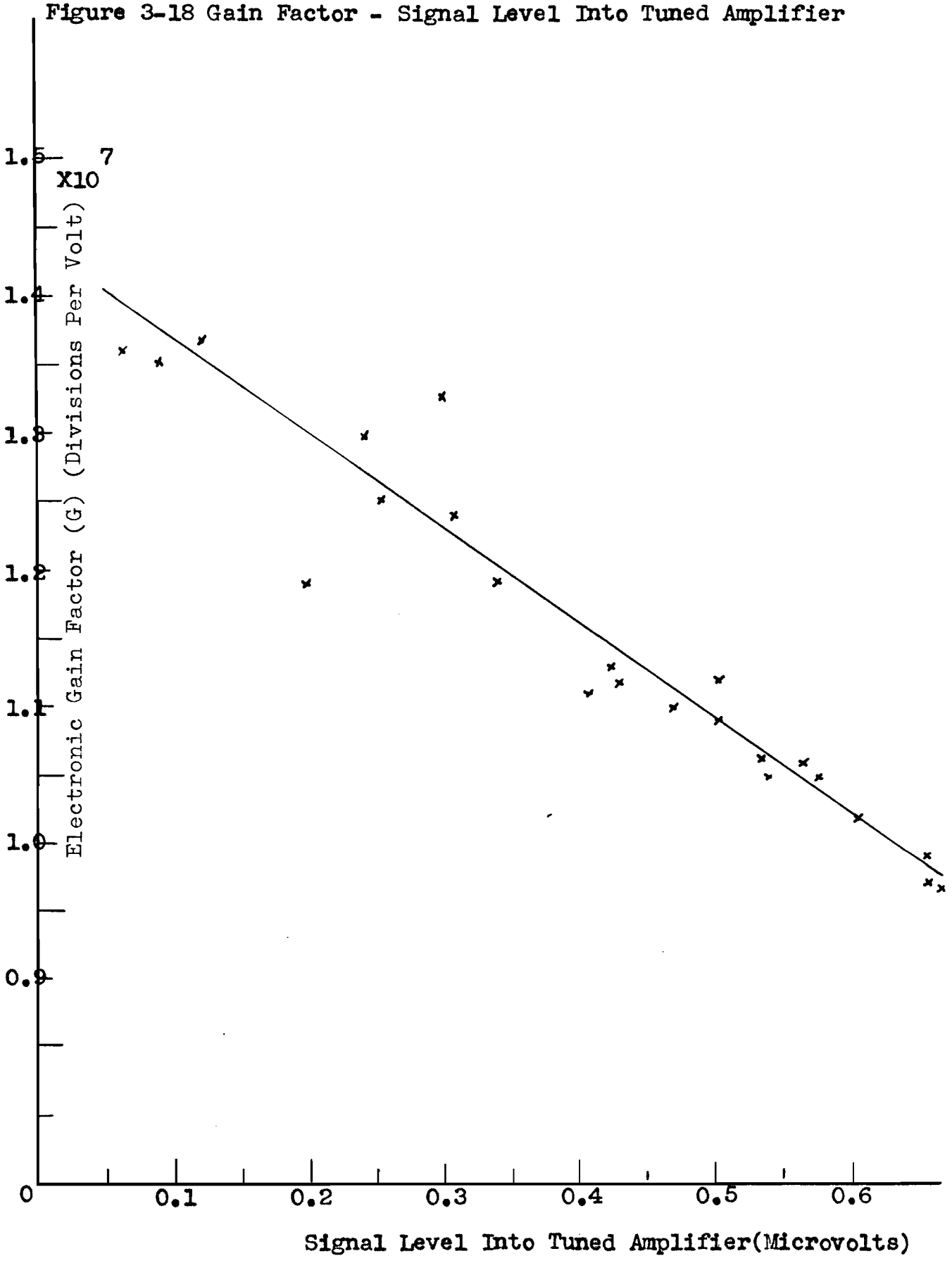

CHAPTER 4

CONCLUSIONS

The electronic sensitivity measurements and the light sensitivity calculation served to demonstrate the feasibility and also the difficulty of measuring a photomagnetism in germanium at room temperature with a photomagnetometer as described in this thesis. The magnetic susceptibility due to the photogeneration of free carriers in germanium at room temperature was shown to have a possible value of -5.6×10^{-10} amp^{2}m^4/joule; the photomagnetometer was shown to be just able to detect a signal of 5.1×10^{-10} amp^{2}m^4/joule.

It was shown that the electronic sensitivity of the photomagnetometer was relatively constant in the xy plane of the sample; the sensitivity was down by 15% at most at the edges of the sample.

The following expression was derived for the recorder deflection to be expected for a magnetic moment M

$$D = \omega' (\phi/M)_{coil} \; M \; G \; \cos\phi \; \cos\beta$$

where ω' is the angular frequency at which the light beam is chopped, $(\phi/M)_{coil}$ the flux linkages for a coil, G the

electronic gain factor, ϕ, and θ angles which describe the angular orientation of the magnetic moment. This expression was substantiated by the measurements.

An expression is derived for the recorder deflection in terms of the photomagnetic susceptibility for a sample of dimensions 3/8" by 3/8" by 1/4"; it is (see section 5.3 of the appendix)

$$D \doteq 3.86 \times 10^{14} R \chi_{sample} H$$

where R is the recorder decade resistance value, χ_{sample} the photomagnetic susceptibility of the sample, and H the magnetic field.

It was shown that a serious source of spurious voltage signal arose from light falling on the detection coils. It was all the more serious in view of the fact that the absorption edge of germanium at room temperature occurs for a wavelength of 1.5 microns, and this is the value of wavelength for which the spurious light generated signal from the coils is a maximum. Therefore the prerequisite of any successful measurement with this apparatus-system is the perfect thermal shielding of the coils from the radiation which is incident on the sample.

The signal to noise ratio for the minimum detectable magnetic moment was shown to be -26 db. The noise figure of the detection system was shown to be

determined primarily by the tuned amplifier noise level; the noise figure of the tuned amplifier was measured and found to be 2.4.

APPENDIX

5.1 Measurement of the Characteristics of the important Component Instruments.

In this section the following components and instruments are considered: pair of evanohm coils, tuned amplifier, phase sensitive detector, DC amplifier, low pass filter, recorder, carbon arc lamp, and monochromator.

5.1.1 Pair of Evanohm Coils.

The sensitivity of the coils is determined by their inherent thermal noise, and the number of turns. The r.m.s. noise voltage present in a bandwidth of 45 c.p.s. at a temperature of 290 ^{o}K was calculated to be $6.66X10^{-8}$ volts. Hence any signal of $6.66X10^{-8}$ volts or less would be masked by thermal noise.

It is possible to detect a signal which is less than the thermal noise of the coils. As was shown in section 3.3 the signal to noise ratio at the coil terminals was -26db for the minimum detectable magnetic moment.

As the temperature is decreased the thermal noise decreases, and hence there is an improvement in the signal to noise ratio.

The coil parameters (copper and evanohm wire wound) are listed in Table 5-1.

Table 5-1 Coil Parameters

Coil	Symbol	Meaning	Units	Value
Copper	d_1	inside diameter of coil	in.	0.130
	d_4	see Fig. 2-2	in.	0.321
	d_6	coil length	in.	0.500
	N_c	turns		8,700 *
	p	resistivity	ohmcm	$1.6X10^{-6}$
	d_w	wire diameter	in.	0.0035
	R	resistance of a coil	Ω	500
	d_2	outside coil diameter	in.	0.420
Evanohm	d_1	inside diameter of coil	in.	0.130
	d_4	see Fig. 2-2	in.	0.321
	d_6	coil length	in.	0.500
	N_c	turns		3,260 *
	p	resistivity	ohmcm	$1.39X10^{-4}$
	d_W	wire diameter	in.	0.004
	R	resistance	Ω	12,260
	$\frac{\text{Area-turns}}{\text{length}}$		$\frac{m^2 \text{ turns}}{\text{in}}$	0.2 **
	d_2	outside diameter of coil	in.	0.420

* The number of turns for a coil was calculated from the formula $N_e = Rd_w^2/2\rho\,(d_2 + d_1)$.

** The area-turns factor was calculated from formula 3-1.

The effect of shielding the pair of evanohm coils with 0.001" aluminum foil was to reduce the sensitivity by a factor of 450.

5.1.2 Tuned Amplifier Sensitivity and Mode of Operation.

The general Radio tuned amplifier and null detector was a sensitive low noise amplifier continuously tunable from 20 c.p.s. to 20 kc.p.s., with additional fixed tuned frequencies of 50 kc.p.s. and 100 kc.p.s..

Full scale meter sensitivity was 1 uv or better over most of the frequency range. The total gain of the amplifier was about 120 db.

The noise level was about 10% of full scale deflection of the output meter; this corresponds to a noise input of about $9.3X10^{-8}$ volts. The noise level was independent of input impedance, and it was the noise level of this instrument which determined the noise figure of the detection system.

The gain control of the tuned amplifier was in the form of a knob on the front panel which could be adjusted to give a gain of from anywhere up to 120 db. To utilize the tuned amplifier as a calibrated attenuator the knob ordinarily supplied with the instrument was removed and replaced with a helipot dial. The tuned amplifier

was then measured as a function of the helipot dial setting (frequency of 1000 c.p.s.).

The circuit used to calibrate the amplifier was as shown in Figure 5-1. The amplifier could not be calibrated with the phase sensitive detector connected onto the output of the amplifier due to the occurrence of a serious ground loop.

The amplifier output was loaded with a 2.5 M resistor shunted by 15 uufd which was the input impedance of the phase sensitive detector. The output voltage from the tuned amplifier was measured with an oscilloscope. Figure 5-3 gives the gain as a function of helipot dial setting.

The amplifier bandwidth between the half power points was measured and found to be 45 c.p.s. The measuring circuit used was as indicated in Figure 5-2. The input was kept constant and the response of the tuned amplifier output meter observed as the frequency of the oscillator was varied. Figure 5-4 gives the results.

5.1.3 Phase Sensitive Detector.

The heart of the detection system was the Phazor Null Meter (Industrial Test Equipment Company). The method of its detection has been outlined in section 2.7

The instrument was used in the low gain position with the gain control fully on. It was impossible to

Figure 5-1 Block Diagram of Instruments Used in Measurement of Gain of Tuned Amplifier

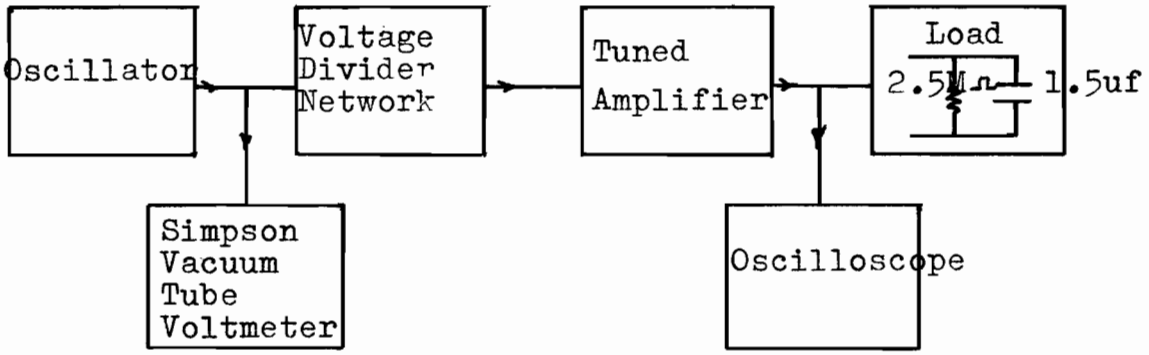

Figure 5-2 Block Diagram of Instruments Used in Measurement of Tuned Amplifier Bandwidth

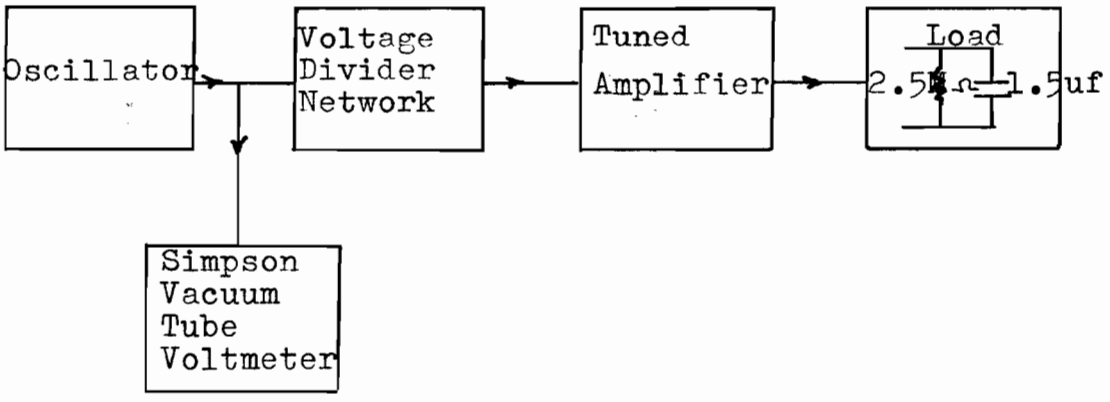

Figure 5-3 Gain of Tuned Amplifier - Helipot Dial Setting

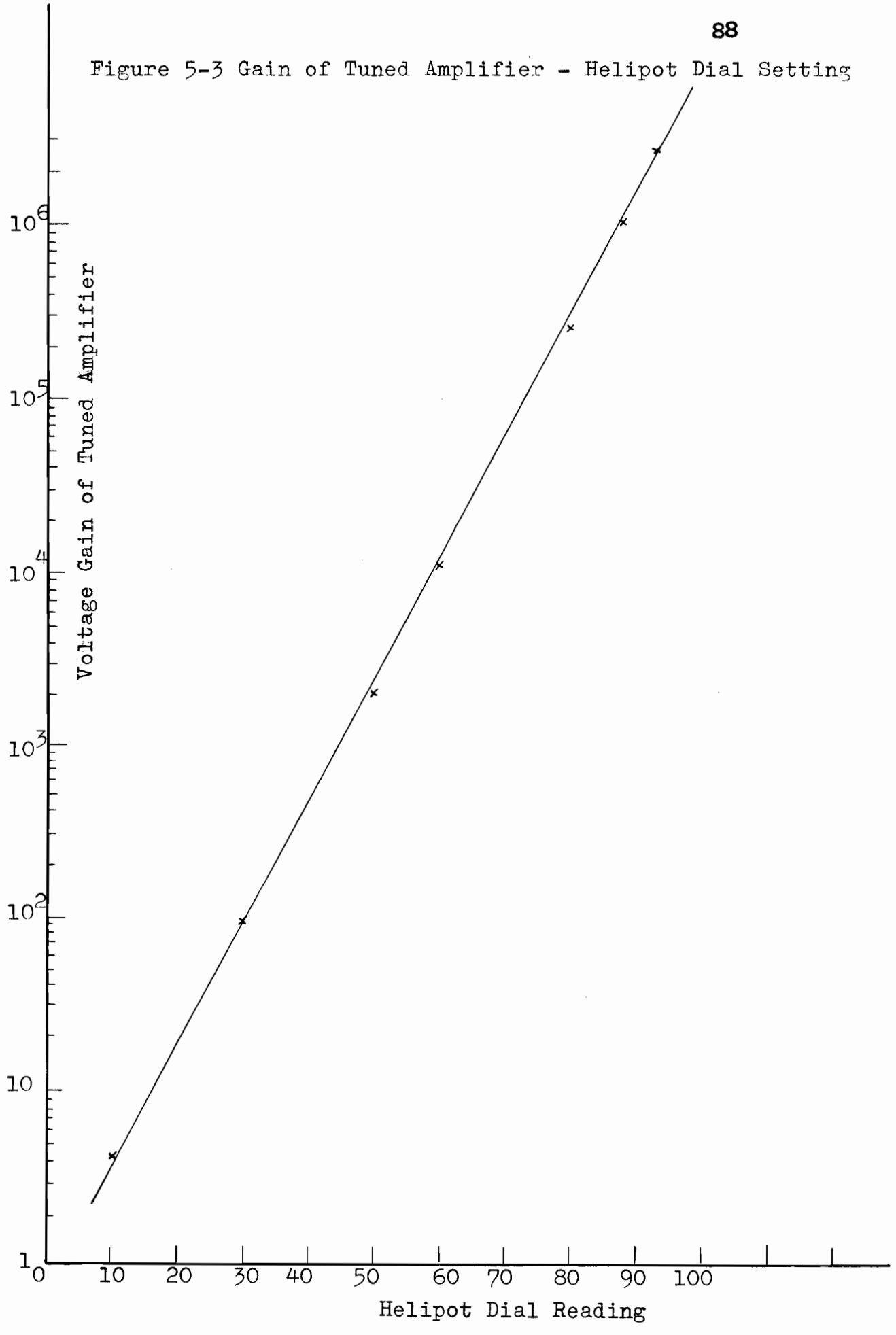

Figure 5-4 Tuned Amplifier Bandwidth

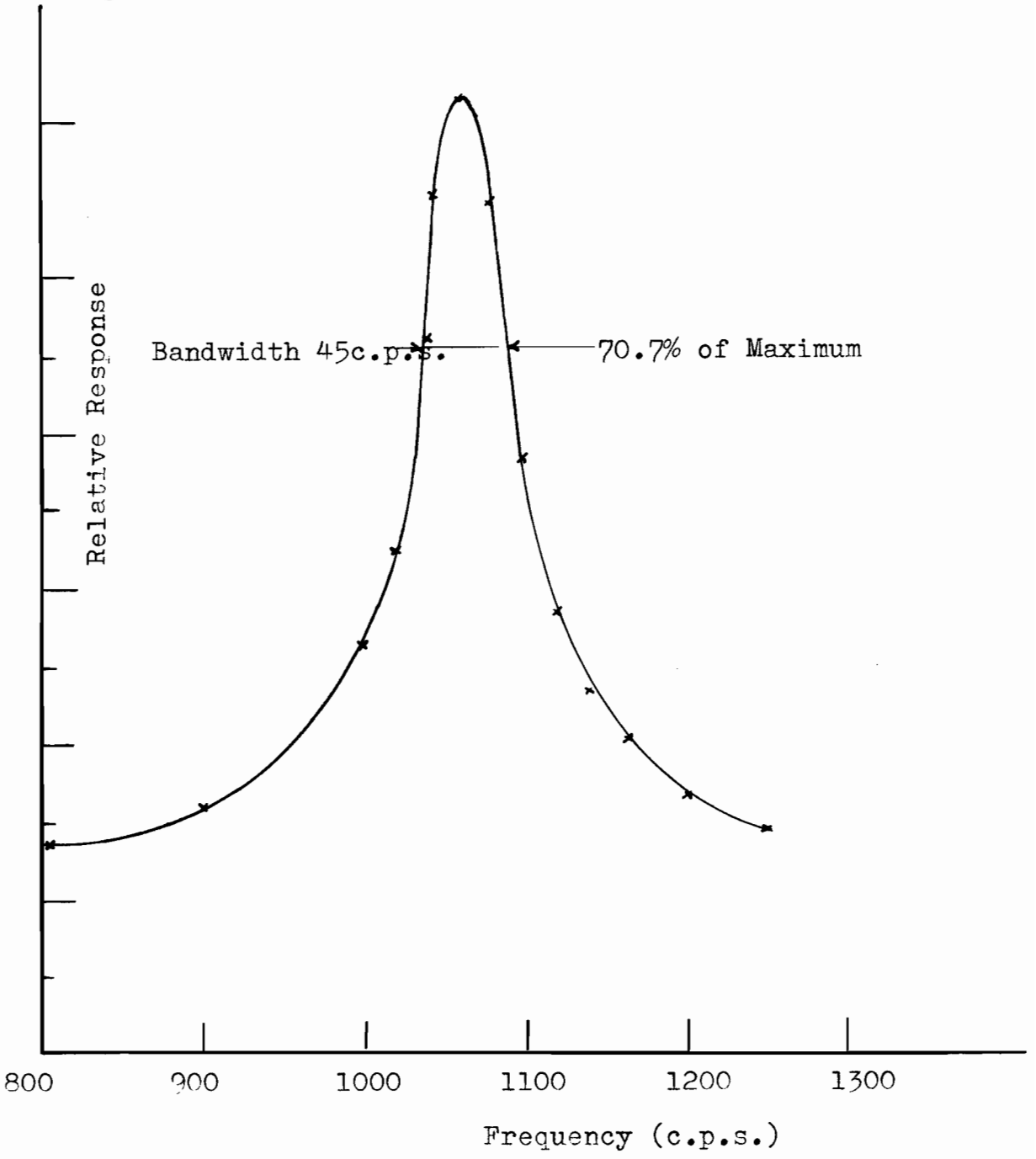

utilize the high gain position owing to the fact that the noise from the tuned amplifier caused the meter needle to fluctuate violently with a large amplitude.

The phase sensitive detector can measure the in-phase or quadrature component of a signal with respect to a reference signal of the same frequency.

The sensitivity of the detector was measured for frequencies of 500, and 1000 c.p.s.. The sensitivity was also measured as a function of gain control position. The circuit used during the measurements was as indicated in Figure 5-5. The results are given in 5-7, 5-8, 5-9 and 5-10. The output as a function of meter deflection was thought to be of some interest and these results are shown in Figure 5-11.

A variable phase shifter was incorporated into the phase sensitive detector; hence, it was possible to null on components other than the in phase or quadrature. This is the variable phase shift referred to earlier in section 2.8.5.

5.1.5. DC Amplifier.

The General Radio DC amplifier and electrometer was used to amplify the small signals from the phase sensitive detector.

Figure 5-5 Block Diagram of Instruments Used In Measuring Characteristics of Phase Sensitive Detector

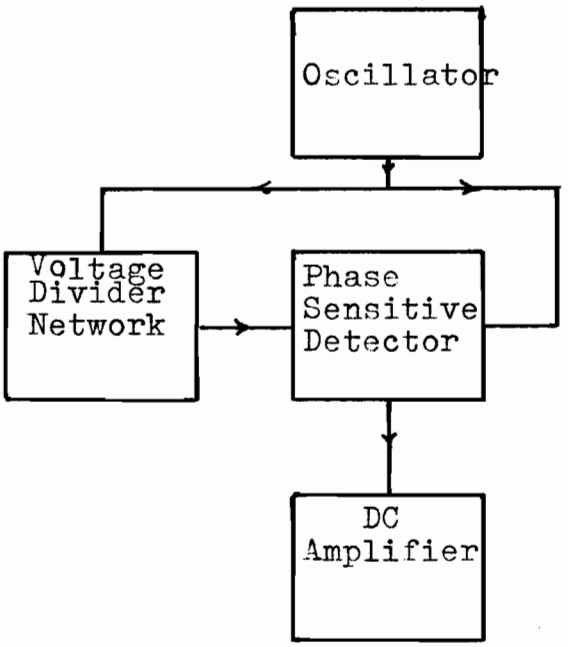

Figure 5-6 Block Diagram of Instruments Used In Measuring the Energy Spectrum of the Carbon Arc

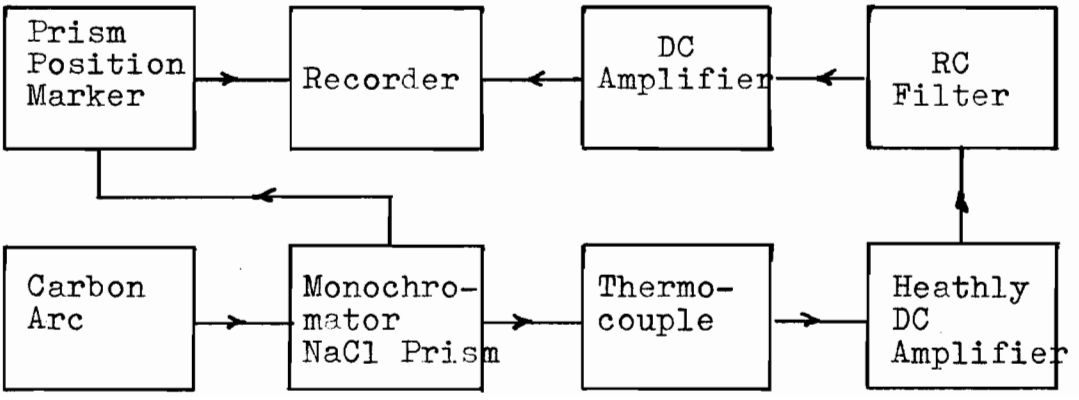

Figure 5-7 Calibration of Phase Sensitive Detector

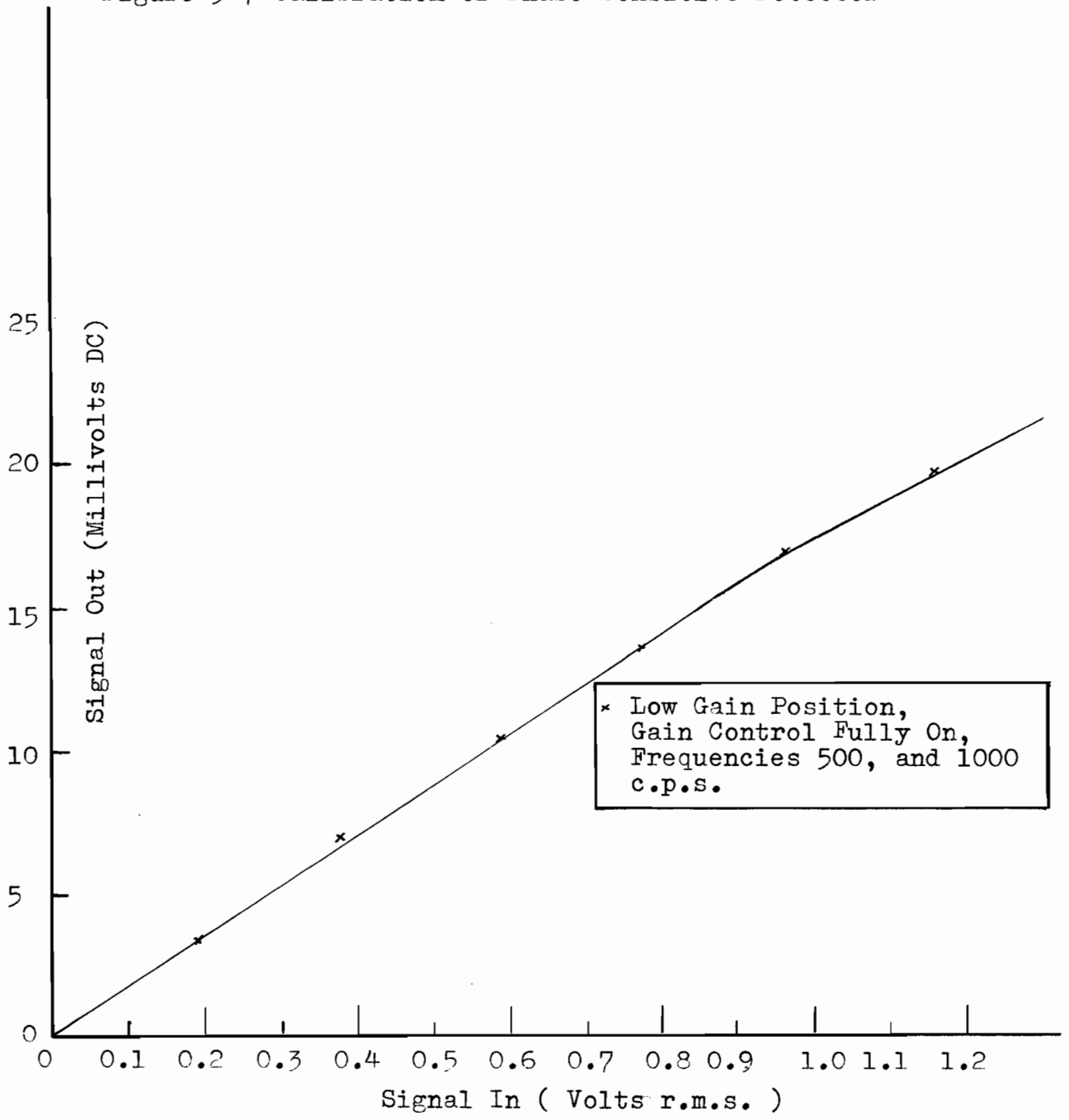

Figure 5-8 Calibration of Phase Sensitive Detector

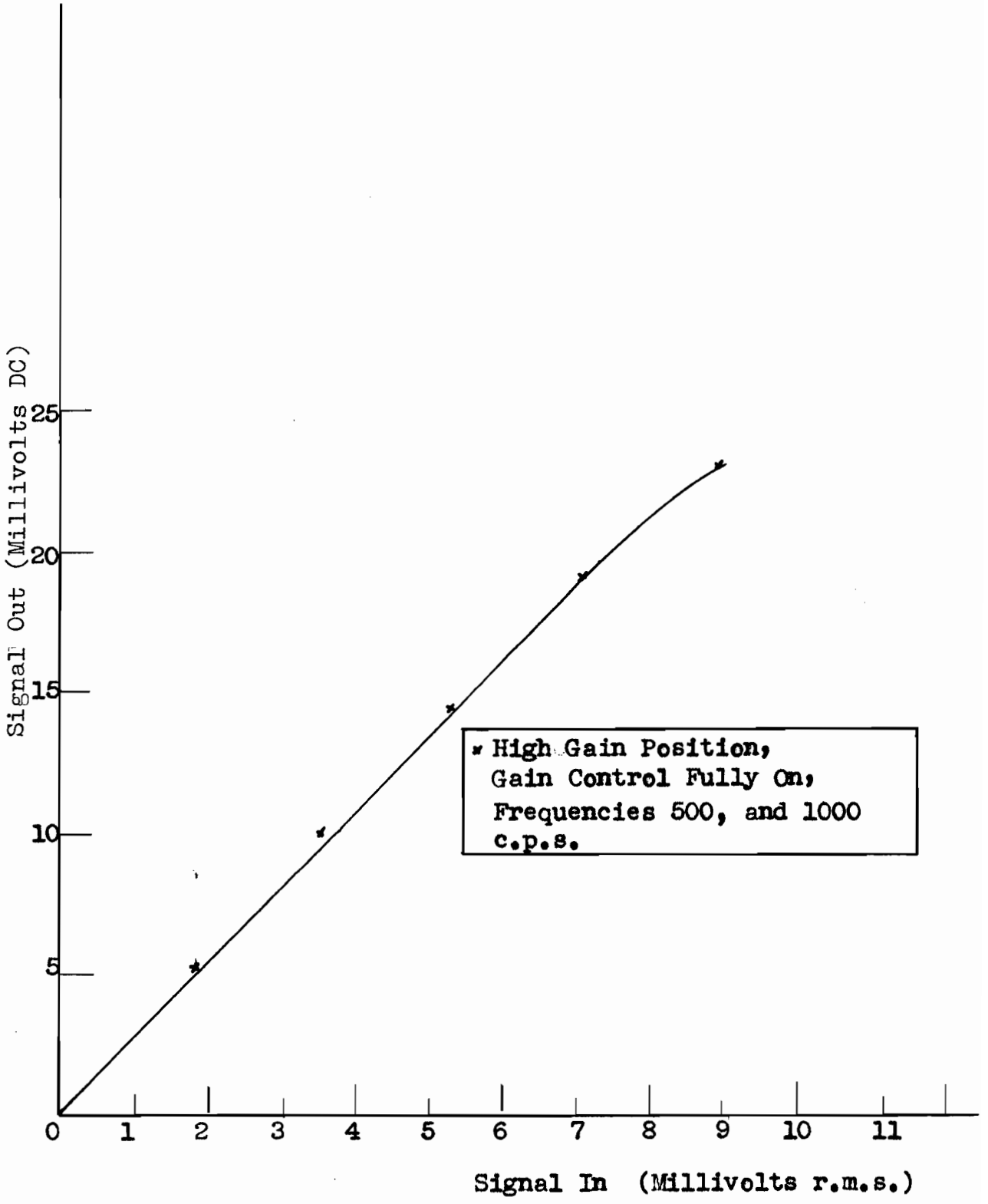

Figure 5-9 Calibration of Phase Sensitive Detector

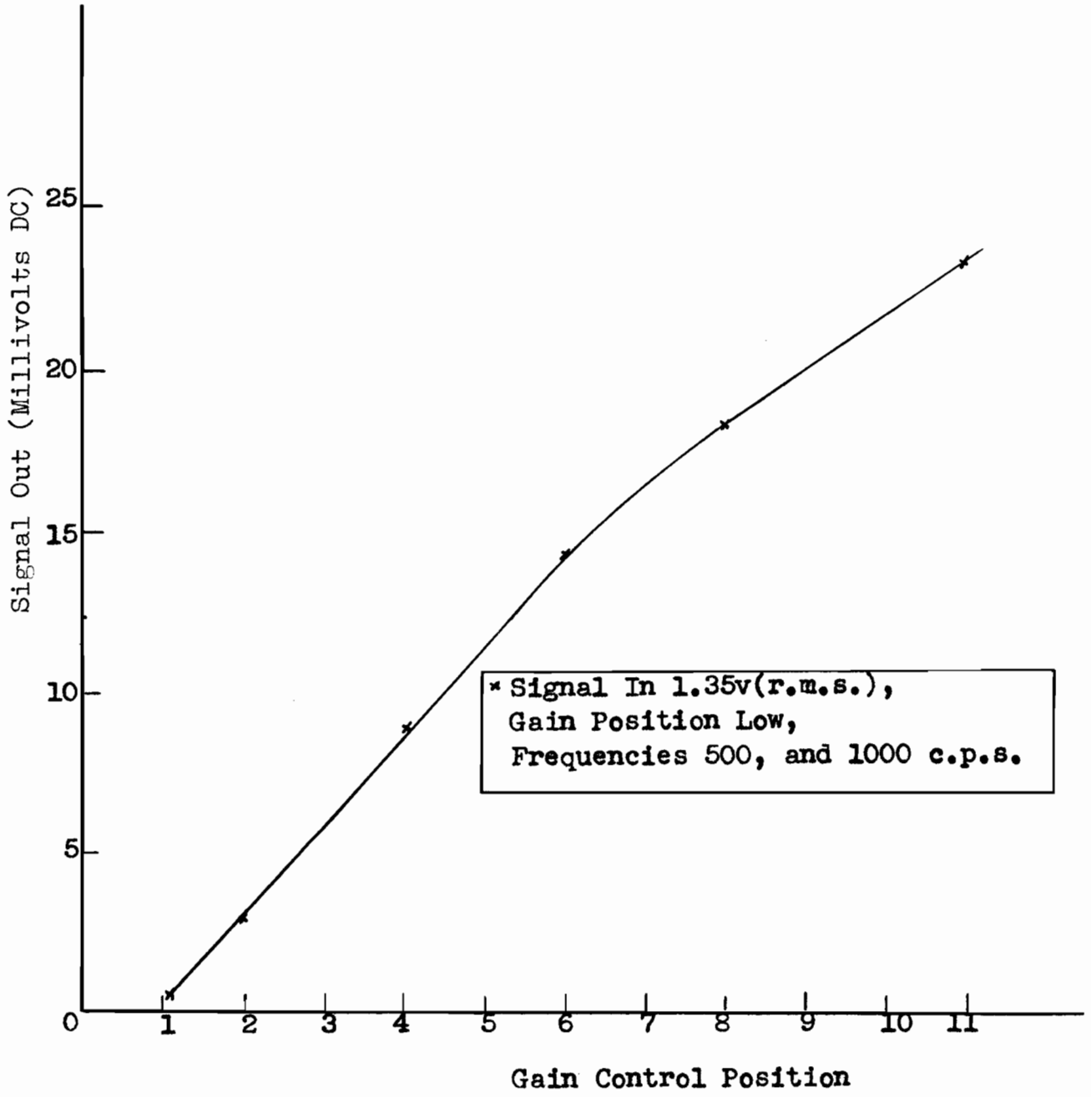

Figure 5-10 Calibration of Phase Sensitive Detector

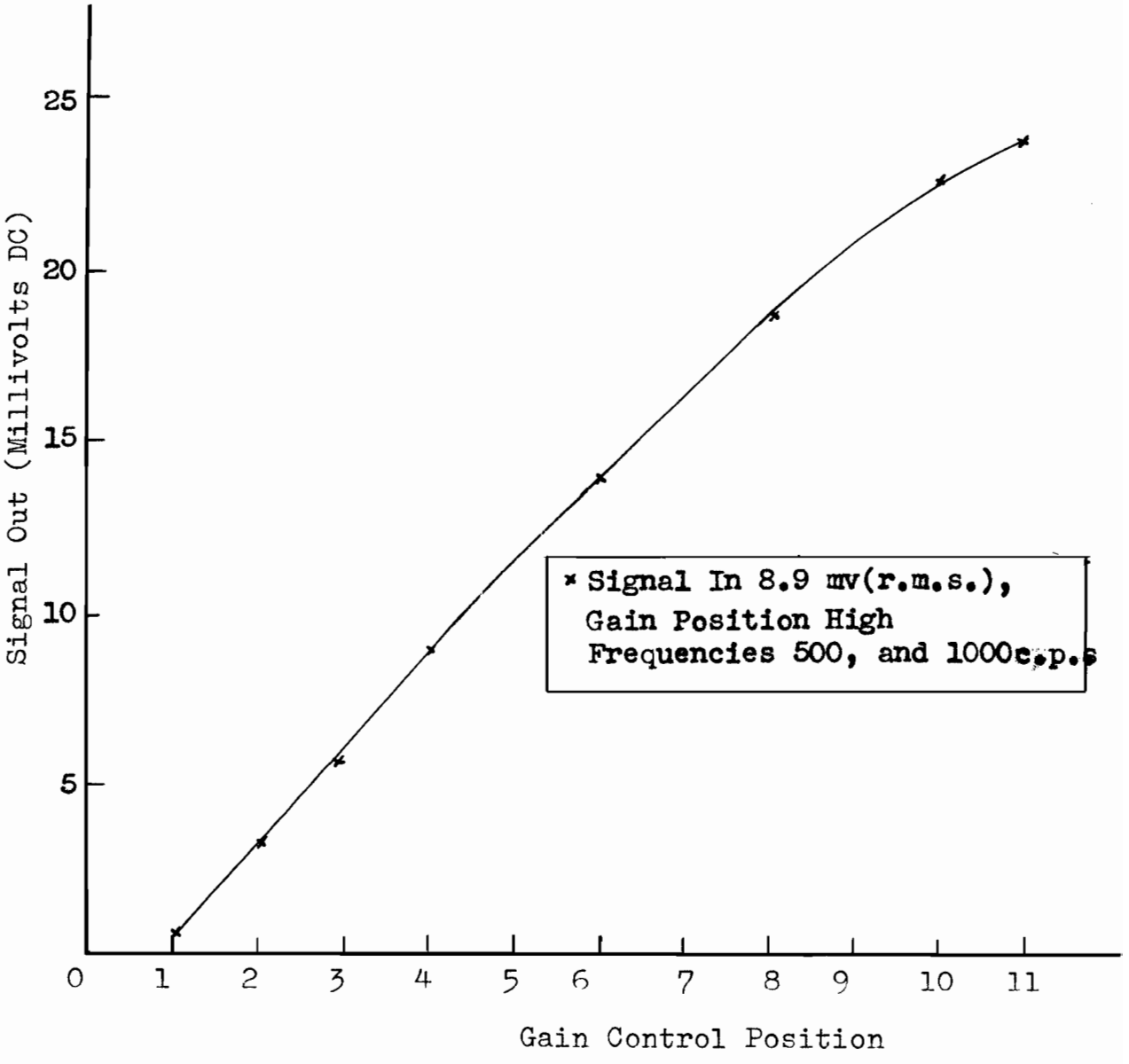

Figure 5-11 Calibration of Phase Sensitive Detector

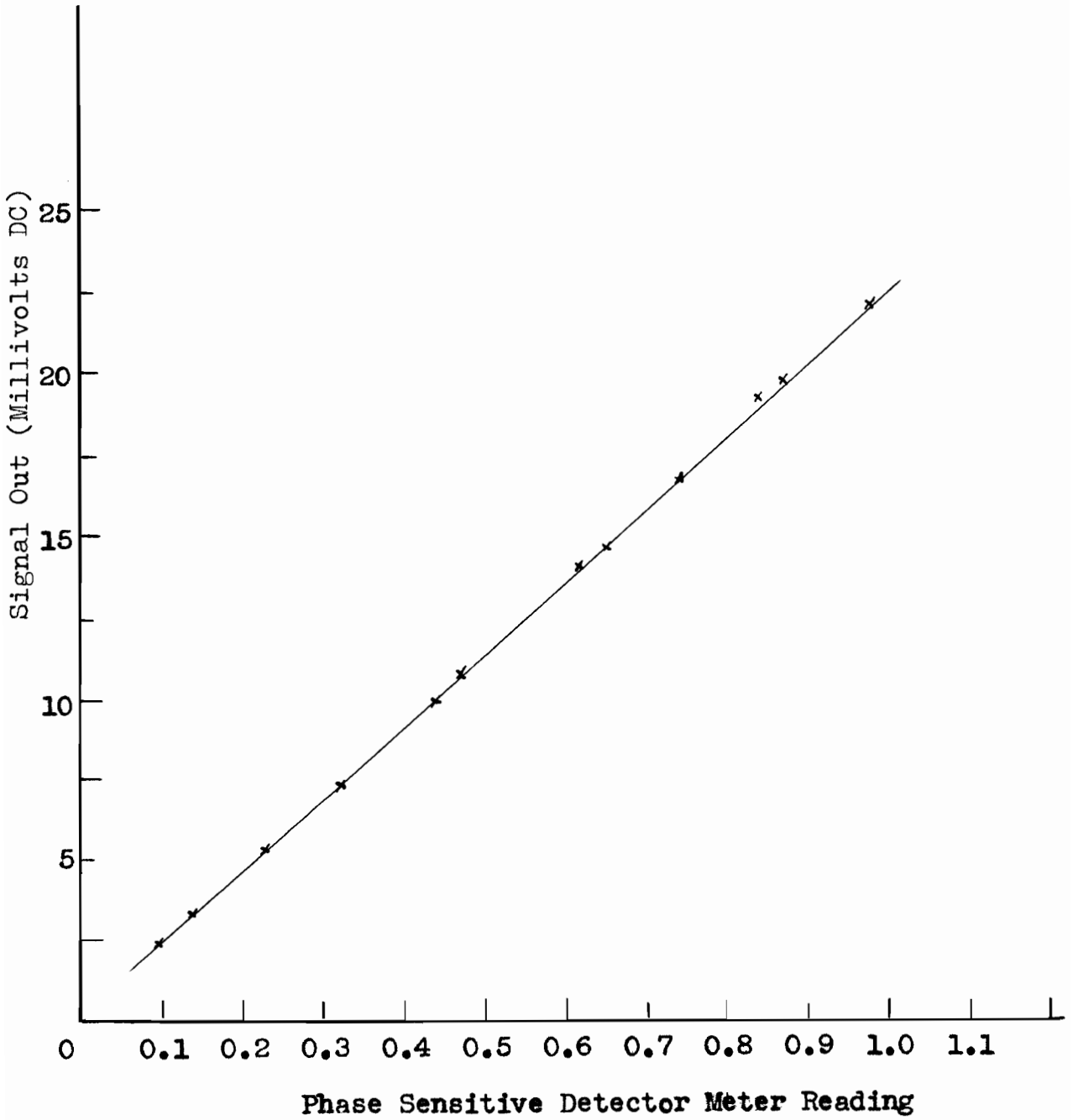

For the majority of the measurements the DC amplifier was used in the most sensitive position (30mv full scale deflection). Four other ranges of sensitivities 100 mv, 300mv, 1v, and 10v were provided.

A high input impedance was used throughout the experiment ($10^8 \Omega$).

The ground selector switch was set at E as recommended by the instruction manual.

The output of the amplifier was loaded with a 1600Ω carbon resistor in series with a variable resistance of maximum value 111Ω.

A warm up period of about two hours was necessary before stable operation of the amplifier was achieved at high sensitivities.

The voltage gain was measured and found to be 2.59, 7.7, 25.4, 78.3, and 258 for sensitivity settings of 3,1v, 300, 100, and 30mv respectively.

The measuring circuit was as shown in Figure 5-12.

The measurements were made with the voltage divider and recorder in place in order that the amplifier load be the same as when in operation.

5.1.5 Low Pass Filter.

This was a very simple network consisting of a

permanent 10% carbon resistor (6.8 MΩ), and a variable decade capacitance (General Radio) of maximum value 1.11 ufd. These were arranged as shown in Figure 2-9.

Since the low pass filter worked into an impedance of $10^8\Omega$ (of the DC amplifier), the voltage divider action of R_1 was very small. It reduced the output from the phase sensitive detector applied to the input of the DC amplifier by 6.3%

As was seen from the theory section the time constant of the low pass filter determines the over all bandwidth of the detection system. This calculated bandwidth was found to be $\Delta f = 0.021$ c.p.s.. The value of the time constant used throughout the measurements was $RC = 7.5\ \text{sec}^{-1}$. The response time of the detection system beyond the low pass filter could be observed on the recorder and was found to agree exactly with the above calculated value.

5.1.6 Recorder.

The signal from the DC amplifier was fed into a voltage divider network and then into a Leeds & Northrup Speedomax recorder (Figure 5-13).

The recorder sensitivity was measured for several values of the load resistance R. The sensitivity was

Figure 5-12 Block Diagram of Instruments Used in Measurement of DC Amplifier Gain

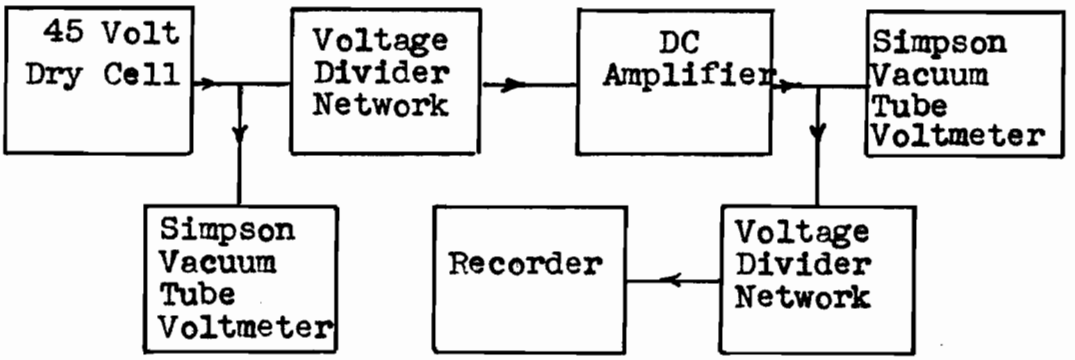

Figure 5-13 Recorder and Voltage Divider Network

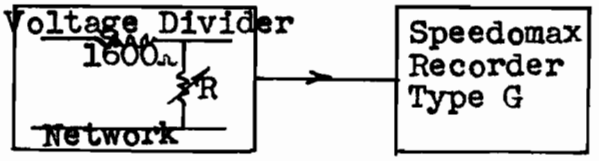

Figure 5-14 Block Diagram of Instruments Used In Measurement of Recorder Sensitivity

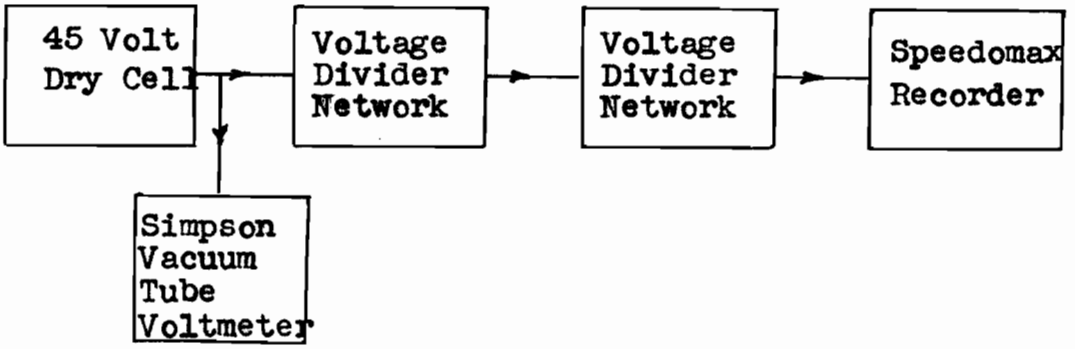

essentially the same $1.1X10^3$ divisions/volt for all three values of R of 1.6, 3.2, and 4.8Ω.

The circuit used in the measurement was as in Figure 5-14.

5.1.7 The Carbon Arc.

The carbon arc (Leiss) energy spectrum (no lens) was measured using a Perkin-Elmer thermocouple. The thermocouple was mounted at the output split of the Leiss monochromator. The monochromator was supplied with a sodium chloride prism. The measuring system was as in Figure 5-6. The prism position was changed by means of a small motor. A marker signal was generated by an off on switch attached to the shaft which altered the prism position. The small marker signal drove the second pen of the chart recorder. The results are shown in Figure 5-15. No attempt was made to adjust the output slit width of the monochromator to compensate for the changing dispersion of the prism. The output slit width during the measurement was 1 mm.

5.1.8 The Monochromator.

A Leiss monochromator was used in the apparatus-system. The monochromator was used with a sodium chloride prism having the transmission limits of 0.25 to 15 microns.

Figure 5-15 Carbon Arc Energy Spectrum

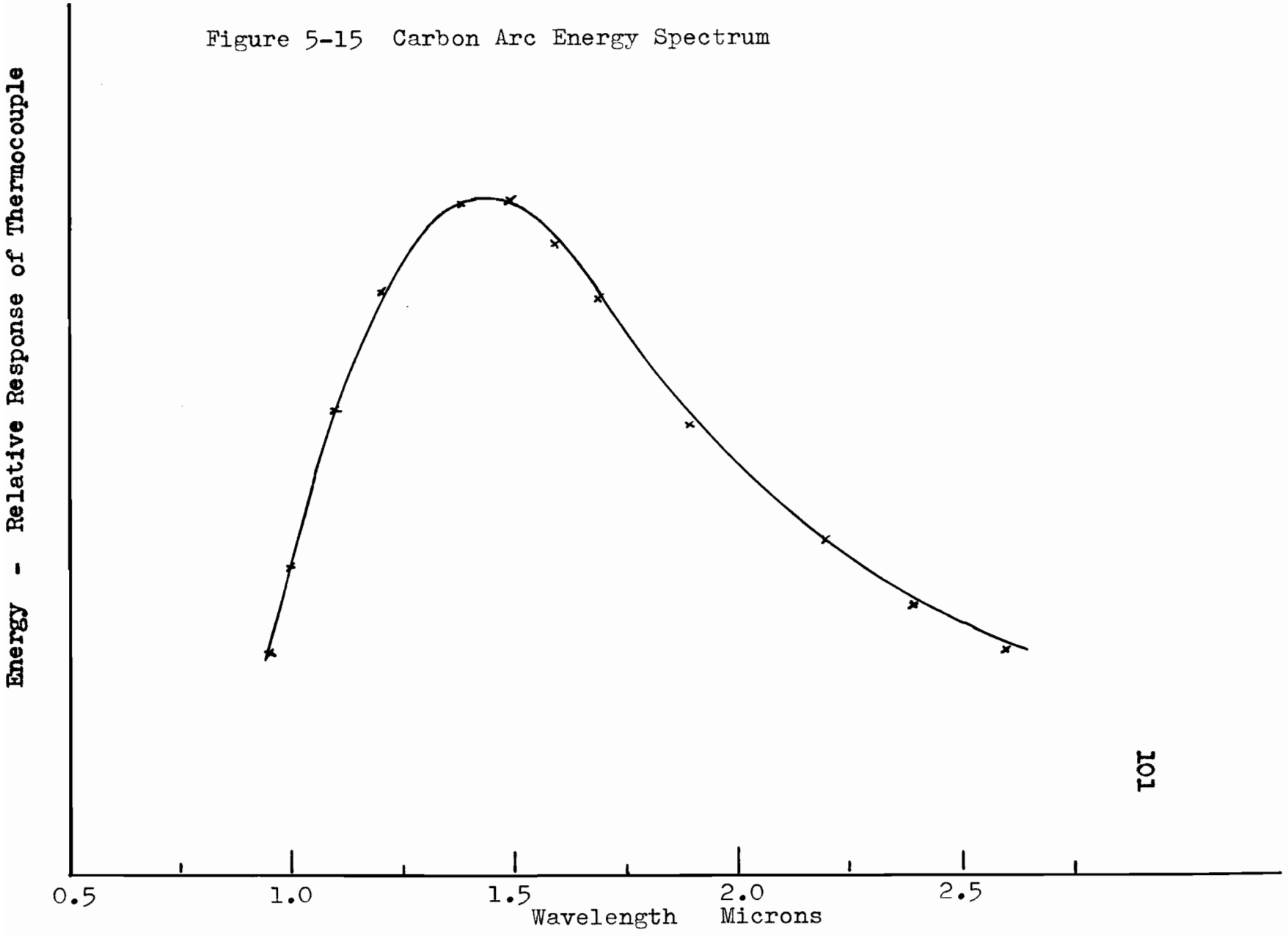

Figure 5-16 Calibration of Leiss Monochromator Against Perkin-Elmer Monochromator (Equipped with Fused Quartz Prism)

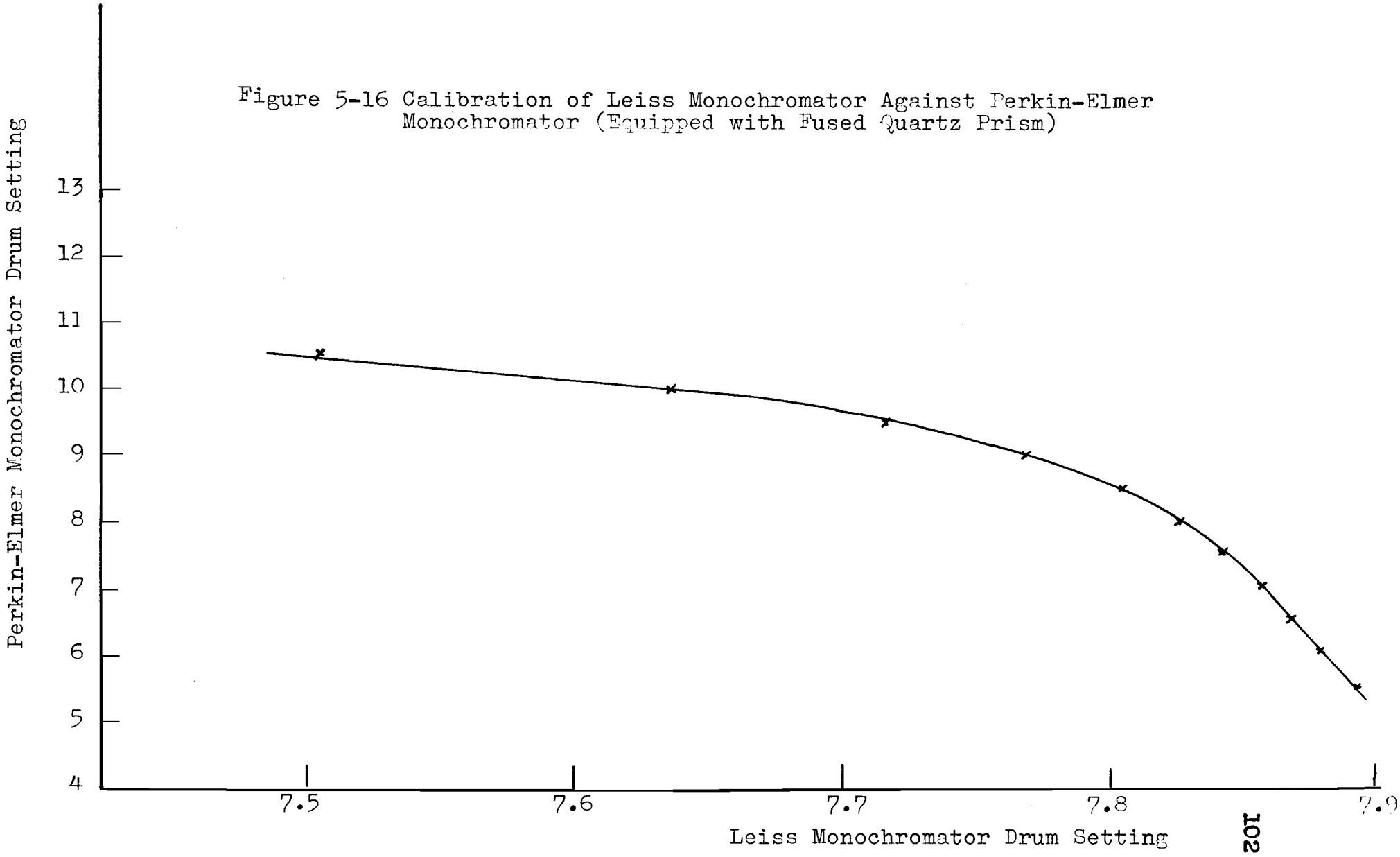

Figure 5-17 Wavelength - Leiss Monochromator Drum Setting

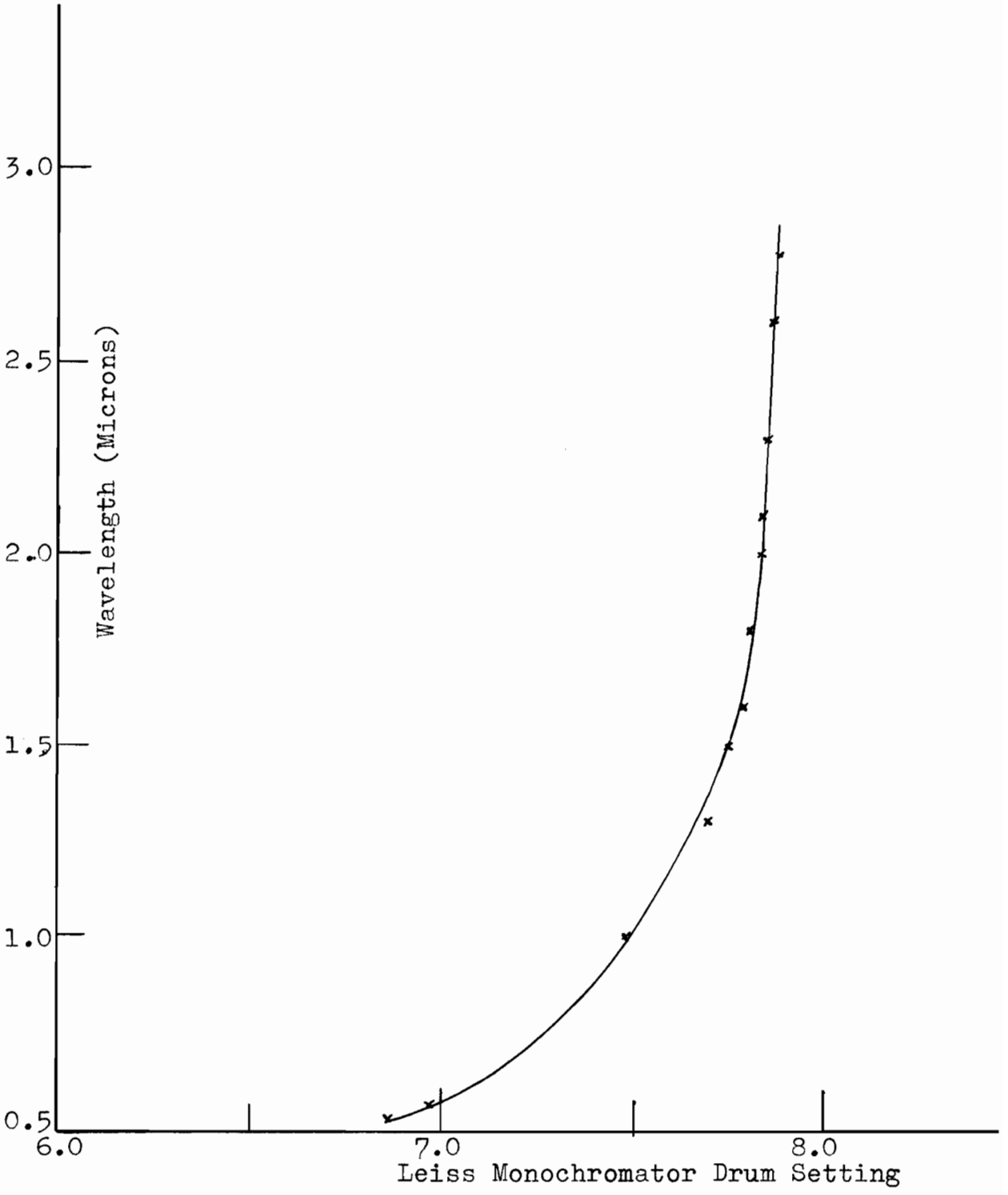

The Leiss monochromator was calibrated in the infra-red against the Perkin-Elmer Universal Monochromator (model 83). The Perkin-Elmer monochromator was calibrated with a mercury lamp. The mercury green line (5461 A^{o}) was found to correspond to a drum setting of the Perkin-Elmer monochromator of 12.063. It is to be noted that the Perkin-Elmer model was equipped with a fused quartz prism during the measurements.

Figure 5-16 gives the Leiss monochromator setting in terms of the corresponding Perkin-Elmer monochromator drum setting.

The calibration curve for the Leiss monochromator is given in Figure 5-17.

5.2 The Magnetic Induction Pattern about a small Dipole the Z Coordinate of which varies periodically with time.

Consider Figure 2-2. The object of the calculation is to find the magnetic induction pattern for a magnetic dipole, one position coordinate of which is changing with time.

Suppose the magnetic dipole has its moment aligned with the X axis, and that the dipole is bodily vibrated in the Z direction. The magnetic potential at a point of

observation $P(x',y',z')$ of a magnetic dipole $\underline{M}$ (13((14) is

$$\phi(x',y',z') = -\frac{1}{4\pi}\underline{M}\cdot\nabla'(1/r) \tag{1}$$

If the Z position coordinate of $\underline{M}$ is caused to change periodically with time according to $a\exp(i\omega' t)$, then the time rate of change of the magnetic potential is given by

$$\frac{\partial\phi}{\partial z}\, a\exp(i\omega' t) \tag{2}$$

The magnetic potential of a dipole oriented in the X direction is given by

$$\phi(x',y',z') = \frac{1}{4\pi}\frac{|\underline{M}|\,x'}{r^3} \tag{3}$$

Hence, the time rate of change of the magnetic potential due to a dipole vibrating in the Z direction is

$$-\frac{3}{4\pi}\frac{|\underline{M}|\,x'z'}{r^5}\, a\exp(i\omega' t) \tag{4}$$

The magnetic induction $B(x',y',z',t)$ is given by

$$\underline{B}(x',y',z',t) = -\nabla'\phi(x',y',z',t) \tag{5}$$

Substituting (4) into (5) there results

$$\underline{B}(x',y',z',t) = \frac{3|\underline{M}|\,a}{4\pi}e^{i\omega' t}\left[\underline{i}\left(\frac{z'}{r^5}-\frac{5x'^2z'}{r^7}\right)+\underline{j}\left(-\frac{5x'y'z'}{r^7}\right)+\underline{k}\left(\frac{x'}{r^5}-\frac{5x'z'^2}{r^7}\right)\right] \tag{6}$$

The X,Y,Z components of the magnetic induction are from (6) then

$$B_x = \frac{3|\underline{M}|}{4\pi}a\exp(i\omega' t)\left(\frac{z'}{r^5}-\frac{5x'^2z'}{r^7}\right) \tag{7}$$

$$B_y = \frac{3|\underline{M}|}{4\pi}a\exp(i\omega' t)\left(-\frac{5x'y'z'}{r^7}\right) \tag{8}$$

$$B_z = \frac{3|\underline{M}|}{4\pi}a\exp(i\omega' t)\left(\frac{x'}{r^5}-\frac{5x'z'^2}{r^7}\right) \tag{9}$$

In spherical polar coordinates (7), (8), (9) become (Figure 18)

$$B_x = \frac{3|\underline{M}|}{4\pi r^4} a \exp(i\omega' t)\cos\theta(1 - 5\sin^2\theta\cos^2\phi) \quad (10)$$

$$B_y = -\frac{3|\underline{M}|}{4\pi r^4} a \exp(i\omega' t)(5\sin^2\theta\cos\theta\sin\phi) \quad (11)$$

$$B_z = \frac{3|\underline{M}|}{4\pi r^4} a \exp(i\omega' t)\sin\theta\cos\phi(1 - 5\cos^2\theta) \quad (12)$$

The arrangement of coils used in this experiment is responsive to changing magnetic induction patterns in the xz plane. Let $\cos\phi = 1$, then equations (10), (11), (12) become

$$B_x = \frac{3|\underline{M}|}{4\pi r^4} a \exp(i\omega' t)\left[\cos\theta(1 - 5\sin^2\theta)\right] \quad (13)$$

$$B_y = 0 \quad (14)$$

$$B_z = \frac{3|\underline{M}|}{4\pi r^4} a \exp(i\omega' t)\left[\sin\theta(1 - 5\cos^2\theta)\right] \quad (15)$$

Equations (13) and (15) are plotted in Figures 5-19 and 5-20 for lines of constant magnetic induction.

5.3 Signal to be Expected from a Sample of Material having a Photomagnetic Susceptibility χ_{sample}

Consider Figure 2-2. Let the photomagnetic susceptibility of the sample be χ_{sample}. It can be assumed that the susceptibility for a thin section in the xy plane of volume abdz is given by

$$\chi_{section} = \frac{dz}{a}\ \chi_{sample}$$

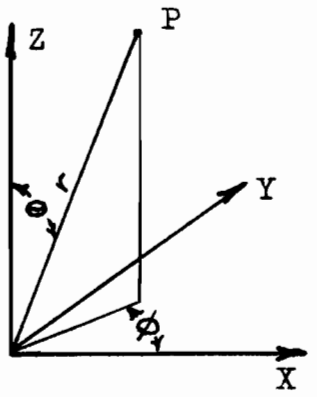

Figure 5-18 Spherical Polar Coordinates

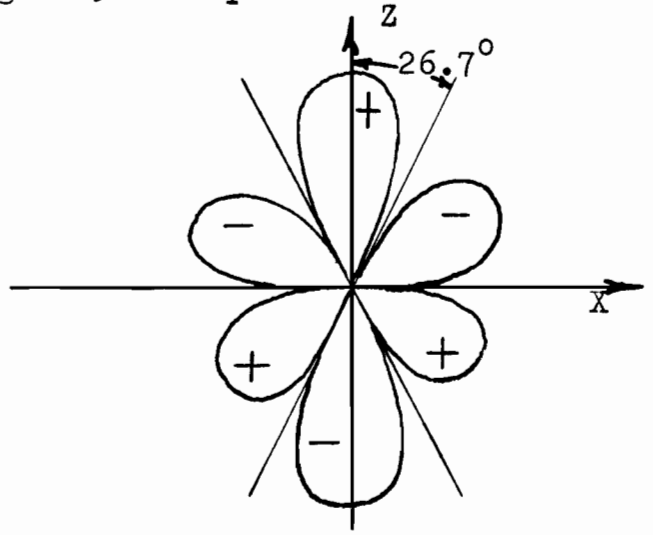

Figure 5-19 Equation 13 - Schematic of Lines of Constant Magnetic Induction (B_x)

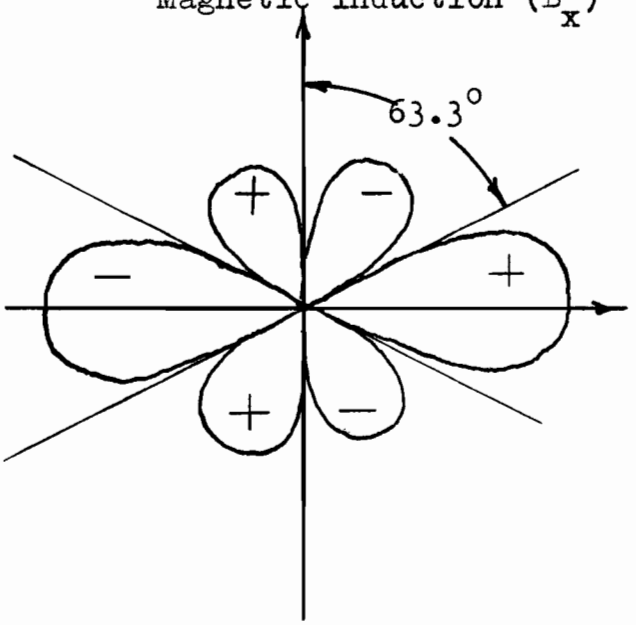

Figure 5-20 Equation 15 - Schematic of Lines of Constant Magnetic Induction (B_z)

The magnetic moment for a thin section is

$$M_{section} = \frac{dz}{a} \chi_{sample} H$$

Since the magnetic moment of the section is changing with time, a small voltage is induced in the detection coils. The recorder deflection arising from this small section is

$$D' = \omega' \frac{dz}{a} \chi_{sample} \frac{HGd_4A''}{2.06} \times 10^{-4} \left\{ \frac{1}{\left[d_4^2 + (d - 0.25)^2\right]^{3/2}} \frac{1}{\left[d_4^2 + (d + 0.25)^2\right]^{3/2}} \right\}$$

where d is the distance in inches of the section to the horizontal plane passing through the geometrical centres of the coils.

Suppose the sample dimensions are 3/8" by 3/8" by 1/4", and that the vertical distance between the plane passing through the geometrical centres of the coils and the centre of the sample is 0.450 inches. Then, if the coordinate system is at the centre of the sample, the recorder deflection to be expected is (replacing d by z+0.45 and integrating)

$$D = \omega' \chi_{sample} \frac{HA''d_4G}{a2.06} \times 10^{-4} \int_{z=-0.187''}^{z=+0.187''} \left\{ \frac{1}{\left[d_4^2 + (z+0.2)^2\right]^{3/2}} - \frac{1}{\left[d_4^2 + (z+0.7)^2\right]^{3/2}} \right\} dz$$

For $\omega' = 6.27 \times 10^3$ rad/sec, a = 0.375 in., $A''(d_4)$ / $2.06 \times 10^{-4} = 3.11 \times 10^2$, and the definite integral = 6, the formula for the recorder deflection becomes

$$D = 3.21 \times 10^7 \, G \chi_{sample} \, H$$

G, the electronic gain factor varies with signal level into the tuned amplifier, and recorder decade resistance R. An average value of G is $G = 1.2 \times 10^{7} R$. The formula for the recorder deflection becomes then

$$D = 3.86 \times 10^{14} R \chi_{sample} H$$

The photomagnetic susceptibility of the sample in terms of the recorder deflection, decade resistance, and magnetic field then is

$$\chi_{sample} = \frac{D}{3.86 \times 10^{14} RH}$$

5.4 Table of Values used in Light Sensitivity Calculation

Table-1 Values used in Light Sensitivity Calculation

Symbol	Meaning	Units	Value
f	Frequency	c.p.s.	10^3
H	magnetic field strength	oersteds	6000
n'	zero frequency refractive index of germanium		4
Q	power supplied to carbon arc	watts	1600
A	lens area	in^2	2.84
v'	lamp efficiency	%	50
v''	chopper, guide tube efficiency	%	30
a	sample width and height	in	3/8
R'	distance of arc to lens	in	1.75
h	Planck's constant	ergsec	$6.62X10^{-27}$
u	Bohr Magneton	$ampm^2$	$9.27X10^{-24}$
k	Boltzmann's constant	$joule/K^o$	$1.38X10^{-23}$
T'	sample temperature	^oK	300
c_1	black body rad, constant	$ergcm^2sec^{-1}$	$3.74X10^{-5}$
c_2	black body rad. constant	cm^oK	1.44
T	lamp temperature	^oK	$1.92X10^3$
σ	Stefan's Constant	$ergcm^{-2}sec^{-1}$ $^oK^{-4}$	$5.67X10^{-5}$
λ_{min}	lamp minimum wavelength	microns	0
λ_{gap}	threshold wavelength	microns	1.5
E_g	germanium energy gap (room temperature)	eV	0.81
c	velocity of light	m/sec	$2.99X10^8$
A'	guide tube cross sectional area	in	0.14
u_o	permeability of space	henry/m	$4\ X10^{-7}$
τ	recombination time in germanium	usec	100
$(\frac{\bar{m}}{m_n})^2+(\frac{\bar{m}}{m_p})^2$			84 *
ω'	angular frequency of chopper	rad/sec	$6.27X10^3$

* See reference (10)

REFERENCES

1. J.O. Kessler, A.R. Moore, Proc. Int. Conf. on Semiconductor Physics (Prague), p.804, (1960).

2. J.O. Kessler and A.R. Moore, Phys. Rev. Letters, 2, 247, (1959).

3. A.R. Moore, J.O. Kesseler, Phys. Rev. Letters, 4, 121, (1960).

4. C. Kittel, Introduction to Solid State Physics, Chapter 9, John Wiley & Sons, Inc., London, (1961).

5. J.F. Nye, Physical Properties of Crystals, chapter 3, Oxford University Press, London, (1960).

6. N.F. Mott, and R.W. Gurney, Electronic Processes in Ionic Crystals, chapter 3, Oxford University Press, London, (1957).

7. T.S. Moss, Optical Properties of Semi-Conductors, chapter 3, Butterworths Scientific Publications, London, (1959).

8. L.L. Korenblit, Zh. tekh. Fiz., Vol. 27, No. 3, 484-94 (1957).

9. W.Von Roosbroeck, Phys. Rev., 101, 1713, (1956).

10. G.A. Busch, O.R. Vogt, Proc. Int. Conf. on Semiconductor Physics (Prague), p.797, (1960).

11. T.S. Moss, Optical Properties of Semi-Conductors, chapter 1, Butterworths Scientific Publications, London, (1959).

12. F.A. Jenkins, H.E. White, Fundamentals of Optics, p.432, McGraw-Hill Book Company, Inc., New York and London, (1957).

13. J.A. Stratton, Electromagnetic Theory, pp.225-230, McGraw-Hill Book Company, Inc., New York, (1941).

14. F.W. Sears, Electricity and Magnetism, p.271, Addison-Wesley Publishing Company, Inc., Reading, Massachusetts, U.S.A., (1958).

15. C.G. Cannon, Electronics for Spectroscopists, p.165 Interscience Publications Inc., New York, (1960).

16. 17. V.C. Rideout, Active Networks, chapter 15, Prentice Hall, Inc., Englewood Cliffs, N.J., (1960).